LEADING PIPELINE RESEARCH

Catalog No. PR-214-203806-R01

Improve Dent/Cracking Assessment Methods

MD-5-2

PR-214-203806

BMT Project: 30839

Prepared for the

Integrity & Inspection Technical Committee

Of

Pipeline Research Council International, Inc.

Prepared by:

BMT Canada Ltd

Authors:

Arnav Rana, Sanjay Tiku, Aaron Dinovitzer

Release Date:

May 30, 2022

Version	Date of Last Revision	Date of Uploading	Comments
Draft 01	March 14, 2022	March 15, 2022	Draft report for project team review
Draft 02	March 29, 2022	March 29, 2022	Draft final report for PHMSA
Final 01	May 30, 2022	May 31, 2022	Final Report

Abstract

This work was funded in part, under the Department of Transportation, Pipeline and Hazardous Materials Safety Administration. The views and conclusions contained in this document are those of the authors and should not be interpreted as representing the official policies, either expressed or implied, of the Pipeline and Hazardous Materials Safety Administration, the Department of Transportation, or the U.S. Government.

This project builds on mechanical damage (MD) assessment and management tools, developed on behalf of Pipeline Research Council International (PRCI), Interstate Natural Gas Association of America (INGAA), Canadian Energy Pipeline Association (CEPA), American Petroleum Institute (API), other research organizations and individual pipeline operators and were included in API RP 1183. These include dent shape, restraint condition and interacting feature characterization; operational maximum and cyclic internal pressure characterization, screening tools defining non-injurious dent shapes based on pipe size and operating condition, failure pressure and fatigue assessment tools for dents with/without interacting features (e.g., corrosion, welds, gouges) in the restrained and unrestrained condition, and direction on available remedial action and repair techniques. In completing this development, areas for improvement were identified.

The current project enhances previously developed tools being adopted in an industry recommended practice (API RP 1183) for pipeline MD integrity assessment and management considering:

- Enhancement of indentation crack formation strain estimation,
- Understanding the role of ILI measurement accuracy on dent integrity assessment, and
- Quantification of assessment method conservatism to support safety factor definition.

Safety factors (Modeling bias) defined in the present study and evaluated for different fatigue life estimation approaches in the present work refer to the conservatism inherent in different fatigue life models and is represented as the ratio of experimental lives to predicted lives.

Project Team

Member	Company
Aaron Dinovitzer	BMT
Adrian Belanger	TDW
Alan Free	Boardwalk
Arnav Rana	BMT
Bryce Brown	ROSEN
David Ransome	Cadent Gas
Edward Newton	SoCalGas
Eric Amundsen	Energy Transfer
Francois Rongere	PG&E
Haakon Ferkingstad	Gassco
Husain Al-Muslim	Saudi Aramco
John Haldiman	Plains
Lisa Madden	ExxonMobil
Marcus Le Roy	Marathon
Mark Gebbia	Williams
Mark Piazza	API
Mark Shook	Buckeye
Maureen Droessler	OTD
Michael Bellamy	Baker Hughes
Michael Pearson	AOPL
Michael Turnquist	Quest
Mike Stackhouse	Phillips 66
Nader Yoosef-Ghodsi	Enbridge
Neil Thompson	DNV
Paul Huddleston	Trans Mountain
Phu Phan	Enterprise
Robert Bood	National Grid
Ron Bessette	Kinder Morgan
Ryan OHara	ATCO
Sanjay Tiku	BMT
Shawn Miller, PE	BHE GT&S
Shenwei Zhang	TC Energy
Taylor Shie	Shell
Taylor Snider	Flint Hills
Tim Burns*	Shell
Tony Dotson	ConocoPhillips
Tyson Cote	TransGas
Walter Crommelin	Gasunie
Zhang Shuli	CPPE

*Team Leader

Contents

List of Figures and Tables

List of Nomenclature

a	Specified Certainty
b_i	Coefficients of Equation (4.11)
d	Dent Depth
E_I	Strain at Indentation
E_p	Strain at Pressure
L	Dent Length
ε_1	Circumferential Bending Strain
L^{AX}	Dent Characteristic Axial Length
L_0	Undeformed Length
L_{def}	Total Deformed Length
L_S	Deformed Length
L^{TR}	Dent Characteristic Transverse Length
L_{undef}	Total Undeformed Length
N_{exp}	Experimental Cycles to Failure
normrnd	Normal Random Number Generator Function
N_{pred}	Predicted Cycles to Failure
p	Equivalent Plastic Strain
Pmax	Maximum Pressure
Pmean	Mean Pressure
r	End of Span Radial Distance
R	Factors of Safety
R_0	Pipe Nominal Outer Radius
R_1	Radius of Curvature of the Circumferential Dent Profile at Dent Apex
R_2	Radius of Curvature Axial Dent Profile at Dent Apex
r_p,	Peak Radial Distance
s	Scaling Factor
t	Pipe Wall Thickness
ε	Strain
ε_0	Critical Strain
ε_2	Axial Bending Strain
ε_3	Axial Membrane Strain
ε_4	Circumferential Membrane Strain
ε_{eff}	Effective Strain
ε_{eq}	Equivalent Plastic Strain
θ	Angular Distance
σ_{eq}	von Mises Stress
σ_m	Hydrostatic Stress

List of Acronyms

API	American Petroleum Institute
ASME	American Society of Mechanical Engineers
CCW	Counter Clockwise
CEPA	Canadian Energy Pipeline Association
CW	Clockwise
DFDI	Ductile Failure Damage Indicator
FE	Finite Element
ID	Inner Diameter
ILI	In-line Inspection
INGAA	Interstate Natural Gas Association of America
MD	Mechanical Damage
OD	Outer Diameter
PHMSA	Pipeline and Hazardous Materials Safety Administration
PRCI	Pipeline Research Council International
SMYS	Specified Minimum Yield Strength
SSI	Spectrum Severity Indicator
USDOT	United States Department of Transportation
WT	Wall Thickness

1 Executive Summary

This project builds on mechanical damage (MD) assessment and management tools developed over several years and incorporated in API RP 1183 [1]. The long-term integrity of a dented pipeline segment is a complex function of a variety of parameters, including pipe geometry, indenter shape, dent depth, indenter support, and pressure history at and following indentation. In order to estimate the safe remaining operational life of a dented pipeline, all of these factors must be considered in the analysis. The current project enhances previously developed tools being adopted in an industry recommended practice (API RP 1183) for pipeline MD integrity assessment and management considering:

- Enhancement of indentation crack formation strain estimation,
- Understanding the role of in-line inspection (ILI) measurement accuracy on dent integrity assessment, and
- Quantification of assessment method conservatism to support safety factor definition.

To understand the potential for cracking-during-dent-formation, criteria have been developed to consider the dent shape to infer strains which are compared to a "crack" formation strain. This approach is an important consideration due to the impact of cracks on MD failure pressure and fatigue life criteria. Various methodologies have been developed to predict the indentation strain, two are considered in this report; the American Society of Mechanical Engineers (ASME) B31.8 Appendix R Effective Strain and "Blade Energy Partners Simplified Model" Effective Strain [2] [3]. The accuracy of estimation of indentation strains by these models were assessed against strain data from validated finite element analysis of pipeline dents over a wide range of pipe geometry and dent depths. The dent dataset included dents from full-scale testing, hypothetical dents and in-service dents from several pipelines. Indentation strains for both restrained and unrestrained dents at different pressures were evaluated. Both the ASME B31.8 effective strain and Blade Energy Partner effective strain agreed well with indentation strains for restrained dents, except for deeper and sharper dents where ASME B31.8 effective strain diverged from finite element (FE) estimated dent strain. Both the methodologies do not predict indentation strains for unrestrained dents, as generally, the measured shape of an unrestrained dent is not representative of the shape of the dent at formation and cannot be directly used to infer the dent formation or indentation strain. A simplified modification to the ASME B31.8 effective strain was developed and worked well for deeper and sharper restrained dents and was able to overcome the divergence in data seen in the ASME effective strain. A methodology was developed to estimate indentation strains for unrestrained dents based on the dent shape and pressure information during ILI tool run and the maximum pressure seen by the dent during its history. The indentation strain predictions for unrestrained dents based on the methodology developed agrees very well with the indentation strains derived from FE models.

Ductile Failure Damage Indicator (DFDI) is a strain-based damage prediction model which can be used to assess the MD incurred during indentation [4]. It involves a damage parameter which is calculated using strain at indentation and material critical strain (material property). A damage parameter exceeding a critical value indicates incurrence of MD. In the current project the DFDI methodology was evaluated against 47 full-scale dent test data. In the 47 test results available, no cracks were observed during indentation. The upper bound DFDI model was employed using the

minimum and maximum critical strain values of 0.3 and 0.5 suggested for pipeline steels [3]. Based upon the least conservative and the most conservative options, 0 out of 47 or 16 out of 47 steels were predicted to have cracks during indentation based on Blade effective strain. The data for full-scale dents on pipes where cracks initiate during indentation for a range of dent shapes and pipe materials is required to fully evaluate the DFDI methodology.

Error and/or variation in reported data exists in all measurements. In-line inspection (ILI) systems are not immune to this. The implications of the errors/variation in reported measurements on dent fatigue and indentation strain estimates were assessed and quantified to support the definition of performance requirements for ILI systems and define the certainty of assessments. To understand the role of ILI measurement accuracy on dent integrity assessment, Monte Carlo simulations were carried out where error distributions of the dent dimensions were sampled and applied to the dent profiles, and the fatigue life and strain estimates were calculated from the randomized profiles. The variation in the fatigue lives and the strain estimates for different error distributions were calculated. The collated data provides a measure of the variation observed in the estimates when the dent shapes are subjected to various error distributions. Based on different error distributions evaluated in the current project, the coefficient of variation of fatigue ranged between 12% to 34% for unrestrained dents and between 5% to 17% for restrained dents. The coefficient of variation of strain estimates ranged between 9% to 51% based on different error distributions evaluated in the current project.

In addition to the Monte Carlo simulations performed to investigate the effects of shape variation on the fatigue life and strain estimates, ILI pull trial and laser scan dent data were also used. Multiple ILI Service Providers had run their caliper tools through the same set of dents for which laser scan data was also available. Data from 53 single peak dents was employed for this analysis and each dent had up to 50 ILI and one laser scan measurements, providing a sizable family of variations for each dent. The fatigue life and dent strain values were estimated from the ILI and reference data, and coefficient of variation were evaluated from the resulting distributions. For most dents, the coefficient of variation in fatigue life estimates was within 40%, and in strain estimate was within 60%. The results were in good agreement with the Monte Carlo simulation results.

Safety factors and associated confidence levels were defined for fatigue life screening and assessment methodology developed under PRCI and CEPA sponsored research and incorporated in API RP 1183. For this purpose, full-scale dent fatigue test data carried out on plain dents, dents interacting with welds and dents interaction with corrosion was utilized. Comparison of experimental full-scale dent fatigue life data with the estimates from fatigue life screening and assessment methodology was carried out. Histograms of ratios of experimental to predicted fatigue lives (safety factor) were developed and probability distribution functions were fitted onto these. These functions provided estimates of the probability of the safety factor being above certain values. These fitted probability density functions were scaled so that a minimum factor of safety, with a specified certainty, could be achieved. The evaluated scaling factors can be used to scale the estimated fatigue life to ensure that a minimum amount of factor of safety can be ensured with a specified amount of certainty, for a particular fatigue life assessment criterion. Safety factors and associated confidence levels inherent in different fatigue life approaches were defined for plain dents and dents interacting with secondary features using different stress life fatigue curves.

2 Introduction

Mechanical damage on gas and oil transmission pipelines is one of the major single causes of incidents as identified in the Pipeline and Hazardous Materials Safety Administration (PHMSA) incident databases. Dents in buried pipelines occur due to a number of potential causes; the pipe resting on rock, third party machinery strike, rock strikes during backfilling, amongst others. The long-term integrity of a dented pipeline segment is a complex function of a variety of parameters, including pipe geometry, indenter shape, dent depth, indenter support, pressure history at and following indentation. In order to estimate the safe remaining operational life of a dented pipeline, all of these factors must be accounted for in the analysis.

In the present work, the stated objectives of the project were

- to assess and improve the indentation strain prediction models,
- to assess the effect of ILI data variability on fatigue life and strain estimations and
- to define and develop safety factors inherent in different fatigue life estimation methodologies.

The results of the present investigation will serve as an industry resource supporting dent assessment and management. The tools developed will increase safety by focusing attention on higher risk features, reduce unnecessary maintenance and support the improvement of pipeline standards and codes of practice.

3 Impact from the Research Results

This project directly contributes to the improvement of pipeline safety by enhancing standards and integrity management practice, ensuring that finite resources are focused on features/anomalies of the greatest significance and addresses gaps in the current knowledge base. The results of this research will be of use in improving integrity management decisions and will support further development of industry guides and standards. As such, the information presented in this paper will be of interest to pipeline operators, integrity management specialists, ILI organizations and regulators. The pipeline integrity management community and developers of integrity management tools and guides will benefit from the results generated in the current project. The results will feed into pipeline operating company traditional integrity management plans, guides, and standards including ASME B31, API RP 1183, US DOT regulations (49 CFR 192 / 195) and other best practices and guidance documents.

The long-term goal of this project is to facilitate and improve the effectiveness of pipeline operating companies' integrity management planning in compliance with 49 CFR 192.917 and 49 CFR 195.452, and enhancement of these regulations to further improve pipeline safety. This goal is achieved by enhancing industry standards such as API RP 1183, which will leverage the results of this project.

4 Improvement of Indentation Crack Formation Strain Estimates

Ductile damage in the form of cracking can be incurred during pipeline indentation. A method of assessing the level of damage incurred, is to estimate the indentation strain from dent shape measurements and comparing the calculated value against a defined "crack" formation strain. Various methodologies have been developed to predict the indentation strain, and of those, two are considered in this section – ASME B31.8 Effective Strain and "Blade Energy Partners Simplified Model" Effective Strain, also referred to as ASME strain and Blade strain. The accuracy of estimation of indentation strains by these models are assessed against strain data from validated finite element analysis of dented pipes. Improvements to the ASME B31.8 criteria are proposed based on the observations made from these assessments. Additionally, accuracy of prediction of indentation strains for unrestrained dent shapes under pressure is also addressed and solutions are proposed to resolve this issue.

4.1 Indentation Strain Estimation Models

4.1.1 ASME B31.8 - 2018 Dent Strain Estimation

ASME B31.8 – 2018 provides a means to estimate the strain in plain dents in pipes, using the dent deformation geometry data. The strain formulations are based on thin shell theory and are presented as bending and membrane component strains in the axial and circumferential directions. No formulation for circumferential membrane strain is offered. In addition to the directional strains, an effective or total strain formulation has also been provided. This measure is analogous to the Equivalent Plastic Strain (p) and provides a scalar metric for the evaluation of the triaxial strain magnitude. The strain formulations as provided in ASME B31.8 Appendix R (2018), are as follows [2],

$$\varepsilon_1 = \left(\frac{t}{2}\right)\left(\frac{1}{R_0} - \frac{1}{R_1}\right) \tag{4.1}$$

$$\varepsilon_2 = \left(\frac{t}{2}\right)\left(\frac{1}{R_2}\right) \tag{4.2}$$

$$\varepsilon_3 = \left(\frac{1}{2}\right)\left(\frac{d}{L}\right)^2 \tag{4.3}$$

$$\varepsilon_{eff} = \left(2/\sqrt{3}\right)\left[\,\varepsilon_1^2 + \varepsilon_1\left(\varepsilon_2 + \varepsilon_3\right) + \left(\varepsilon_2 + \varepsilon_3\right)^2\,\right]^{1/2} \tag{4.4}$$

Where, t is the pipe wall thickness, R_0 is the pipe nominal outer radius, R_1 is the radius of curvature of the circumferential dent profile at the dent apex, R_2 is the radius of curvature of the axial dent profile at the dent apex, d is the depth of the dent, L is the length of the dent, ε_1 is the

circumferential bending strain, ε_2 is the axial bending strain, ε_3 is the axial membrane strain and ε_{eff} is the effective strain. The sign convention adopted for the radii of curvature assigns a negative value to R_1 and R_2 for re-entrant dent profiles and positive for non-re-entrant cases [2]. The bending strains are assigned positive values for the inside diameter (ID) surface and negative value for the outside diameter (OD) surface, as the ID and OD surfaces are under tension and compression, respectively. The axial membrane strain is assumed to be always in tension [2].

4.1.2 Blade Energy Partners Simplified Model for Dent Strain Estimation

The "Blade Energy Partners Simplified Model" was assessed as an alternative to the ASME B31.8 strain measure [3]. It is a relatively simple model that only requires ILI caliper data to predict the deformed pipe wall (dent) strain. There are other advanced models available that require finite element (FE) tools in addition to the caliper data [5] [6]. The bending strain formulations are the same as that offered by ASME B31.8. The membrane strain formulations are based on evaluating the change in the length of an undeformed segment near the dent apex, brought upon by the rotation induced by bending. This can account for the membrane strain induced by rotation but not for the in-plane extension. For the axial membrane strain, a method for evaluating the in-line extension was used based on the work of Rosenfeld et al [7]. A formulation for circumferential membrane strain has been offered in this model and similar to that used for the axial membrane strain, the value is evaluated using the difference in deformed and undeformed length of a circumferential span at the dent apex. The membrane strain equation is as follows [3],

$$\varepsilon = (L_s - L_0) / L_0 \tag{4.5}$$

Where, L_S is the deformed length and L_0 is the undeformed length of a span near the dent apex. Since, the circumferential strain is also present, the effective strain formulation is as follows,

$$\varepsilon_{eff} = \left(2/\sqrt{3}\right)\left[(\varepsilon_1 + \varepsilon_4)^2 + (\varepsilon_1 + \varepsilon_4)(\varepsilon_2 + \varepsilon_3) + (\varepsilon_2 + \varepsilon_3)^2\right]^{1/2} \tag{4.6}$$

Where, ε_4 is the circumferential membrane strain, while the remaining variables are as described in Equation (4.1)(4.4).

4.2 Assessment of Indentation Strain Estimation Models

For the purpose of the comparison of ASME and Blade estimated strains with strains from finite element dent modeling, geometry and strain data were extracted from the validated BMT FE Dent Database. The database consists of hypothetical dents, as well as FE models of dent full-scale tests and in-service field dents. The hypothetical FE models employed for the present analysis consist of plain restrained and unrestrained dents. A matrix of hypothetical FE models used for this analysis, consisting of multiple pipe geometries, pipe grade, indenter geometries, indentation depth, pressures at indentation, maximum pressures experienced by pipe and pipe mean pressures, is presented in Table 1. A matrix for the full-scale dent test FE models is presented in Table 2 and a matrix of in-service field dent FE models is presented in Table 3. For more information regarding the full scale dent models used please refer to [8], [9] and [10]. The deformed geometry and FE strain data were extracted at indentation and at various operating mean pressures listed in the tables, and the ASME and Blade strains were calculated for both cases.

Table 1- Matrix of Hypothetical Dent FE Models

Parameter	Values
Pipe Outer Diameter/Wall Thickness (in)	4.5/0.188, 6.625/0.188, 8.625/0.218, 10.75/0.188, 12.75/0.312, 16/0.218, 18/0.312, 24/0.25, 24/0.281, 30/0.25, 32/0.281, 36/0.281, 42/0.42
Pipe Grade	X42, X52, X70
Indenter Shapes	4 inch Spherical, 12, 24, 30, 48 inch Elliptical 2:1, 12, 24, 30, 48 inch Elliptical 6:1, 4, 8-inch Transverse Cylinder
Indentation Depth (% OD)	Restrained - 0.5, 1.5, 2.5, 4, 5, 6, 7, 8, 9, 10 Unrestrained – 5, 10
Indentation Pressure (%PSMYS)	0, 20, 40, 60, 90
Maximum Pressure (%PSMYS)	20, 30, 40, 50, 60, 70, 80, 90
Mean Pressure (%PSMYS)	15, 20, 25, 30, 35, 40, 45, 50, 55, 60, 65, 70, 75

Table 2- Matrix of Full-Scale Test FE Models

Parameter	Values
Pipe Outer Diameter/Wall Thickness (in)	18/0.312, 20/0.281, 24/0.311, 24/0.35, 24/0.375
Pipe Grade	X52, X70 of various vintages
Indenter Shapes	2, 4, 8, 12, 24, 48-inch Semi-Elliptical, Transverse Long Bar, 45o Long Bar, Axial Short Bar
Indentation Depth (% OD)	1 – 20 % OD
Indentation Pressure (%PSMYS)	0, 15, 30, 40, 80
Maximum Pressure (%PSMYS)	60, 70, 80, 90, 100
Mean Pressure (%PSMYS)	30, 40

Table 3- Matrix of Field Dent FE Models

Parameter	Values
Pipe Outer Diameter/Wall Thickness (in)	4.5/0.125, 8.625/0.188, 8.625/0.203, 12.75/0.25, 16/0.25, 24/0.281, 24/0.375, 30/0.25, 36/0.53, 36/0.625, 42/0.42, 42/0.448
Pipe Grade	Grade A, Grade B, X42, X52, X70
Indentation Depth (% OD)	0.5 - 14 % OD

The deformed geometry data from the dented pipe models was used to evaluate the ASME and Blade strain estimates. The computation of the strain estimates required the extraction of the axial and circumferential pipe profile passing through the dent apex. The geometry data points had been sampled from the FE models at an interval of 4 mm, on average, in the axial direction and at an interval of two degrees in the circumferential direction. Due to the discretized nature of the geometry data points, polynomial curve fitting was required to generate continuous profiles. The fitting was confined to the vicinity of the dent apex as the curvature at that region was required. For the axial profile a span of 11 points was used, and for the circumferential profile, a span of four points was taken, with the dent apex at the center of the span for both cases. For the circumferential

profile, the data points had been mapped into the polar coordinate system and the curve fitting was performed in the parametric system. The curvature of the circumferential profile was evaluated accounting for the polar coordinate parameterization. For both axial and circumferential profiles, 4th degree polynomials were used to evaluate the curvatures. For the evaluation of the ASME axial membrane strain, the dent axial length and depth, as described in Equation (4.3), needed to be extracted. No guidance is provided on how the depth and length are to be extracted in ASME B31.8 [2]. The process adopted to extract these values is described in section 4.4.1. For the Blade axial and circumferential membrane strain evaluation, slope and curvature values calculated from the fitted curves were used in the arc length formulation to calculate the deformed length. The entire process of geometry data extraction, curve fitting, curvature and strain evaluation was performed using MATLAB®. The curve fitting was accomplished using the *lsqnonlin* MATLAB® function, which is a nonlinear least squared regression tool [11]. Once the curvatures, dent depth, dent length and deformed span lengths were established, Equations (4.1) to (4.6) were used to evaluate the ASME and Blade effective strains on the ID and OD surfaces. The maximum of the effective strains on the ID and OD surfaces was assigned as the final ASME and Blade effective strains of the dent. Sample calculations for evaluating ASME and Blade strains have been presented in Appendix A.

The FE dent models in the BMT database were developed using ANSYS® Mechanical (version 17 and 19) commercial software [12]. These models were assigned nonlinear material properties and the solver was made to account for large deformations and strains. A calibrated Chaboche nonlinear kinematic hardening model was used to define plastic deformation. Eight node quadratic curved shell elements (SHELL281) were used to mesh the pipe geometry. The region of indenter contact required for refined mesh (2 to 4 mm depending on indenter size), while away from the contact region, the mesh smoothly transitioned into coarser mesh. Indenters were assumed to be rigid and were meshed with ANSYS Target 170 rigid elements. Contact elements on the pipe were generated using ANSYS 3D 8-node SURF 174 contact elements. A rigid/deformable general surface to surface contact option was used to model the contact between the pipe and the indenter.

During the analysis, for a particular case from the FE model matrix, the loading process followed the following steps:

1. The pipe was pressurized to an indentation pressure (refer to Table 1).
2. The indenter was made to travel to a specific indentation depth and was held there for restrained and removed for unrestrained dents (refer to Table 1). The indentation geometry and strain data were extracted after indentation was completed, with the indenter in place.
3. A maximum pressure was applied (refer to Table 1).
4. Then different mean pressures, equal to or less than the maximum pressure, were applied. The deformation and strain data were extracted after the dent experienced maximum pressure and the various mean pressures.

The stress-strain values were extracted at the centroid of the shell elements on the inner diameter (ID) and outer diameter (OD) surfaces, in the element coordinate system. Four components were extracted – circumferential, axial, radial and in-plane shear. The strain values associated with the shell element at the dent apex were extracted. The deviatoric components of the strain tensor were calculated for these strain values, Equation (4.7). The deviatoric components were used to evaluate

the Effective Strain, analogous to the Equivalent Plastic Strain, Equation (4.8). The equations for deviatoric strain tensor and effective strain tensor are as follows [13]:

$$dev(\varepsilon_{ij}) = \varepsilon_{ij} - \frac{1}{3}\, trace(\varepsilon_{ij})\delta_{ij} \tag{4.7}$$

$$\varepsilon_{eff} = \sqrt{\frac{2}{3}\, dev(\varepsilon_{ij})\, dev(\varepsilon_{ij})} \tag{4.8}$$

The maximum of the effective strains of the ID and OD surfaces was taken as the final FE effective strain for the dent. This value was compared with the corresponding ASME and Blade effective dent strains.

For the purpose of comparison, 4600 hypothetical dents, 60 FE models of dent full-scale tests and 100 FE models of field dents, were used to derive strains at indentation and at various operating mean pressures.

4.2.1 Use of the Strain Formulation with Regards to Dent Restraint Condition

The strain formulations presented in sections 4.1.1 and 4.1.2 are intended to be used for measuring indentation strains. Sections 4.2.2 and 4.2.3 compare the effective strains from these prediction models (evaluated using the FE geometry of dent during indentation), against the FE strains during indentation. Therefore, the procedure followed in these sections are indifferent to the restraint conditions as only the data during the indentation is used. In practical applications, ILI data must be used for measuring strain but the dent shape at ILI measurement depends on the restraint condition of the dent. If the indenter is in place, then the ILI shape reflects the shape at indentation, hence, the strains estimated for restrained dents are essentially the indentation strains. This is not the case if the indenter is removed after indentation. In this case, the shape of the unrestrained dent does not reflect the shape (or strains) at indentation. Hence, the shapes measured during ILI run of the unrestrained dents cannot be used to estimate the strains at indentation. This is further elaborated in section 4.3.

Improvements to the ASME strain model have been proposed in section 4.4. These include general improvements to the formulation to better predict the strains using the dent shape at indentation (restrained dent shape). The strains predicted (using FE shapes at indentation) by the improved model are compared with the FE strains at indentation, in section 4.4.3. Additionally, a prediction model has been proposed that can estimate the strain at indentation using the ILI measured shape of unrestrained dents. Equations for predicting ASME and improved ASME strain at indentation for unrestrained dents are presented in section 4.4.4.

4.2.2 Comparison of Indentation ASME Effective Strains against FE Equivalent Strains

The ASME strain values were calculated from the deformed FE geometry at indentation and these values were compared with FE equivalent strains extracted from the dent peak. The collated data showed good agreement, with 76% of hypothetical, 82% of full-scale and 79% of field dent data falling within a 20% error band (Figure 1). The percentage of ASME axial bending strain

predictions within the 20% error bands were, 87% for hypothetical, 75% for full-scale and 68% for field dent data, respectively. The percentage of ASME circumferential bending strain predictions within the 20% error bands were, 70% for hypothetical, 55% for full-scale and 66% for field dent data, respectively. The predictions of the ASME axial membrane strains, compared to the FE axial membrane strains, were generally poor. The ASME axial membrane strain predictions were orders of magnitude lower than the FE values. Regardless of the inaccuracy of ASME axial membrane strain predictions, the ASME effective strain predictions demonstrated good agreement with FE, due to the fact that on average, the FE axial membrane strains were an order of magnitude lower than the FE bending strains. Due to the dominance of bending strains at the dent peak, the effect of the inaccuracy of the axial membrane strain predictions on the ASME effective strain predictions, were reduced.

From Figure 1(c) it can be inferred that for several data points the ASME strains, significantly diverge from the corresponding FE values. These data points belong to deep (>= 6% OD) and sharp (radii of curvature of dent peak between -200 mm to 0 mm) hypothetical dents, subjected to high indentation pressures (>= 60% PSMYS). Deep indentation, at high pressures, produce significant plastic damage in the form of high axial and circumferential membrane strains, at the dent apex. As mentioned earlier, the ASME axial membrane strain formulation underpredicted the axial membrane strain and additionally, there is no formulation to predict circumferential membrane strain in ASME B31.8 Appendix R. This results in the ASME effective strains underpredicting when compared to the FE equivalent strains in these cases. This is especially evident in hypothetical dents formed by the “4-inch Spherical” indenter. Due to the small size of the indenter and the depth of indentation, the profiles that were formed possessed sharp curvatures at the dent peak, which resulted in large membrane strain. The effect of indentation depth and indentation pressure on the accuracy of ASME effective strain can be observed in Figure 2, which presents the unity plot of FE equivalent strain and ASME effective strain, at indentation, for the dents formed by “4-inch Spherical” indenter. It can be observed that for these sharp dents, the increase in indentation depth and indentation pressure leads to greater divergence of ASME strain from the FE values, which is due to the inability of ASME strain to properly account for high membrane strains. The unity plot of ASME versus FE strains without these deep and sharp dents, formed at high indentation pressure is presented in Figure 3. It can be observed that the predicted ASME strain values are in good agreement with FE strains. Additional plots comparing various ASME and FE strains can be found in Appendix B.

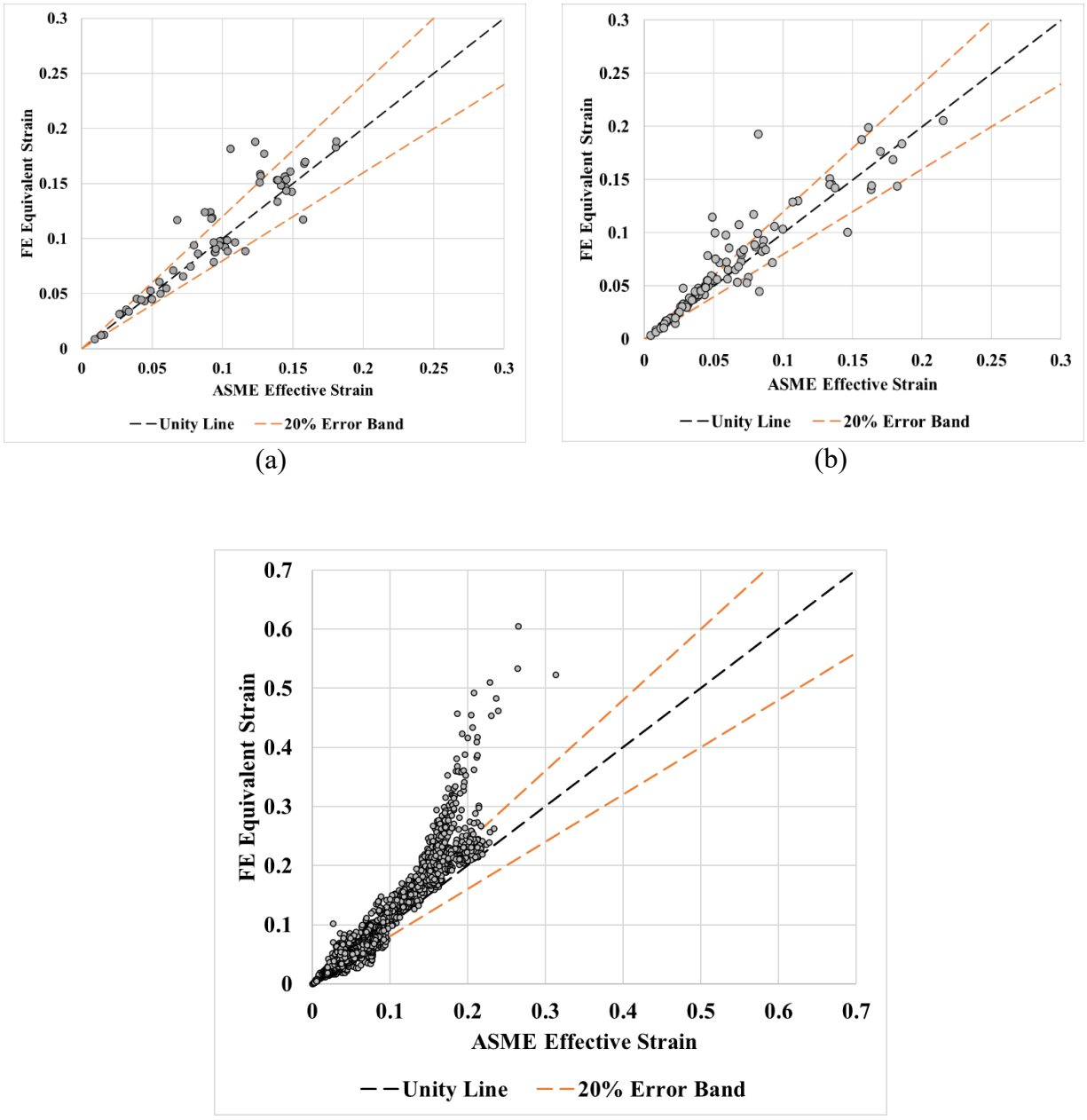

Figure 1- Unity Plots of ASME Effective Strain vs FE Equivalent Strain

Calculated using FE models from (a) Full-Scale (b) Field Dents (c) Hypothetical Dents

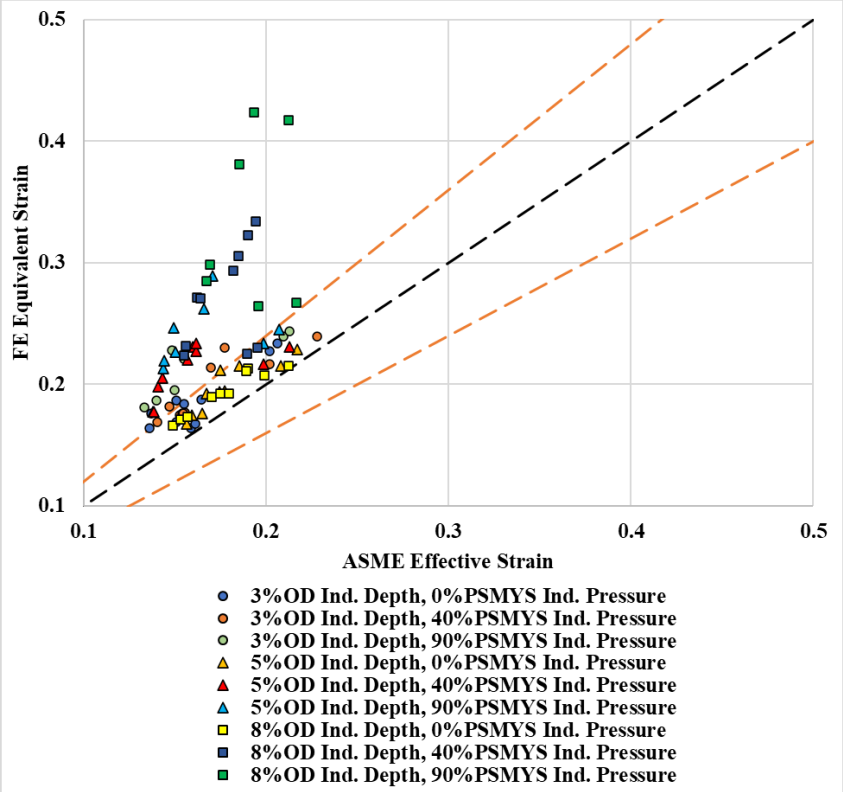

Figure 2- Unity Plot of FE Equivalent Strain vs ASME Effective Strain for Hypothetical Sharp Dents Formed by "4 inch Spherical" Indenter (- 200 to 0 mm radius of curvature).

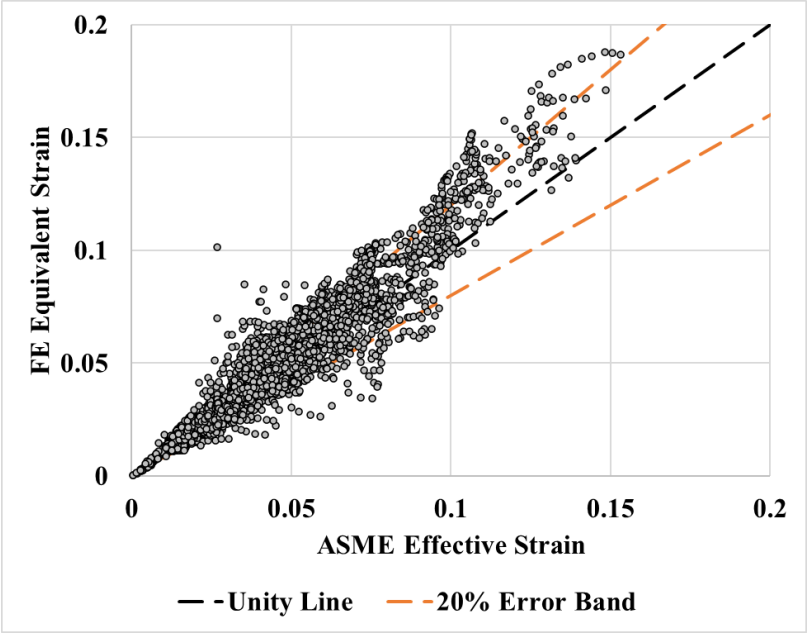

Figure 3- Unity Plot of FE Equivalent Strain vs ASME Effective Strain for Hypothetical Dents Without the deep and sharp dents.

From the analysis of the data, it can be inferred that deep dents (>= 6% OD) with low circumferential or axial radius of curvature, within the following range, -200 mm to 0 mm (following convention set in ASME B31.8 Appendix R), formed under high indentation pressure (>= 60% PSMYS), are subjected to high membrane strains that render the ASME effective strain predictions lower than the FE equivalent strain. Plots comparing the FE axial membrane and bending strain distribution near the dent peak, for two deep and sharp dents formed at high indentation pressure, are shown in Figure 4. For the case in Figure 4(a), the circumferential and axial curvatures were -24.7 mm and -35.3 mm, respectively. For the case in Figure 4(b), the circumferential and axial curvatures were -172.3 mm and -346.9 mm, respectively. It can be observed that the membrane strains are in the same order of magnitude as the bending strains, hence, accurate prediction of membrane strains is crucial for these cases.

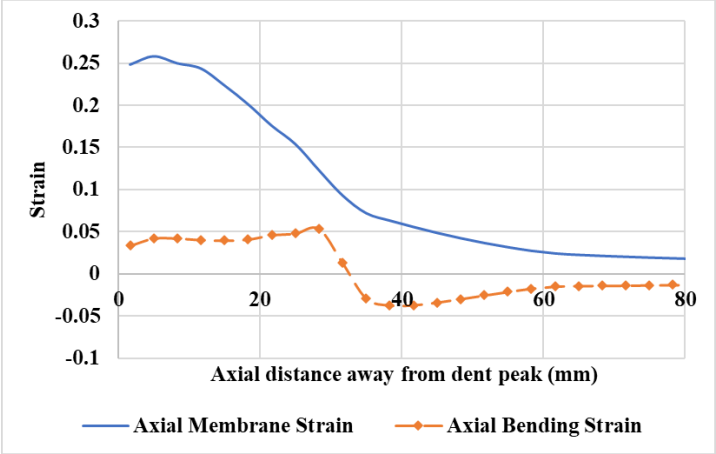

(a)

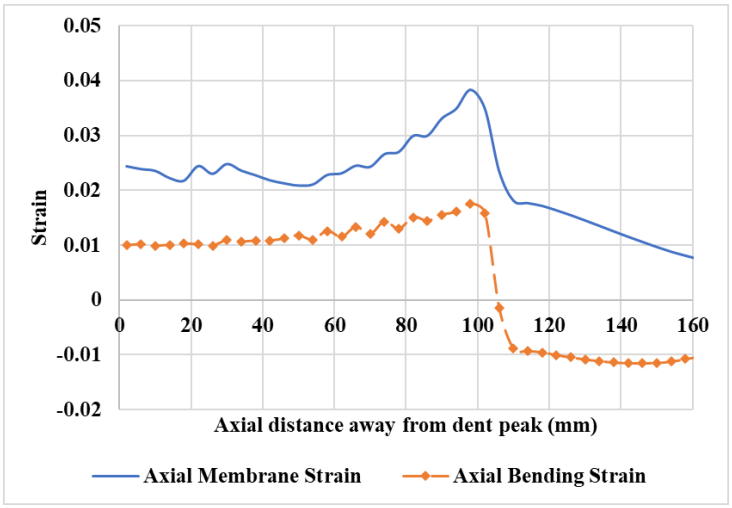

(b)

Figure 4- Axial Distribution of FE Axial Membrane and Bending Strains

For (a) OD 30 in, WT 0.25 in, X52, "4-inch Spherical" Indenter, 10% OD Depth, 90% PSMYS Indentation Pressure
(b) OD 30 in, WT 0.25 in, X52, "12-inch Elliptical 2:1" Indenter, 10% OD Depth, 90% PSMYS Indentation Pressure

4.2.3 Comparison of Indentation Blade Effective Strains against FE Equivalent Strains

"Blade Energy Partners Simplified Model" utilizes the same bending strains as the ASME B31.8 Appendix R formulation. The difference is in the formulation of the membrane strains. Comparison of the Blade effective strains against the FE equivalent strains showed good agreement, with 86% of hypothetical, 83% of full-scale and 77% of field dent data falling within 20% error band (Figure 5). Furthermore, the accuracy of effective strain estimates for deep and sharp dents is significantly improved over the ASME estimates (Figure 6). This can be attributed to the presence of a circumferential membrane strain formulation and the improvement in prediction of axial membrane strain. Although the accuracy of the membrane strain estimates when compared against the FE values is low (90% of data outside 20% error band), the improvement in prediction of these values over the ASME formulation allows for a better estimation of the effective strains (Figure 7).

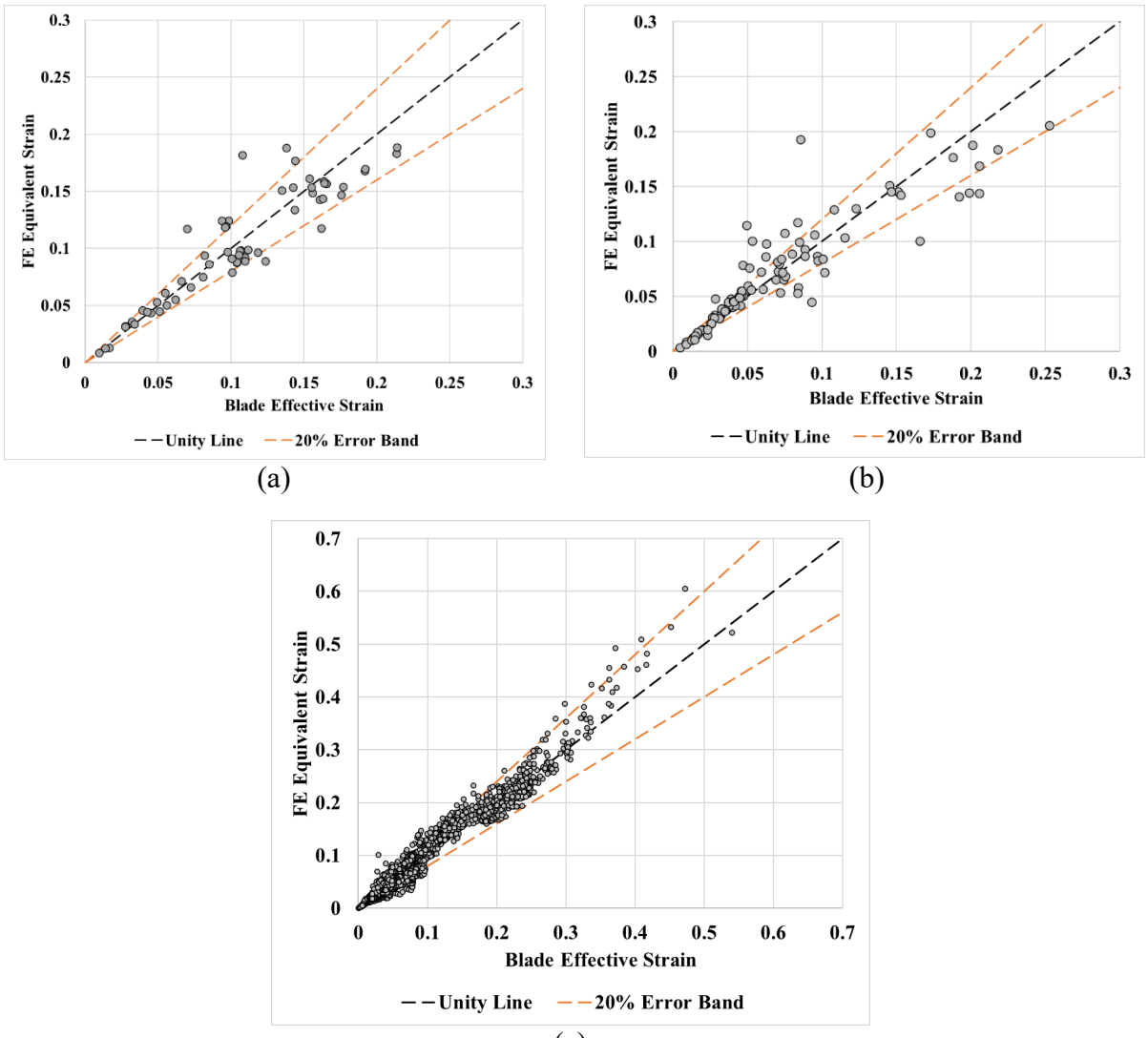

Figure 5- Unity plots of Blade Effective Strain vs FE Equivalent Strain

Calculated using FE models from (a) Full-Scale (b) Field Dents (c) Hypothetical Dents

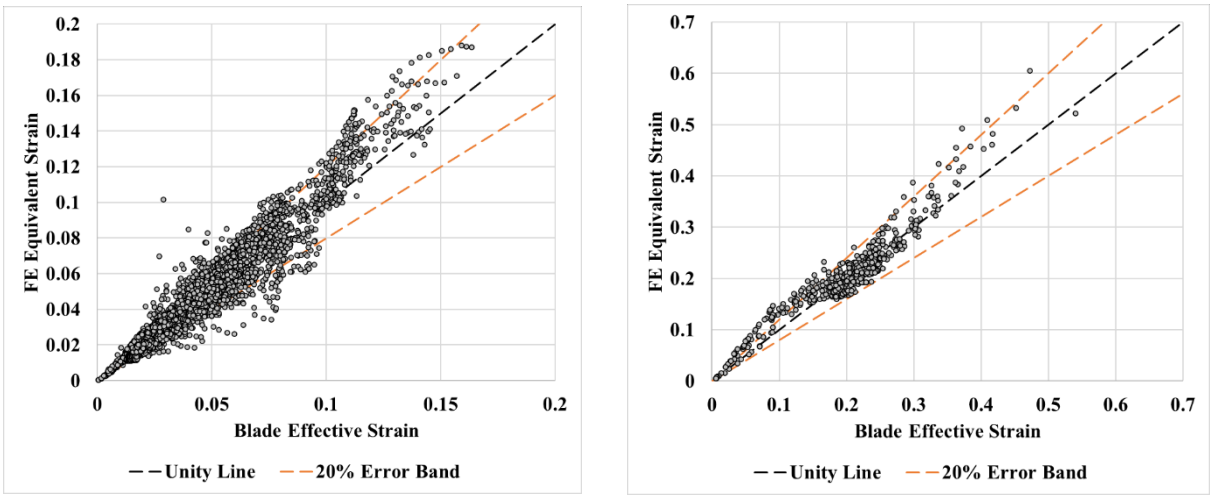

Figure 6- Unity Plot of FE Equivalent Strain vs Blade Effective Strain for Hypothetical Dents

(a) Without the Deep and Sharp Dents (b) Only Deep and Sharp Dents

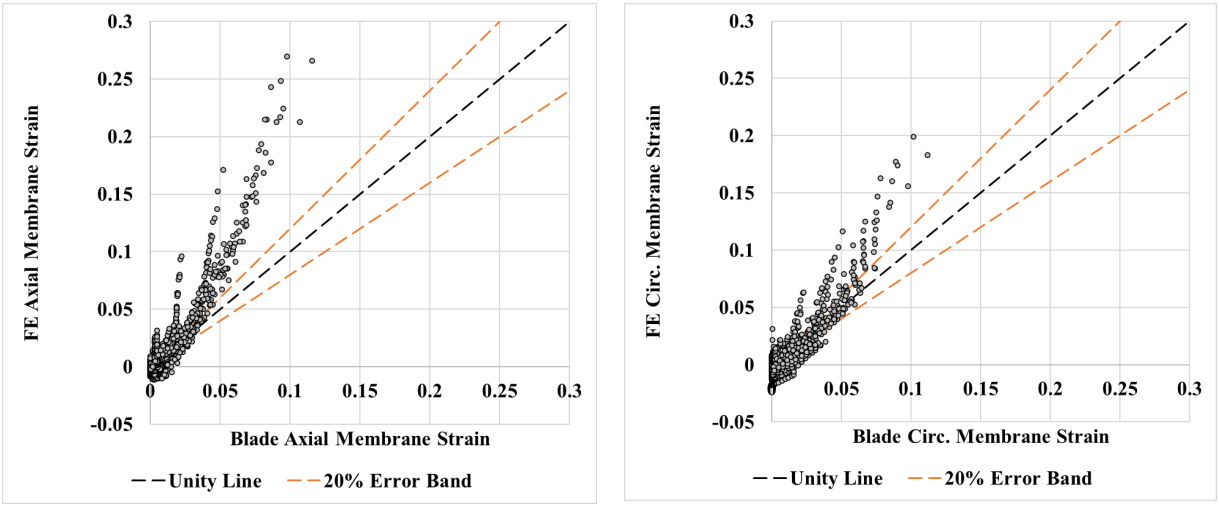

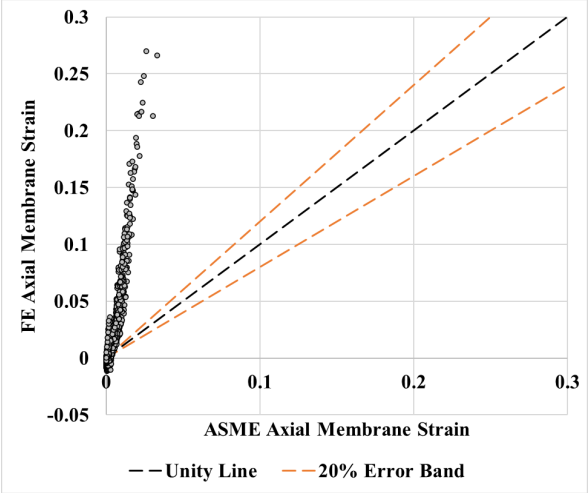

(c)

Figure 7- Unity plot of FE Membrane Strain vs (a) Blade Axial Membrane Strain (b) Blade Circumferential Membrane Strain (c) ASME Axial Membrane Strain, for Hypothetical Dents

4.3 Prediction of Indentation Strain for Unrestrained Dents

The strain estimates discussed in the previous sections have been developed to infer the damage incurred during indentation based on the detailed dent shapes from the FE models. In practice, the dent shapes that are used to estimate the indentation strains are measured at pressure during ILI runs. If the dent is restrained after indentation, then the shape at pressure does not differ significantly from the indentation shape. This is not the case for unrestrained dents, which experience significant re-rounding after the indenter removal and application of pressure. This can be observed in the examples shown in Figure 8. These unrestrained dents experience significant re-rounding with an almost 80% reduction in depth in one case. Along with the reduction in depth, the dent peak curvatures can also be altered. Since the shapes after re-rounding can differ considerably, from the indentation shape, the strain estimate based on the shape at pressure should differ from the indentation strain when indenter is still in contact. This can be observed in Figure 9, where ASME and Blade strain estimates for unrestrained dent shapes at pressure are compared with the estimates evaluated using the shapes at indentation. For both estimates, the strains evaluated from the unrestrained dent shapes at pressure are significantly underpredicted when compared to values evaluated from dent shapes at indentation. Therefore, for unrestrained dents, the strain estimates evaluated for a dent after indenter removal and at pressure should not be used as a measure of indentation strain. For restrained dents, the relatively fixed shape after indentation due to the indenter still in contact permits the use of shape at pressure to estimate indentation strains. It can be observed in Figure 10, that the strain estimates for restrained dents evaluated from shapes at pressure and indentation have good agreement and the majority of the data points are clustered about the unity line.

All the unrestrained dents shown in Figure 9 have experienced a maximum pressure of 90% PSMYS, and their strains are presented at different mean operating pressures. Since the dents have been subjected to a high pressure beforehand, the dent shape and strains have stabilized, and dent strains do not vary if measured subsequently at lower pressures. The dependence of the shape and strains of unrestrained dents on maximum pressure (e.g., hydro test) can be observed in Figure 11.

In this case, the dents have not seen prior higher pressures and the dent shape and resulting strains are dependent on the pressure at which the dent shapes are being measured. There is significant difference in dent strains when measured at different pressures.

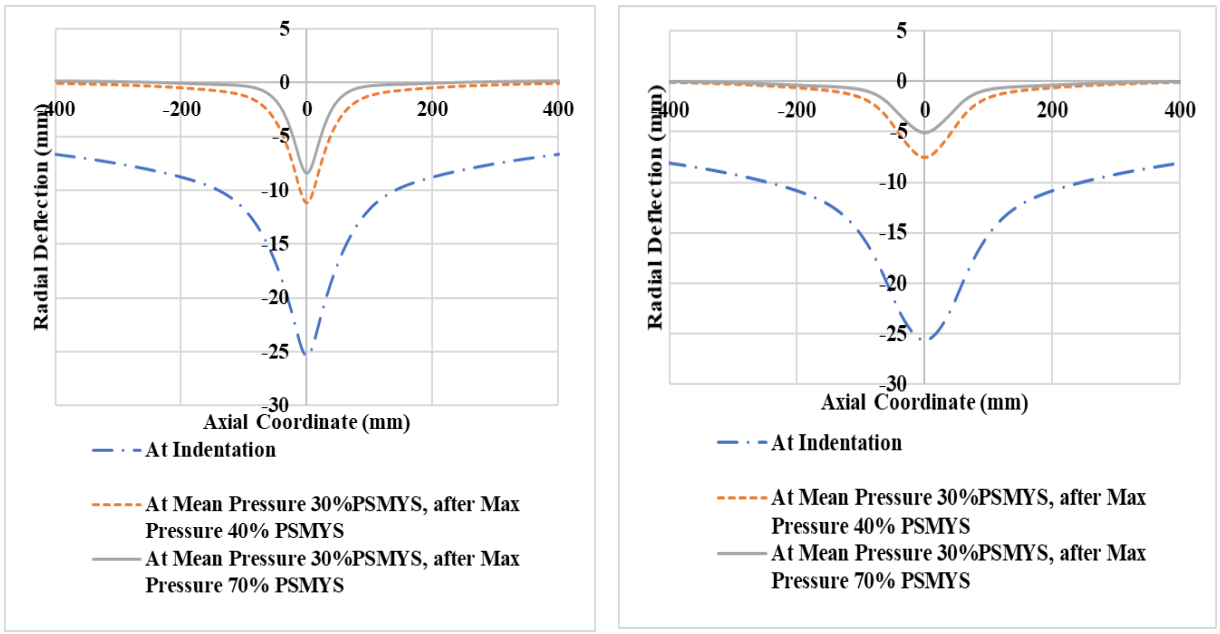

Figure 8- Axial Profiles at Indentation and After Re-Rounding

Dents created on OD 24 in, WT 0.25 in, Grade X52 pipes under the following conditions (a) “4 inch Spherical” Indenter, 5% OD Indentation Depth (b) “12 inch Elliptical 2:1” Indenter, 5% OD Indentation Depth, 0% PSMYS Indentation Pressure

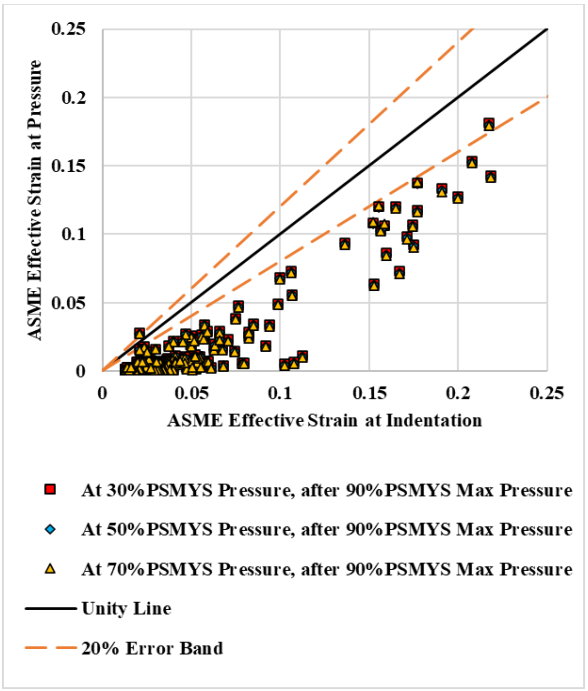

(a)

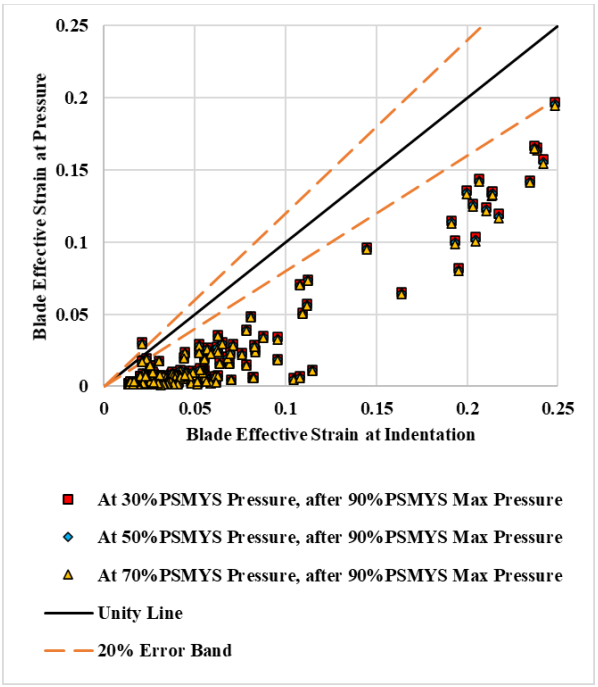

(b)

Figure 9- Comparison of Strain Estimates Evaluated from Hypothetical Unrestrained Dent Shapes at Pressure and Indentation

(a) ASME Effective Strain (b) Blade Effective Strain

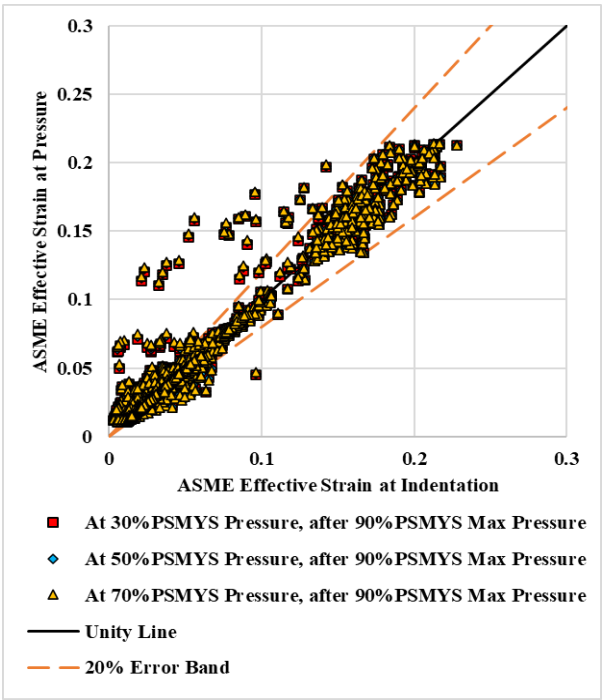

(a)

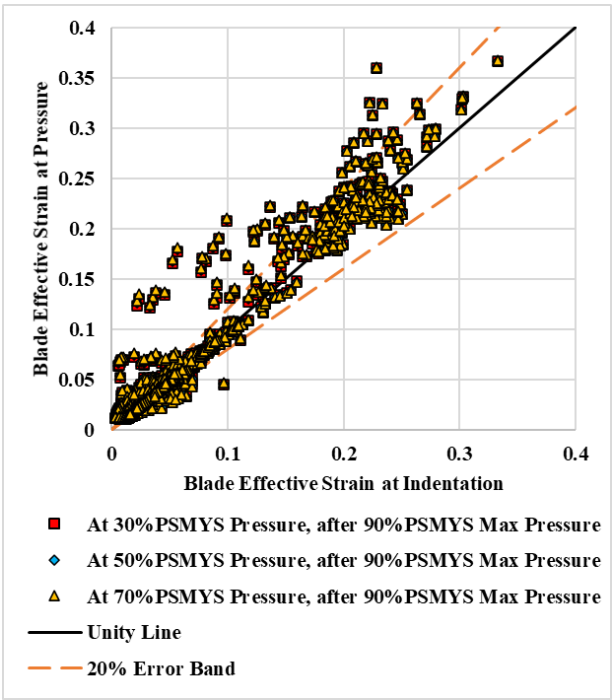

(b)

Figure 10- Comparison of Strain Estimates Evaluated from Hypothetical Restrained Dent Shapes at Pressure and Indentation (a) ASME Effective Strain (b) Blade Effective Strain

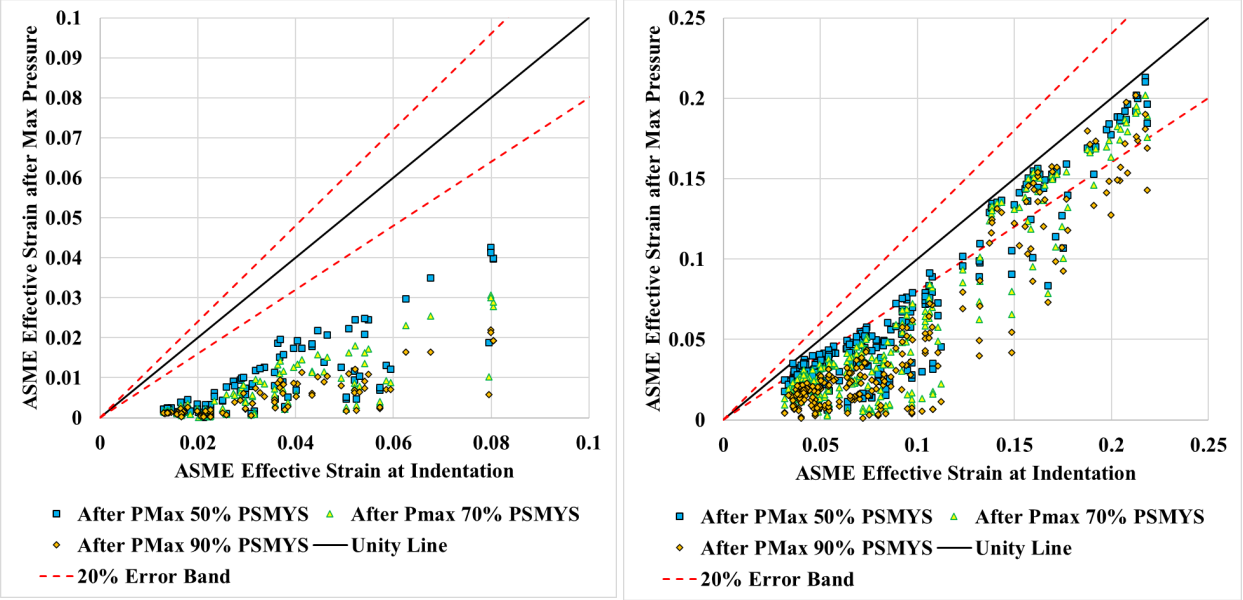

Figure 11- Comparison of ASME Strains at Indentation vs ASME Strains of Unrestrained Dents After Experiencing Various Maximum Pressures

(a) Smoother Dents (b) Sharper Dents

4.4 Improvements to the ASME B31.8 Effective Strain Model

Improvements to the ASME B31.8 strain prediction model have been proposed in this section. From the assessments made in the previous sections, the major shortcomings of the model were regarding the prediction of the membrane strains and the inability of the model to predict the indentation strains for unrestrained dents measured under pressure. The latter issue can be addressed using the information presented in the previous section. The former issue can be solved within the framework of the current model using the modification proposed in the following sections. The "Blade Energy Partners Simplified Model" can be adopted to improve the prediction of membrane strains. The modifications presented here follow the current ASME B31.8 framework and have performance comparable to Blade strain model.

4.4.1 Modification of the ASME Axial Membrane Strain Formulation

As discussed in Section 4.2, it was observed that the ASME axial membrane strain formulation is significantly underpredicted when compared to corresponding FE values. This can be attributed to two factors. Firstly, the inappropriate references used to extract the depth and length values and secondly, the constant value (1/2) used in the formulation. The first factor can significantly contribute to the underprediction of strain, due to inappropriate depth and length definitions in Equation (4.3). Excessively long length values can reduce the membrane strain prediction. This can lead to overestimation of the length values and underprediction of the strains. Various references were investigated along the dent profile at various depths. It was observed that references closer to the dent peak yielded better results and taking the 85% dent depth (as per API RP 1183 [1]) as the reference, was found to be suitable (Figure 12).

ASME membrane strain formulation is based on a triangular approximation of the deformed dent feature [5]. The membrane strain is assumed to be the ratio of change in length of the deformed section to the length of the undeformed section. As can be observed in Figure 13, the arc length of the deformed section (L_S) can be approximated using the lengths of the hypotenuse of the triangles. Then the membrane strain can be presented as follows:

$$\varepsilon = \frac{L_S - L}{L} = \frac{2\sqrt{d^2 + \left({}^{L}/_{2}\right)^2} - L}{L} = \sqrt{4\left({}^{d}/_{L}\right)^2 + 1} - 1$$

$$\varepsilon + 1 = \sqrt{4\left({}^{d}/_{L}\right)^2 + 1}$$

Squaring both sides and assuming that $\varepsilon \ll 1$ ($\varepsilon^2 \to 0$), we get the following:

$$2\varepsilon + 1 = 4\left({}^{d}/_{L}\right)^2 + 1$$

$$\varepsilon_3 = 2\left({}^{d}/_{L}\right)^2 \tag{4.9}$$

Where, d and L are reference depth and length at 85% dent depth, as defined in Figure 13. This modification to the ASME membrane strain formulation predicts strains four times higher than the original formulation. This modification has also been suggested in Reference [5]. Adopting two instead of one-half as the constant in the formulation, contributes to remedying the underprediction of the original formulation.

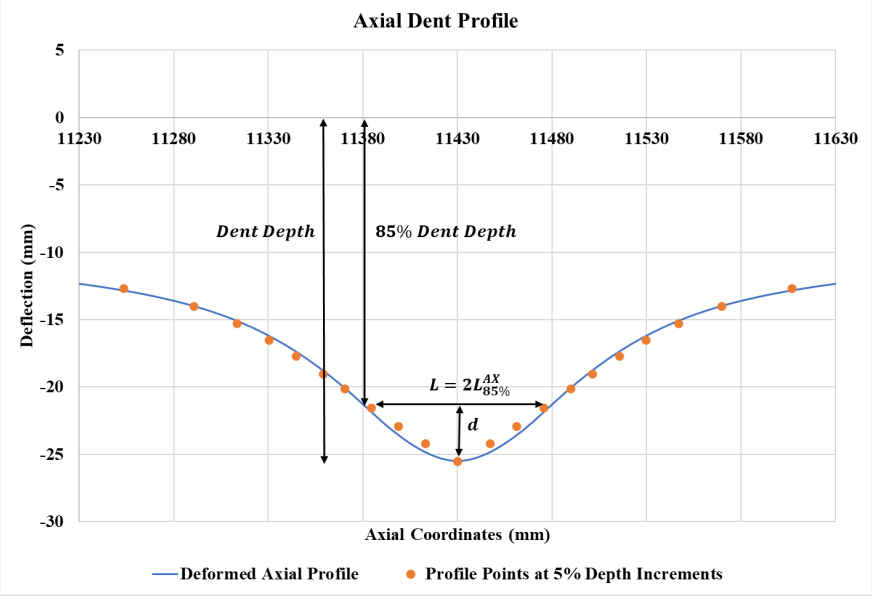

Figure 12- Alternate Reference for Evaluating ASME Axial Membrane Strain

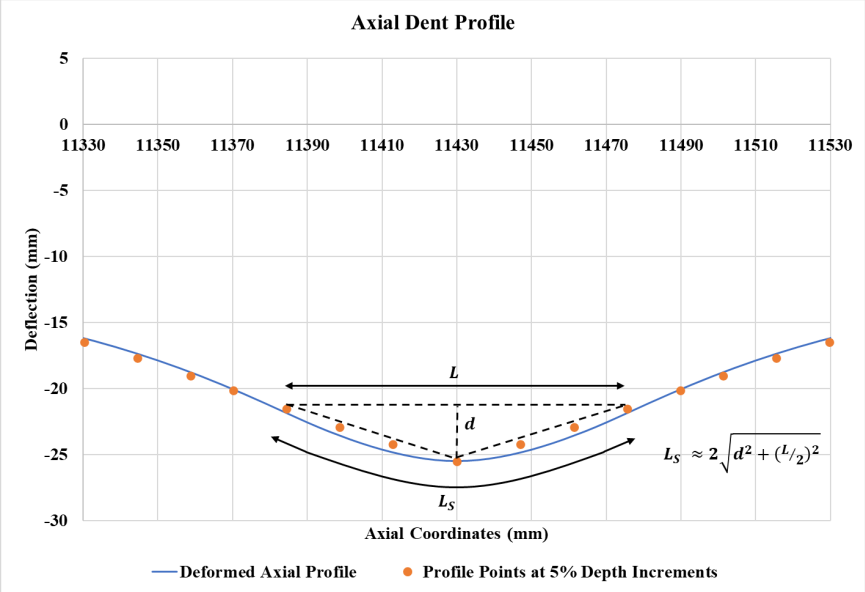

Figure 13- Approximation of Deformed Section Length using Right Triangles

4.4.2 Circumferential Membrane Strain Formulation

In addition to the modification to the axial membrane strain formulation, a circumferential membrane strain formulation is proposed here in a framework similar to that of the axial membrane strain. The formulation is based on predicting the membrane strain by comparing the deformed and undeformed lengths about the dent peak, using linear distance approximation to evaluate the arc lengths. The first step requires extracting a circumferential deformed span about the dent peak, as shown in Figure 14. The radial distance of the peak is represented by r_p, and the radial distance of an end of the span as r and the angular distance of that end away from the peak as θ. The undeformed and deformed spans have been illustrated in Figure 15. It can be observed that the deformed curve and undeformed curve configurations have been approximated using the linear distance approximation between the center and the ends of the spans. The approximate L_S and L_0 lengths are evaluated for the clockwise (CW) and counterclockwise (CCW) spans and the total deformed and undeformed lengths are used in the strain formulation to predict the circumferential membrane strain. The equations required to calculate the strain are as follows,

$$L_S = \sqrt{r^2 + {r_p}^2 - 2\, r\, r_p \cos\theta} \qquad L_0 = r\sqrt{2(1 - \cos\theta)}$$
$$L_{def} = L_S\, cw + L_S\, ccw \qquad L_{undef} = L_0\, cw + L_0\, ccw \qquad (4.10)$$
$$\varepsilon_4 = \left(L_{def} - L_{undef}\right) / L_{undef}$$

Where, L_S and L_0 are the deformed and undeformed lengths, respectively. These values have to be evaluated for both clockwise and counter-clockwise directions and then summed to get the total deformed (L_{def}) and undeformed (L_{undef}) lengths. These values are then used to evaluate the circumferential membrane strain estimate, ε_4.

As in the case of axial membrane strain, the judicious selection of the span about the peak is required for better approximation of the strain. For the assessment of the modified model, the points

on the circumferential profile associated with 85% dent depth (as per API RP 1183) were taken as the ends of the span about the dent peak, as seen in Figure 16. The radial distance of the peak and the span ends were extracted. The angular distance of a span end from the peak can be given by $\theta = L_{85\%}^{TR}/R$, where, $L_{85\%}^{TR}$ is the transverse length associated with 85% dent depth and R is the nominal pipe radius. Using, these points as a reference resulted in, on average, an end-to-end span of 12 degrees ($\theta \approx 6°$, CW and CCW of the peak). Extracting excessively long span can invalidate the linear distance approximation used for the formulation.

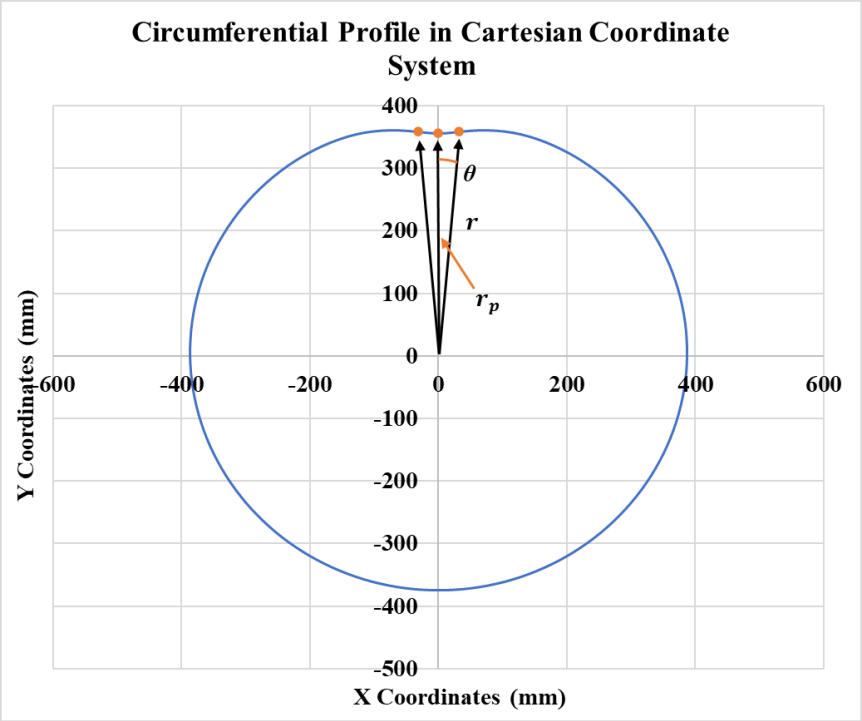

Figure 14- Deformed Circumferential Profile and Extracted Span for Membrane Strain Calculation

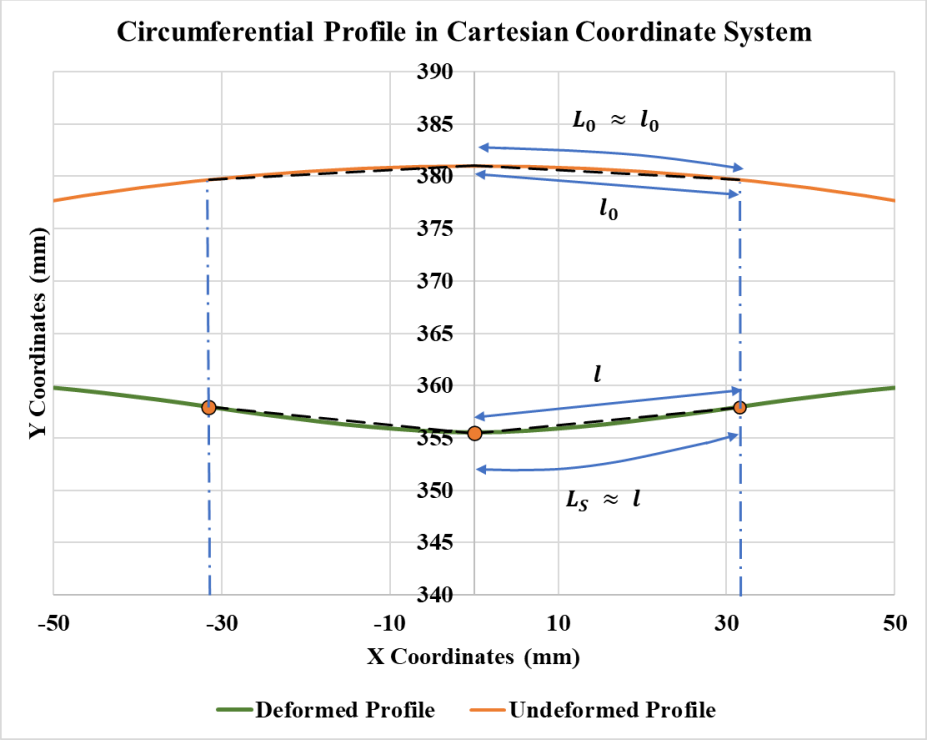

Figure 15- Undeformed and Deformed Spans Used for Estimating the Circumferential Membrane Strain

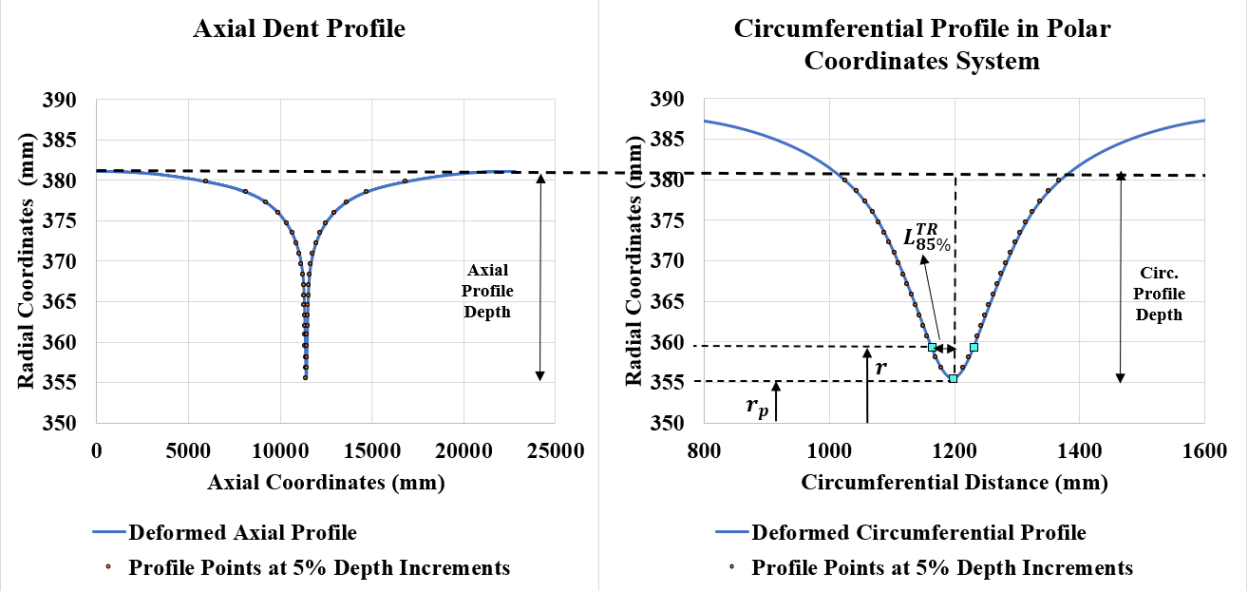

Figure 16- Defining the Ends of the Circumferential Span About the Dent Peak Based on 85% Dent Depth

4.4.3 Assessment of BMT Modified ASME Model Indentation Strain Prediction

An assessment of the accuracy of prediction of effective strain for the modified strain formulation was carried out following the same procedure adopted for the ASME B31.8 strain and Blade strain assessments. For the calculation of the bending strains, Equations (4.1) and (4.2) were used while the membrane strain evaluations were based on Equations (4.9) and (4.10). Since a circumferential formulation has been adopted, the effective strain was evaluated using Equation (4.6). The comparison between the modified ASME effective strain calculated from the FE indentation strains and FE equivalent strains produced good agreement, with 82% of hypothetical, 80% full-scale and 75% field dent data falling within 20% error band. The unity plots comparing the values are given in Figure 17. This model was able to correct for the inability of the ASME strain model to accurately predict the effective strain for deep and sharp dents formed at high indentation pressures (Figure 18). Additionally, the unity plots of the predicted membrane strains against the FE membrane strains have been given in (Figure 19). As in the case of Blade membrane strains, the predictions accuracy compared to FE strains is low, but is much improved over the original ASME formulation and this allows for better overall approximation of the effective strains.

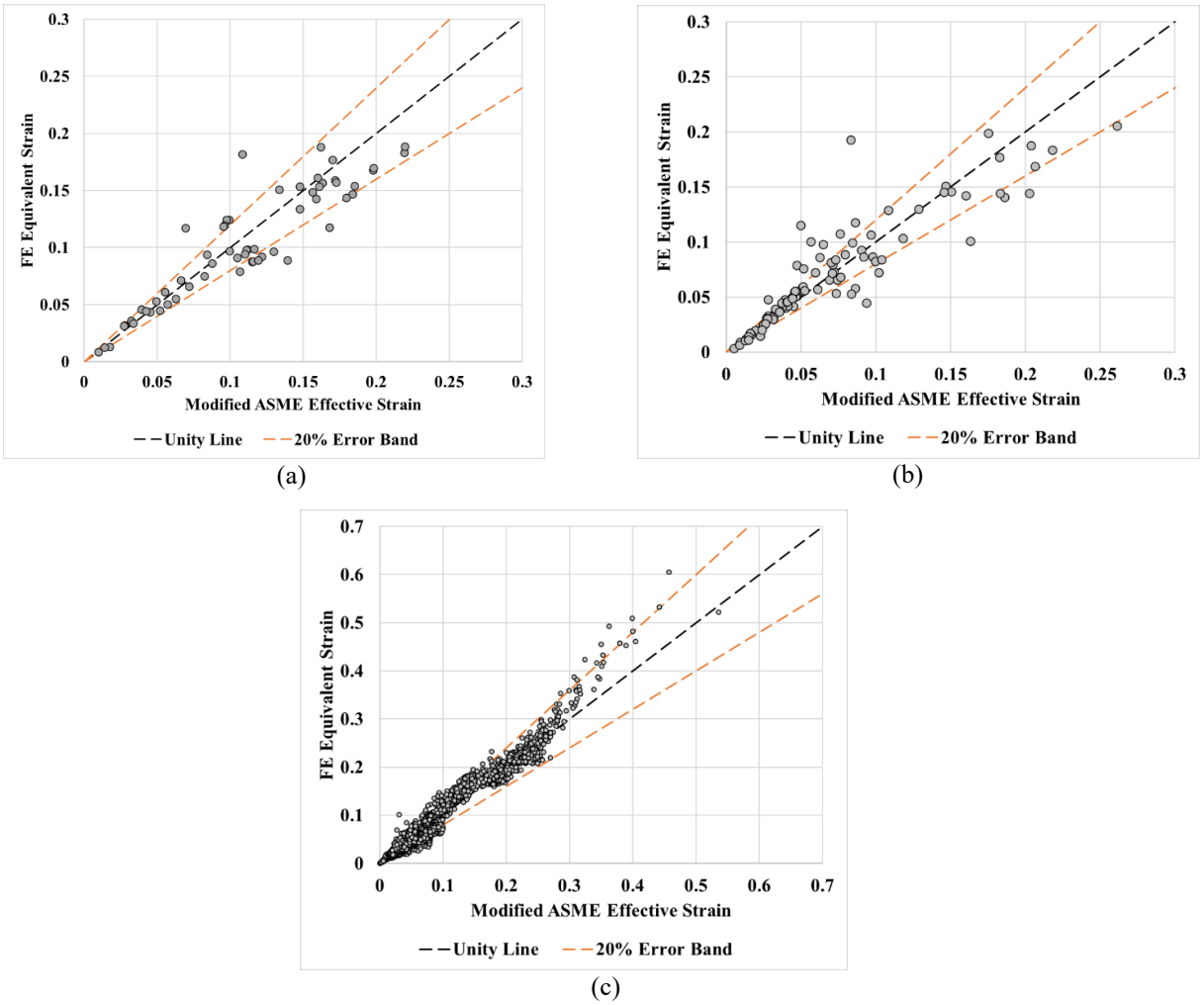

Figure 17- Unity plots of Modified ASME Effective Strain vs FE Equivalent Strain

Calculated using FE models from (a) Full-Scale (b) Field Dents (c) Hypothetical Dents

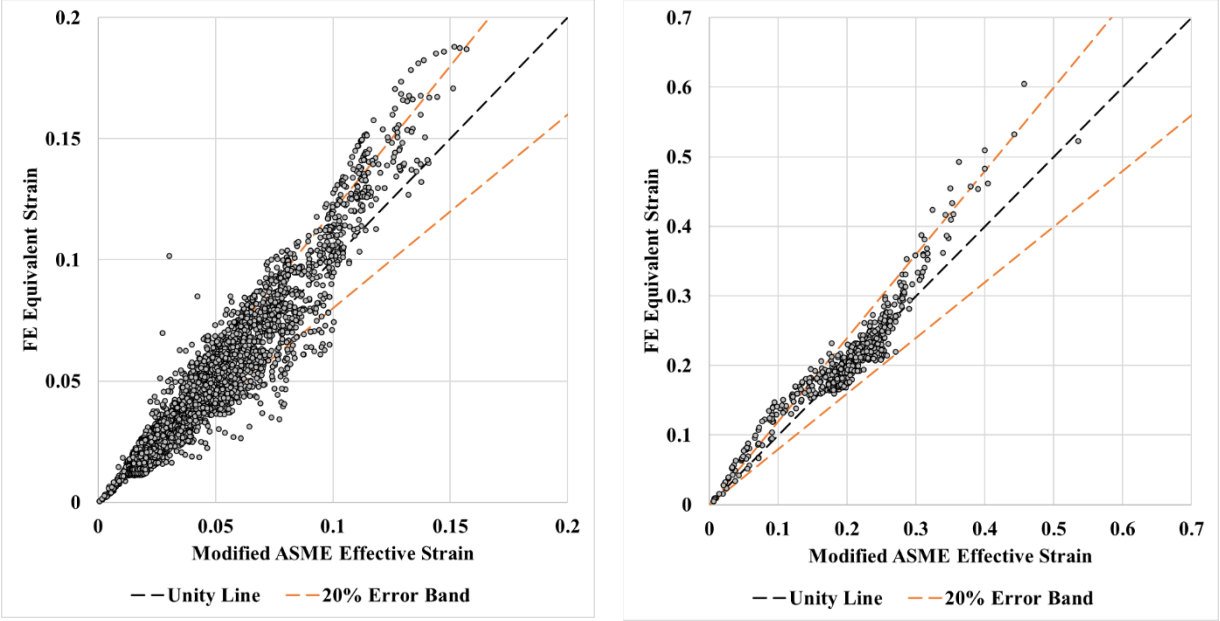

Figure 18- Unity Plot of FE Equivalent Strain vs Modified ASME Effective Strain for Hypothetical Dents

(a) Without the Deep and Sharp Dents (b) Only Deep and Sharp Dents

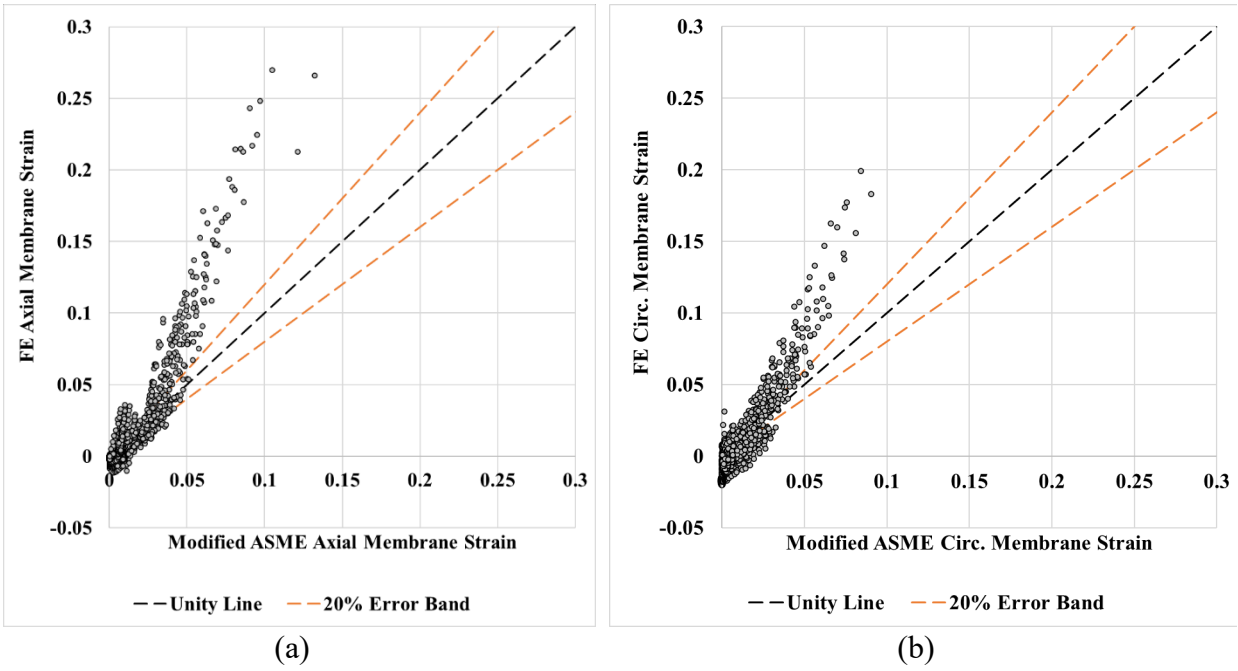

Figure 19- Unity Plot of FE Membrane Strain vs (a) Modified ASME Axial Membrane Strain (b) Modified ASME Circumferential Membrane Strain for Hypothetical Dents

4.4.4 Prediction of Indentation Strain for Unrestrained Dents

From the discussions and observations made in the previous section, it can be concluded that for unrestrained dents, the strain estimates calculated using the current dent shapes after re-rounding

do not represent indentation strains. A means of estimating the ASME effective strain at indentation from ASME effective strain evaluated at pressure for unrestrained dents is discussed in this section. A simple functional relationship which predicts the indentation, ASME effective strain using ASME effective strain evaluated at pressure, has been developed. Additionally, the mean pressure at which the ILI measurements of the dent were taken, and the maximum pressure experienced by the dent are also required as inputs. This relationship was developed by relating the ASME indentation strain and ASME strain at various pressures of unrestrained dents in the BMT FE database. The hypothetical unrestrained dents were used for training the regression model, with about 24,000 data points. The regression equation is as follows:

$$\boldsymbol{E_I = c_1 * E_P + c_2 * E_P^{|c_3|}}$$
$$\boldsymbol{c_1 = b_1 + b_2 * Pmax + b_3 * Pmean + b_4 * OD/WT} \quad (4.11)$$
$$\boldsymbol{c_2 = b_5 + b_6 * Pmax + b_7 * Pmean + b_8 * OD/WT}$$
$$\boldsymbol{c_3 = b_9 + b_{10} * Pmax + b_{11} * Pmean + b_{12} * OD/WT}$$

Where, E_I is the predicted ASME effective strain at indentation, E_P is the ASME effective strain evaluated from the unrestrained dent shape at pressure, $Pmean$ is the mean pressure at ILI measurement of dent shape as percentage of P_{SMYS}, $Pmax$ is the maximum pressure experienced by the dent as percentage of P_{SMYS} and OD/WT is the ratio of pipe outer diameter to wall thickness. The coefficients b_i's are given below in Table 4. The unity plot comparing the ASME indentation strain predicted by Equation ((4.11)) vs the ASME strain evaluated using FE dent shape at indentation has been given in Figure 20 (a). About 73% of the compared values fall within the 20% error band.

An upper bound regression analysis was also performed, in which the upper bounds of the data sets were weighted, resulting in a conservative prediction model. The same equation, Equation (4.11), was used to perform the data fit, resulting in a different set of coefficients. These coefficients are listed in Table 5. The unity plot comparing the predicted upper bound ASME indentation effective strains with the ASME effective strains evaluated using FE dent shapes at indentation has been given in Figure 20(b). 95% of the data points were above the unity line, demonstrating the conservative nature of the fitting.

Table 4- Coefficients in Equation (4.11)

b1	b2	b3	b4	b5	b6	b7	b8	b9	b10	b11	b12
8.0397 E-01	-2.1443 E-05	-4.8577 E-04	1.5435 E-03	3.4513 E-02	3.6336 E-04	7.8631 E-05	-2.9772 E-04	2.1983 E-02	1.8032 E-05	-1.2964 E-06	-9.8010 E-04

Table 5- Coefficients of (4.11) for Conservative Upper Bound Predictions

b1	b2	b3	b4	b5	b6	b7	b8	b9	b10	b11	b12
8.6890 E-01	-5.8945 E-03	1.8710 E-05	-6.4826 E-04	1.1248 E-02	1.9675 E-03	-9.9039 E-05	1.0360 E-03	1.2677 E-01	-1.4761 E-05	-2.1076 E-04	1.7274 E-03

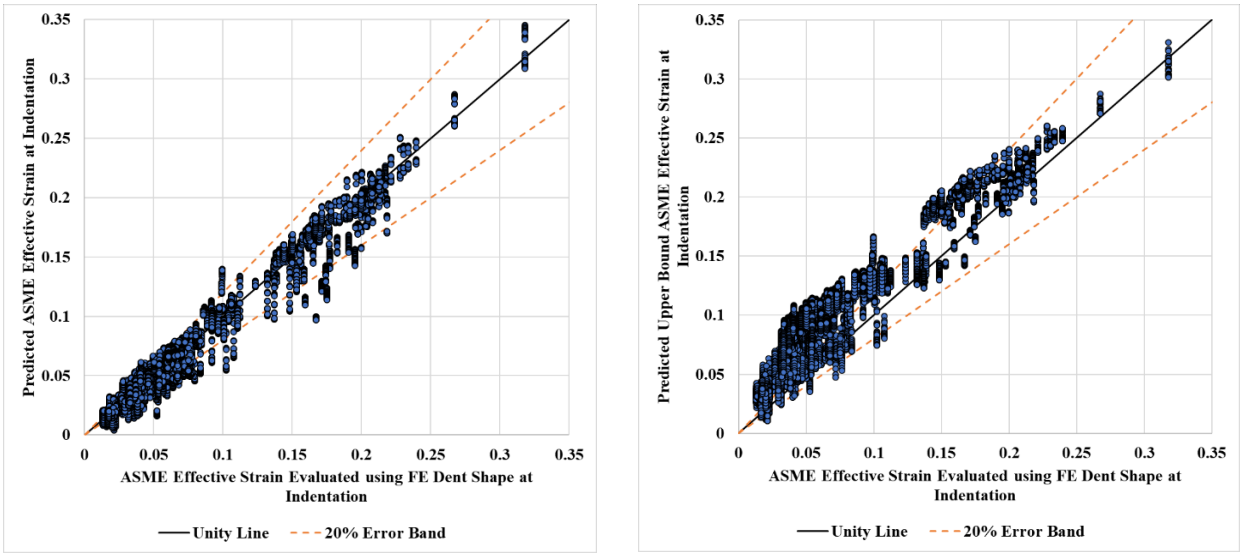

(a) (b)

Figure 20- Unity Plot
Comparing (a) ASME effective strain at indentation predicted by Equation (4.11) vs the ASME effective strain evaluated using FE dent shape at indentation. (b) Upper Bound ASME effective indentation strain predictions vs the ASME effective strain evaluated using FE dent shape at indentation. Data set used for training.

A set of 55 unrestrained dent FE models from the full-scale test database was used to test the regression equations. The ASME effective strains at pressure and indentation for these cases were evaluated from the FE dent shapes. The pressure information and strain at pressure were used with Equation (4.11) to predict the strain at indentation. These predicted indentation strains were compared with the effective strains evaluated using the indentation dent shapes. 81% of the predictions made using the standard coefficients (Table 4), were within the 20% error band, while 85% of predictions made using the upper bound coefficients (Table 5), were above the unity line. The comparison unity plots for the standard and upper bound predictions are given in Figure 21.

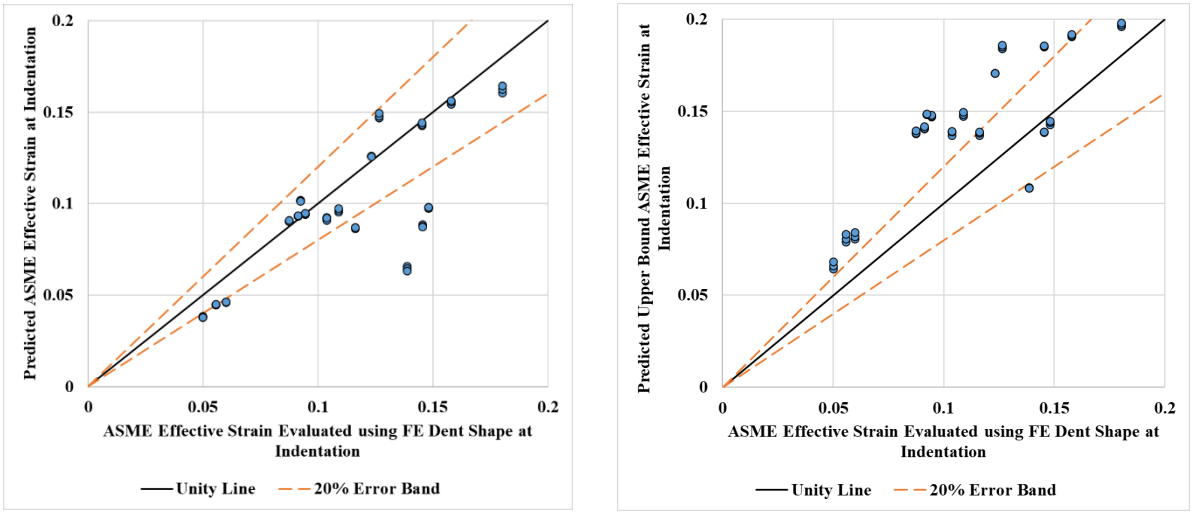

(a) (b)

Figure 21- Unity plot comparing predicted ASME Effective Strain at indentation vs ASME effective strain evaluated using FE dent shape at indentation

(a) Standard Prediction (b) Upper Bound Prediction. Data set used for testing regression model.

As in the case of ASME strain estimation of indentation strains of unrestrained dents, the BMT modified model cannot approximate the indentation strains using the dent shapes at pressure. Therefore, the indentation strain prediction regression model Equation (4.11) was fitted for the modified ASME strain model. Using, Equation (4.11) and the coefficients in Table 6 (standard) and Table 7 (upper bound), the indentation strains can be predicted using modified ASME effective strain evaluated at pressure. The same fitting and testing data used previously was used to fit and validate the equation. About 77% of the fitted data fell within the 20% error band for the standard prediction coefficients and 95% of the fitted data was predicted above the unity line for the upper bound prediction coefficients (Figure 22). About 82% of the predicted values from the test data fell within the 20% error band for standard prediction, while 84% of the upper bound predictions were above the unity line (Figure 23).

Table 6- Coefficients for Equation (4.11)
For standard prediction of Modified ASME effective indentation strains from strains evaluated at pressure, for unrestrained dents

b1	b2	b3	b4	b5	b6	b7	b8	b9	b10	b11	b12
7.0567 E-01	1.9833 E-03	1.1354 E-04	3.1260 E-03	2.6672 E-02	4.2429 E-04	8.3458 E-05	-2.2784 E-04	-3.0317 E-02	1.7133 E-05	2.4208 E-06	1.2294 E-03

Table 7- Coefficients for Equation (4.11)
For upper bound prediction of Modified ASME effective indentation strains from strains evaluated at pressure, for unrestrained dents

b1	b2	b3	b4	b5	b6	b7	b8	b9	b10	b11	b12
7.5550 E-01	1.0615 E-04	2.5154 E-04	1.8056 E-03	2.4727 E-02	8.7182 E-04	1.4291 E-04	5.2805 E-04	3.1122 E-02	-4.9341 E-04	1.9003 E-04	2.2123 E-03

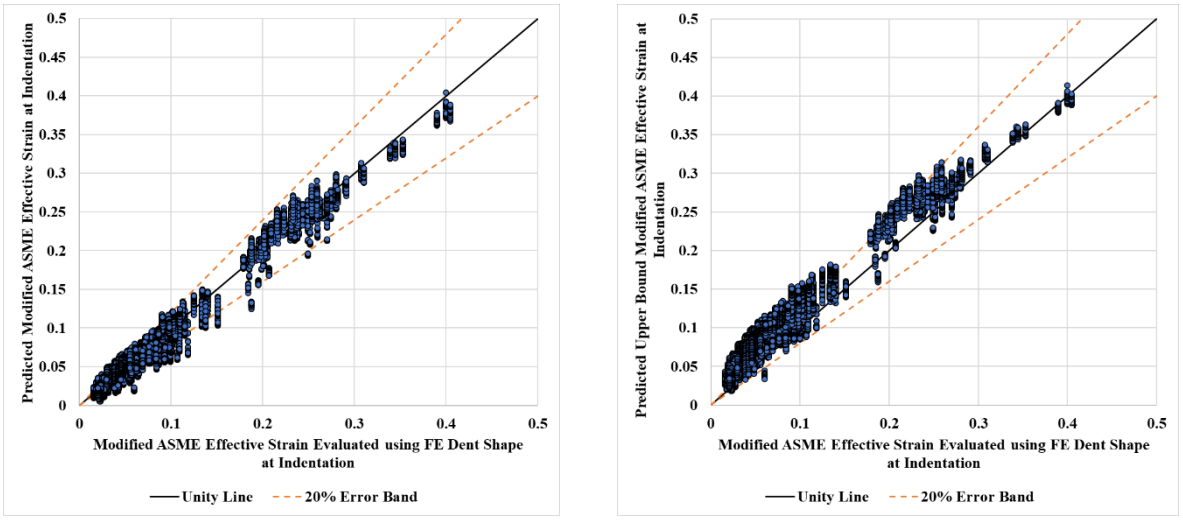

(a) (b)

Figure 22- Unity Plot Comparing

(a) Modified ASME effective strain at indentation predicted using standard coefficients (Table 6) (b) Modified ASME effective strain at indentation predicted using upper bound coefficients (Table 7), vs the Modified ASME effective strain evaluated using FE dent shape at indentation. Data set used for training.

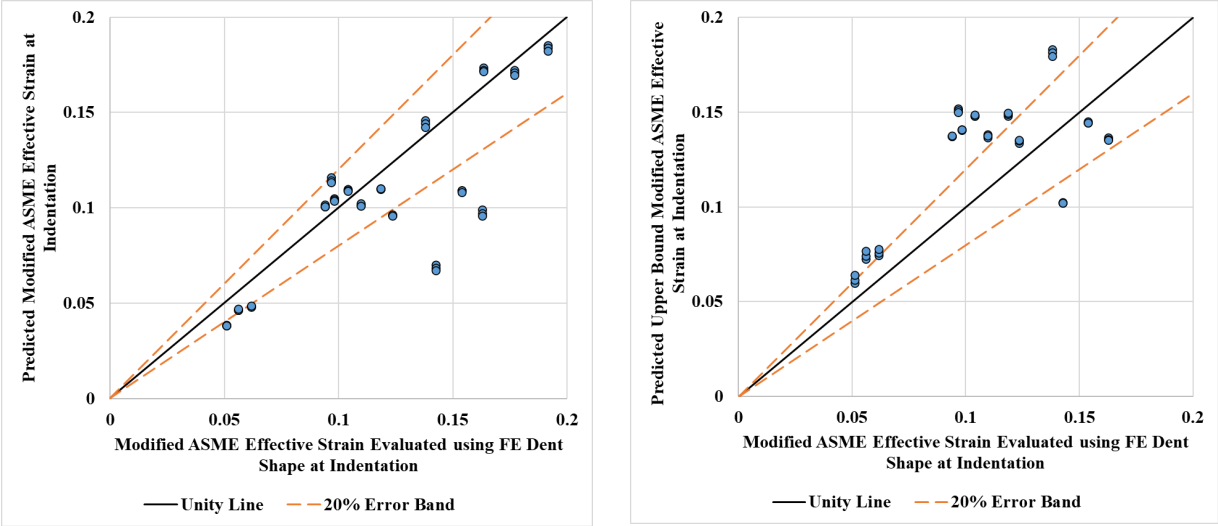

Figure 23- Unity plot comparing predicted Modified ASME Effective Strain at indentation vs Modified ASME effective strain evaluated using FE dent shape at indentation

(a) Standard Prediction (b) Upper Bound Prediction. Data set used for testing regression model.

4.5 Dent Strain Cracking Criterion

4.5.1 Ductile Failure Damage Indicator

The Ductile Failure Damage Indicator (DFDI) is a phenomenological damage prediction model which predicts the onset of cracking due to large plastic deformation [3]. It is a decoupled post-processing model which utilized the strain and stress triaxiality evolution in the FE analysis of the deformation of an undamaged material. The DFDI is given by the following equation [3],

$$DFDI = \int_0^{\varepsilon_{eq}} \frac{d\varepsilon_{eq}}{1.65\varepsilon_0 \exp\left(-\frac{3\sigma_m}{2\sigma_{eq}}\right)} \tag{4.12}$$

Where, ε_{eq} is the equivalent strain, ε_0 is a material property called critical strain which represents crack inception true strain under uniaxial testing, σ_m is the hydrostatic stress and $\sigma_{eq}$is the von Mises stress. A simplified upper bound screening criteria has also been developed and does not require the evolution of stress and strain quantities across the deformation, but only requires the material critical strain and final equivalent strain. The upper bound equation is as follows:

$$DFDI_{Upper\ Bound} = \frac{1.65\varepsilon_{eq}}{\varepsilon_0} \tag{4.13}$$

The evaluated indentation effective strains can be used as the equivalent strain to estimate the state of damage incurred by the pipe due to indentation [3] [14]. The critical strain for pipeline materials is usually between 0.3 to 0.5 [3]. DFDI = 0 represents the undamaged state, while DFDI = 1.0 represents the damaged state. A damage limit of DFDI = 0.6 can be employed and has been suggested as a conservative option [3].

The upper bound DFDI was evaluated for 47 dents involved in the full-scale tests. These values were evaluated using all three strain estimates – ASME, Blade and BMT Modified ASME. The DFDI values were evaluated using critical strain of 0.3 and 0.5, the lower and upper bound values of the suggested range. The results have been plotted in Figure 24. None of the dents from the full-scale tests had incurred cracking due to indentation. The predicted DFDI values are in agreement with this fact and are below 1.0, except a few points. With the more conservative case (ε_0=0.3), 2, 4 and 8 dents predict DFDI greater than 1.0 using ASME, Blade and Modified ASME formulations, respectively, while for the less conservative case (ε_0=0.5), none of the dents have DFDI values greater than 1.0. DFDI upper bound evaluations using the FE indentation strains were also performed. For the case where ε_0=0.3, 4 dents had DFDI upper bound predictions greater than 1, while no dents exceeded the cracking limit for ε_0=0.5. The results can be found in Figure 25.

On the other hand, if a damage limit of DFDI = 0.6 is used as a more conservative option [3] along with the lower bound critical strain value of 0.3, 15, 16 and 21 dents predict DFDI greater than 0.6 using ASME, Blade and Modified ASME formulations, respectively. While with the upper bound critical strain value of 0.5, 2, 4 and 8 dents predict DFDI greater than 0.6 using ASME, Blade and Modified ASME formulations, respectively. With the lower bound critical strain value of 0.3, 19 dents predict DFDI greater than 0.6 using FE equivalent strains and 3 dents predict DFDI greater than 0.6 while using critical strain value of 0.5.

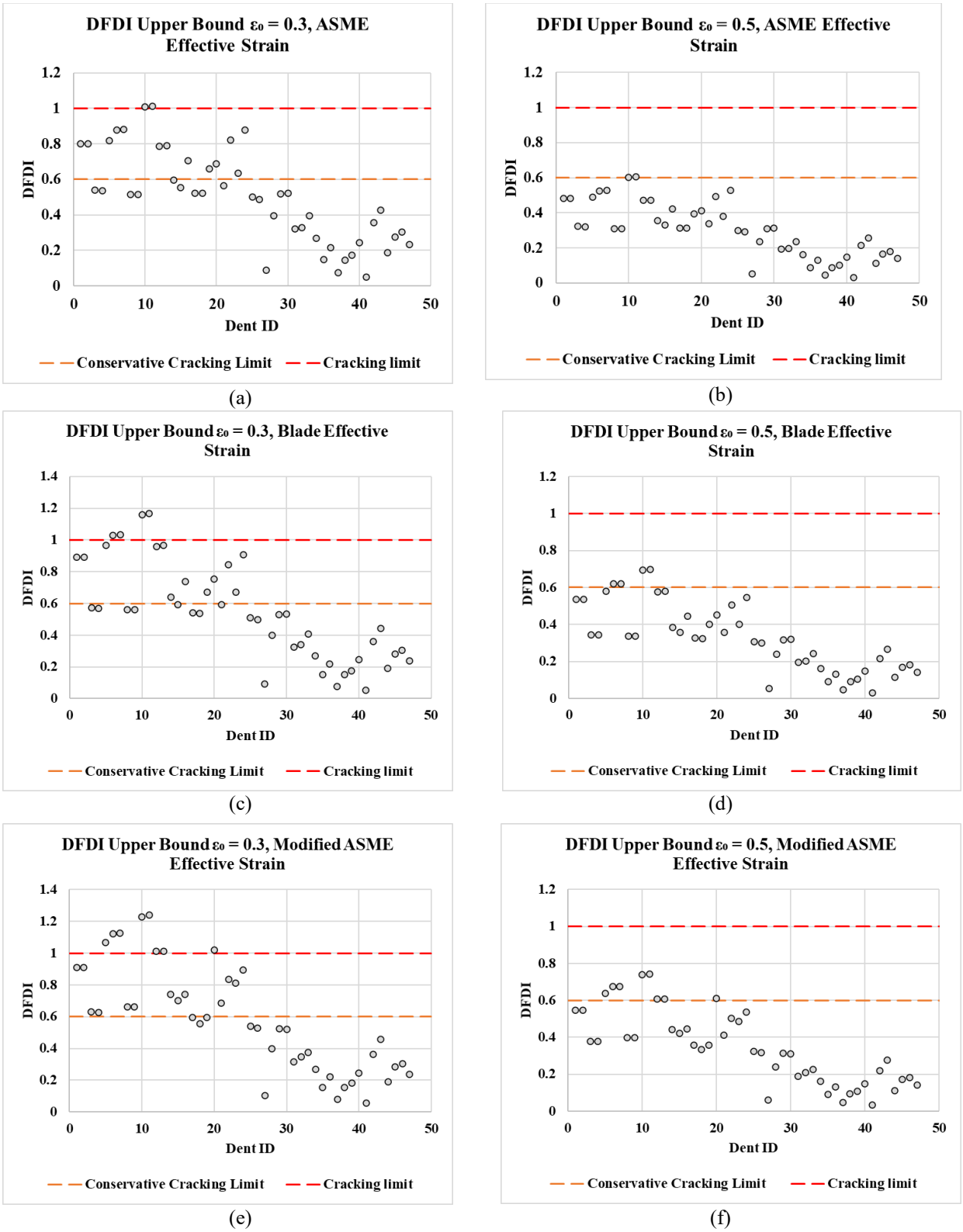

Figure 24- DFDI Upper Bound Values For Full-Scale Test Dents Evaluated Using (a) ASME strain with ε_0=0.3 (b) ASME strain with ε_0=0.5 (c) Blade strain with ε_0=0.3 (d) Blade strain with ε_0=0.5 (e) Modified ASME strain with ε_0=0.3 (f) Modified ASME strain with ε_0=0.5

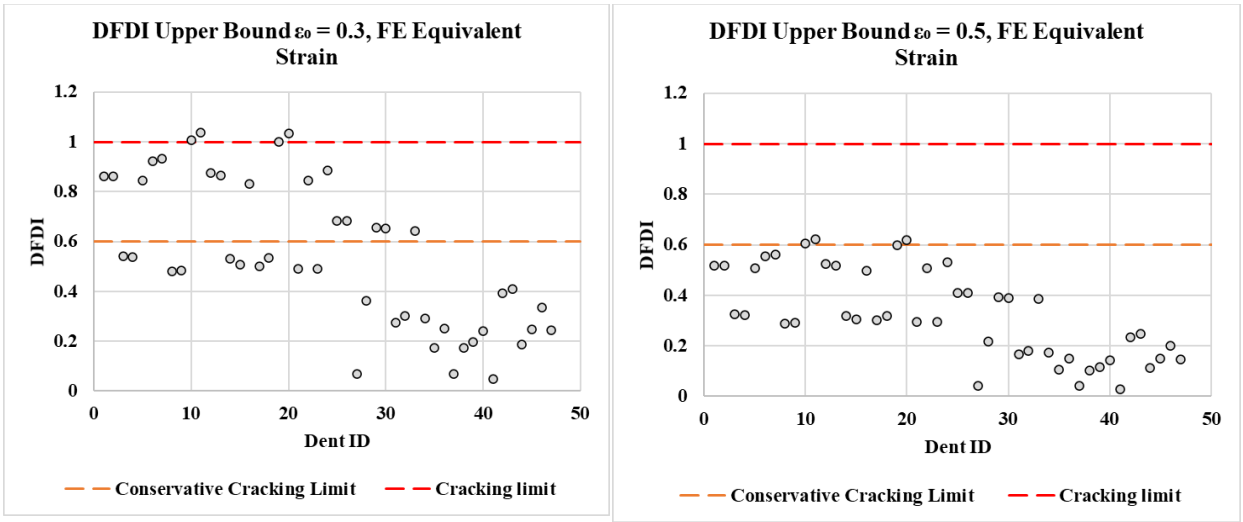

Figure 25- DFDI Upper Bound Values for Full-Scale Test Dents Evaluated using FE Strains (a) ε_0=0.3 (b) ε_0=0.5

4.5.2 ASME B31.8 Limit Strain Criterion

ASME B31.8 provides a guideline stating that the likelihood of cracking is high if an indentation with strains exceeding 6% occurs [2]. The effective strains (ASME, Blade, Modified ASME) exceeding this limit suggests that the dent might have incurred cracking during indentation. This criterion was applied to the 47 full-scale dents and based on it and the three different effective strain measures, ASME strain: 32 of 47 dents, Blade strain: 33 of 47 dents and Modified ASME strain: 33 of 47, have exceeded the critical value. Based on the FE equivalent strain, 33 of 47 dents have exceeded 6% strain. These results can be observed in Figure 26.

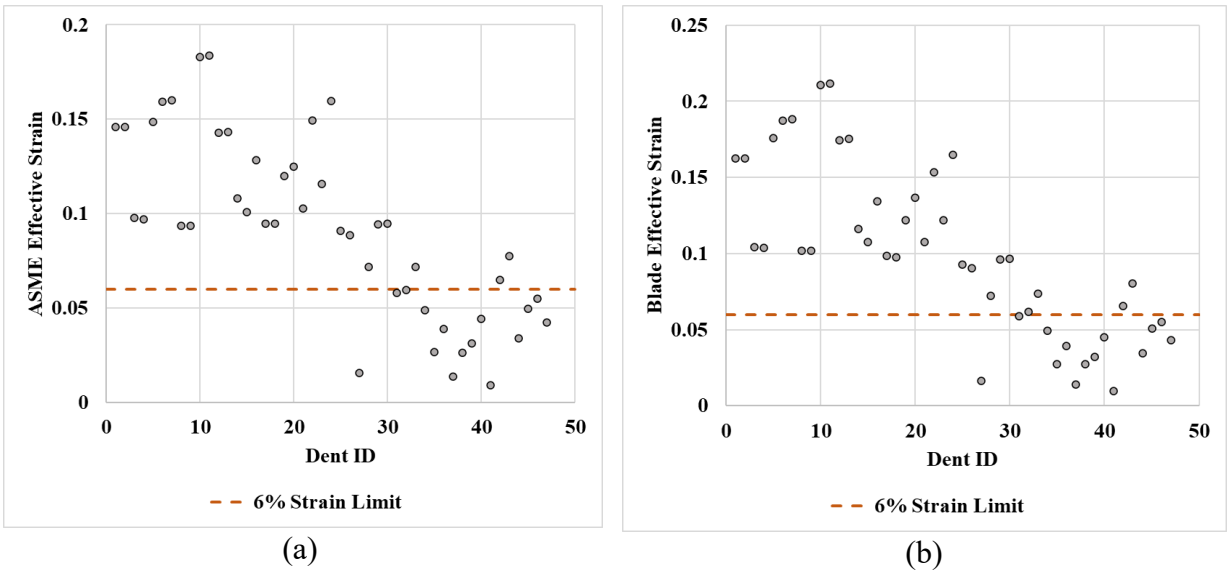

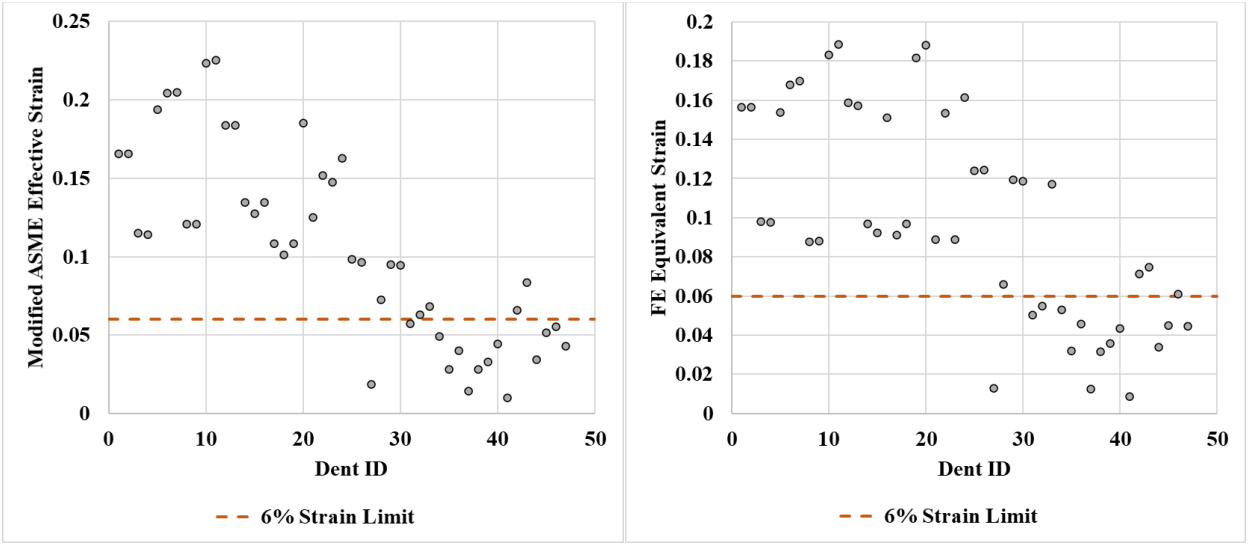

(c) (d)

Figure 26- Effective Strain Estimates of Full-Scale Dents Compared Against the 6% Strain Limit

(a) ASME Effective Strain (b) Blade Effective Strain (c) Modified ASME Effective Strain (d) FE Equivalent Strain

4.5.3 ***Comparison of Cracking Effective Strain from DFDI and ASME Limit Strain Criteria***

Upper Bound DFDI criterion quantifies damage based on material property (critical strain) and indentation equivalent strain. The ASME B31.8 effective strain estimate from ILI data can be used as the equivalent strain, in the DFDI equation to back calculate limit strain and compare it with 6% limit strain as defined in ASME B31.8 Appendix R, as they are conceptually similar [3] [14]. Use of different critical strain (ε_0) values (0.3 to 0.5 for pipeline steels) and cracking DFDI limit (0.6 or 1), can produce a range of effective strain limits [14]. The evaluation of these limit strains is presented below.

$$DFDI_{Upper\ Bound} = \frac{1.65\varepsilon_{eq}}{\varepsilon_0}$$

$$Effective\ Strain\ Limit = \ \varepsilon_{eq} = \frac{DFDI_{Upper\ Bound} \times \varepsilon_0}{1.65}$$

For DFDI cracking limit of 0.6 and $\varepsilon_0 = 0.3$, the strain limit is given by,

$$\varepsilon_{eq} = \frac{0.6 \times 0.3}{1.65} = \ 0.11\ (11\%\ Limit\ Strain)$$

Similarly,

- for cracking limit of 0.6 and critical strain of 0.5, the calculated strain limit would be 0.18 (18% limit strain),

- for cracking limit of 1 and critical strain of 0.3, the calculated strain limit would be 0.18 (18% limit strain), and
- for cracking limit of 1 and critical strain of 0.5, the calculated strain limit would be 0.3 (30% limit strain).

There is a large discrepancy between 6% strain limit as defined in ASME B31.8 Appendix R and the range of 11% - 30% strain limit calculated from the DFDI methodology. This is the primary reason that a larger portion of full-scale test specimens show potential for cracking using ASME criterion as compared to the DFDI methodology

5 Effects of Variation of ILI Data on Fatigue Life and Strain Estimation of Dents

The variation in ILI tool reported measurement of dent shape can introduce variations in fatigue life (PRCI Level 1/2, API RP 1183 [1]) and dent strain (ASME B31.8 [2]) estimation, as these models are dependent on the dent shape. This section is dedicated to the investigation of the sensitivity of these models to ILI measurement variability. This investigation was conducted by employing Monte Carlo simulations, where error distributions of the dent dimensions were sampled and applied to the dent profiles, and the fatigue life and strain estimates were calculated from the randomized profiles. The variation in the fatigue lives and the strain estimates for different error distributions were calculated. The collated data provides a measure of the variation observed in the estimates when the dent shapes are subjected to various error distributions. In addition to the artificially induced errors, variation in estimates were also obtained from multiple ILI measurements of a set of dents which were part of ILI pull tests (PRCI NDE-4-18 PHMSA contract 693JK31910014). Laser scan data for these dents was also available. The fatigue life and dent strain distributions calculated from multiple measurements from different ILI Service Providers and laser scan data were compared against the Monte Carlo simulation results.

The ILI data sets used for the Monte Carlo simulations are given in Table 8. The data sets (Sets 1 to 4) consist of caliper data obtained from in-service ILI runs carried out on a wide range of pipe geometries and dent depths. Sets 5, 6 and 7, consist of laser scanned dent geometries from pipe sections used for full-scale testing. The first step in processing the data involved extracting the axial and transverse profiles of the dents. Then the shapes of these profiles were altered based on a randomization scheme that resulted in a very large number of dent shape variations. The randomization was performed using percentage error normal distributions with different standard deviations. These errors were then applied to the depth, length and width of the dent profiles to get a family of variations for each dent. The dent geometry parameters as per API RP 1183, were extracted for these variations, and then the PRCI Level 1 and 2 fatigue life estimation was performed on each variation, assuming a pressure cycle equivalent to a 13 ksi (90 MPa) hoop stress and a fixed spectrum severity indicator (SSI) (i.e., number of cycles). Statistical measures of the resulting distributions of the fatigue life for each dent were evaluated. Similarly, the profiles were processed as described in section 4 to evaluate the ASME effective strains for the family of variations, and the statistics of the resulting strain distributions for each dent were calculated. As mentioned earlier, fatigue life and strain estimates were also evaluated for the laser scan and ILI data from dents involved in ILI pull trials. Examination of the average spread of the fatigue life and strain

estimates from the Monte Carlo simulations and ILI pull trial data, can help quantify the sensitivity of these models to ILI measurement variation.

Table 8- Dent Data Sets Used for Monte Carlo Simulations

Data Set	No. of Single Peak Dents	No. of Unrest./Rest. Dents	Outside Diameter, OD (in)	Wall Thickness, t (in)	Grade	Depth Range (% OD)	No. of Simulations
1	256	84/172	12.75	0.188	X46	0.61-6.98	6,000,000
2	172	38/134	40	0.4	X60	0.27-0.65	6,000,000
3	182	73/109	36	0.281	X52	0.2-4.25	6,000,000
4	177	53/124	24	0.35	X70	0.29-5.28	6,000,000
5	55	55/0	20	0.281	X52	0.36-8.19	6,000,000
6	26	26/0	10.75, 24, 36, 40	0.218, 0.25, 0.312, 0.344	X52	0.66-10.98	6,000,000
7	24	24/0	10.75, 24, 36, 40	0.218, 0.25, 0.312, 0.344	X52	0.22-10.74	6,000,000

5.1 Variation of Dent Profiles

The first step in generating a family of variations of a dent for the Monte Carlo simulation was to sample percentage error values from normal distributions of percentage errors. These normal distributions were generated using the normal random number generator function, *normrnd*, in MATLAB [15]. The function required mean and standard deviation values to randomize the errors. The mean percentage errors were all set at 0, while three different standard deviation values were considered, 10%, 15% and 20%. Six shape variation schemes were implemented which required six sets of error distributions. These involved the variation of depth, length, and width, individually, each with a standard deviation of 20%. The next three sets consisted of coupled variations of the three dimensions at 10%, 15% and 20% standard deviations. For each distribution, a million samples were extracted. Hence for each dent, approximately 6,000,000 simulations were performed.

The application of percentage error to vary the dent profiles is illustrated in Figure 27. Based on an instance of percentage error from the distributions, the profiles are scaled in the manner illustrated in Figure 27. The dent peak of the axial and transverse profiles is offset to the origin and the axial length (length), transverse length (width) and deflection (depth) are scaled according to the respective percentage error instances. After the family of varied dent profiles have been generated based on the six randomization schemes, the dent geometry parameters and the dent peak curvatures are evaluated for the fatigue life and strain estimation for each variation. These values are then used to calculate the fatigue life and strain distributions, associated with the dent, generated due to the simulated variations in dent shape. The mean, standard deviation and coefficient of variation of the resulting distributions are evaluated. The coefficient of variation provides a means to quantify the sensitivity of the model to the ILI measurement errors, as it is an average measure of spread of the resulting distribution, normalized to the mean. A sample error distribution and resulting distribution in fatigue life and strain estimate is given in Figure 28.

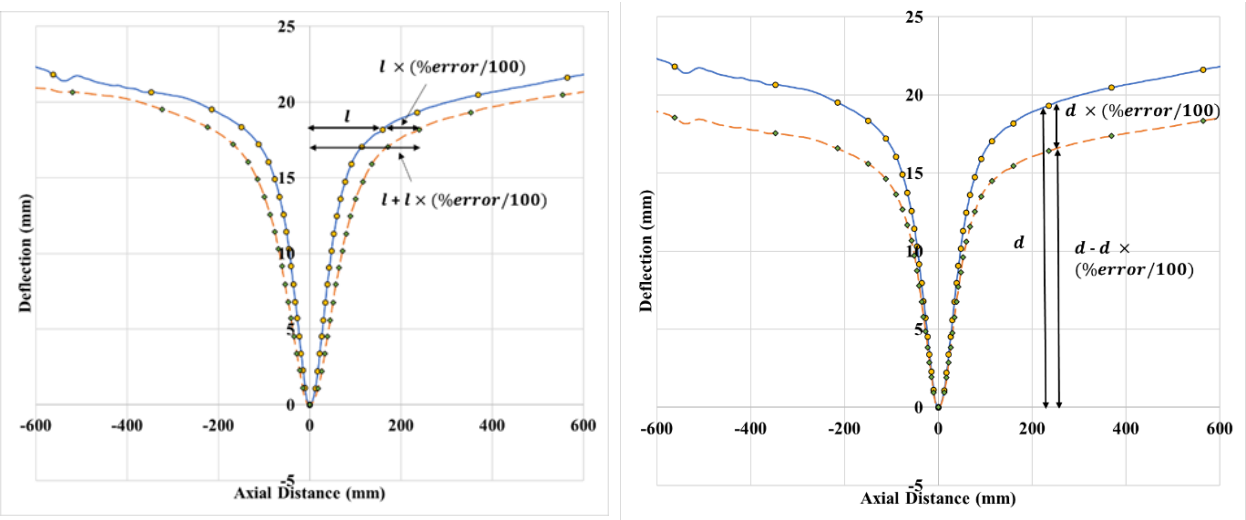

(a) (b)

Figure 27- Illustration of Variation of Profile (a) Length (b) Depth, By Application of Percentage Error

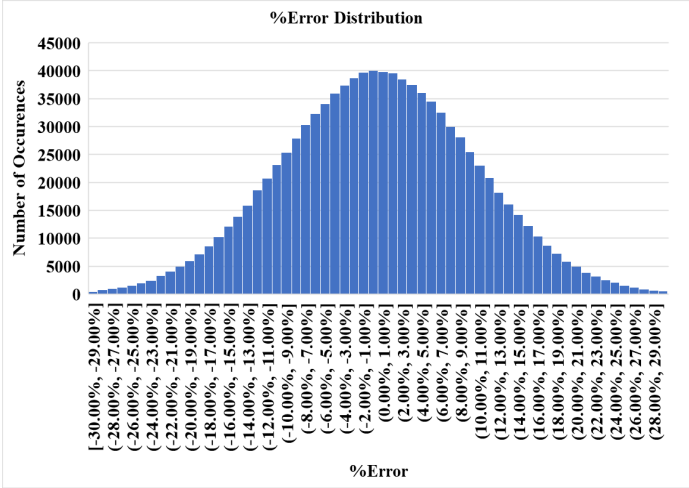

(a)

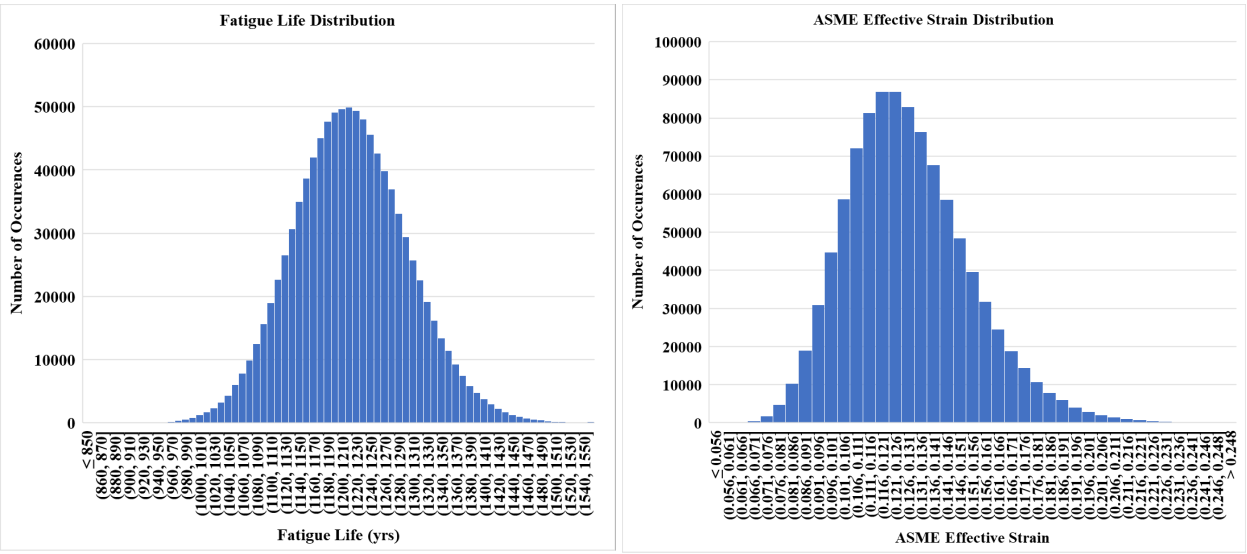

(b) (c)

Figure 28- (a) Sample % Error Histogram (b) Sample Fatigue Life Histogram Monte Carlo Simulation Output (c) Sample ASME Effective Strain Histogram Monte Carlo Simulation Output

The sample percentage error distribution displayed in Figure 28(a), was extracted from the normal random number generator with a mean of 0% and standard deviation of 10%. As can be seen in Figure 28(a), the errors can be as high as 30% but the frequency is low for such values at the tails. Most percentage errors values can be found within 10% (68% of data). Three distinct sets of error distributions were sampled each with a million instances. These errors were applied to the sample dent which created a simulated family of variations of dent shapes. Then these shapes were processed to calculate the fatigue life and strain estimates, resulting in the distributions seen in Figure 28(b) and Figure 28(c), respectively. The coefficient of variation for the fatigue life and strain distributions were 6% and 18%, respectively. These values indicate the average percentage error that can be expected when using an ILI tool with a specified percent(age) error normal distribution of standard deviation of 10%. The coefficient of variation for fatigue life distribution, ASME effective strain and modified ASME effective strain for some of the cases listed in Table 8, are provided in Figure 29, Figure 30 and Figure 31, respectively. As can be seen in these figures, each dent has six coefficient of variation values associated with the six variation schemes. The information shown in these figures is summarized in Table 9, Table 10 and Table 11, as the average of the coefficients of variation of the dents for the different variation schemes.

The coefficient of variation is used as the measure of spread of the resulting fatigue and strain distributions. It is used as the ratio of standard deviation to mean of distribution in percentage form. It can be observed from the figures and tables that the maximum variation in fatigue life (average coefficient of variation 32% - 34% for unrestrained dents and 15% - 17% for restrained dents) and strain (average coefficient of variation 45% - 51% for ASME strain and 46% - 52% for modified ASME strain) estimates occurs for the variation scheme where all three dimensions are varied using three distinct normal distributions of percentage errors, each with a standard deviation of 20%. Based on the current analysis, as an approximate rule of thumb, for errors applied to all of the dent dimensions, the fatigue life coefficient of variation for the unrestrained dent features is approximately 1.5 times the error standard deviation magnitude, whereas the restrained dent

fatigue life coefficient of variation is equal to the error standard deviation magnitude for the cases investigated in this study.

In the case of dimensions being varied individually, the fatigue life estimates appear to be most sensitive to depth (average coefficient of variation is 22% - 23% for unrestrained dents and 3% - 13% for restrained dents) variations while least sensitive to the width (average coefficient of variation 12% for unrestrained dents and 5% - 11% for restrained dents). The strain estimates appear to be most sensitive to width variation (average coefficient of variation is 29% - 44% for both ASME strain and modified ASME strain, respectively). It can be observed that the fatigue life estimation criteria for unrestrained dents is more sensitive to dent shape variations compared to the restrained dents. This is reasonable since the unrestrained dent profiles are highly variable on account of the change in shape under pressure variation. Hence, the regression model for the estimation of fatigue life of unrestrained dents is more susceptible to variations in the dent shape, as it was trained using greater variety of dent shapes.

Table 9- Average Coefficient of Variation of Fatigue Life Estimates for the Dents in the Data Sets Listed in Table 8 for the Six Different Variation Schemes

	Average Coefficient of Variation of Fatigue Life Estimates For Unrestrained Dents					
Data Set	Depth, Length, Width %Error, 10% Standard Deviation	Depth, Length, Width %Error, 15% Standard Deviation	Depth, Length, Width %Error, 20% Standard Deviation	Depth %Error Only, 20% Standard Deviation	Length %Error Only, 20% Standard Deviation	Width %Error Only, 20% Standard Deviation
1	14.27	22.22	31.86	21.61	19.33	11.80
2	14.75	23.03	33.78	22.35	21.84	11.78
3	14.67	22.89	33.00	21.61	20.94	11.80
4	14.47	22.57	32.45	22.50	20.16	11.79
5	14.93	23.29	33.94	22.32	21.91	11.78
6	14.90	23.28	33.68	21.61	21.88	11.79
7	14.81	23.10	33.29	21.71	21.51	11.78
	Average Coefficient of Variation of Fatigue Life Estimates for Restrained Dents					
Data Set	Depth, Length, Width %Err or, 10% Standard Deviation	Depth, Length, Width %Error, 15% Standard Deviation	Depth, Length, Width %Error, 20% Standard Deviation	Depth %Error Only, 20% Standard Deviation	Length %Error Only, 20% Standard Deviation	Width %Error Only, 20% Standard Deviation
1	7.84	12.12	17.04	12.87	5.50	5.33
2	7.80	11.96	16.61	13.36	5.07	4.89
3	7.06	10.78	14.76	9.19	6.25	6.09
4	7.33	11.17	15.35	2.50	10.09	10.61

Table 10- Average Coefficient of Variation of ASME Effective Strain Estimates for the Dents in the Data Sets Listed in Table 8, for the Six Different Variation Schemes

	Average Coefficient of Variation of ASME Effective Strain Estimates					
Data Set	Depth, Length, Width %Error, 10% Standard Deviation	Depth, Length, Width %Error, 15% Standard Deviation	Depth, Length, Width %Error, 20% Standard Deviation	Depth %Error Only, 20% Standard Deviation	Length %Error Only, 20% Standard Deviation	Width %Error Only, 20% Standard Deviation
1	19.71	31.38	46.46	21.55	20.05	35.39
2	21.59	34.37	51.02	21.06	8.91	44.44
3	20.09	32.01	47.51	20.65	16.37	38.46
4	20.17	32.14	47.75	20.10	15.38	39.39
5	19.97	31.70	46.99	21.99	21.28	35.39
6	19.76	31.42	46.61	21.16	22.87	33.30
7	19.25	30.63	45.43	20.90	27.44	29.02

Table 11- Average Coefficient of Variation of Modified ASME Effective Strain Estimates for the Dents in the Data Sets listed in Table 8, for the Six Different Variation Schemes

Average Coefficient of Variation of Modified ASME Effective Strain Estimates						
Data Set	Depth, Length, Width %Error, 10% Standard Deviation	Depth, Length, Width %Error, 15% Standard Deviation	Depth, Length, Width %Error, 20% Standard Deviation	Depth %Error Only, 20% Standard Deviation	Length %Error Only, 20% Standard Deviation	Width %Error Only, 20% Standard Deviation
1	20.40	32.40	47.77	23.75	19.73	35.59
2	21.91	34.84	51.62	22.44	9.13	44.18
3	20.40	32.45	48.07	21.87	16.51	38.30
4	20.27	32.28	47.94	20.48	15.33	39.40
5	21.27	33.66	49.35	26.16	20.02	36.24
6	20.08	31.85	47.14	22.61	22.64	33.52
7	19.60	31.14	46.10	22.11	27.19	29.24

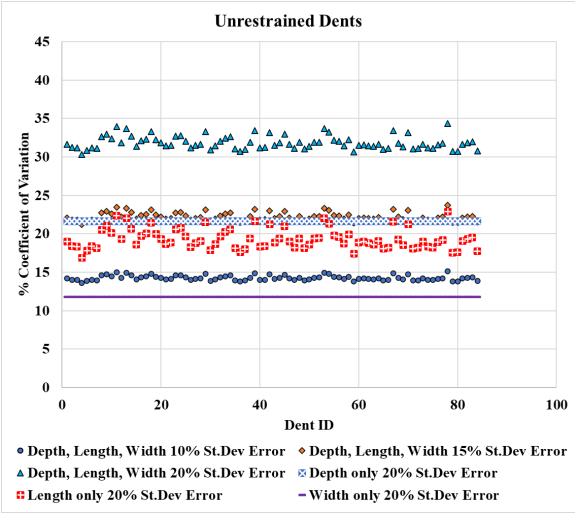

(a) Set 1 – Unrestrained

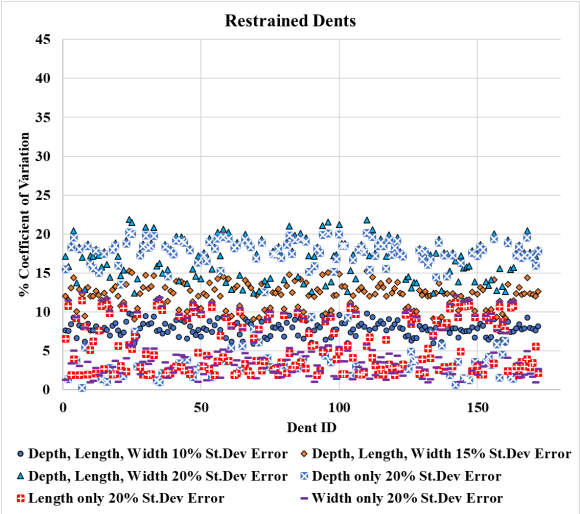

(b) Set 1 – Restrained

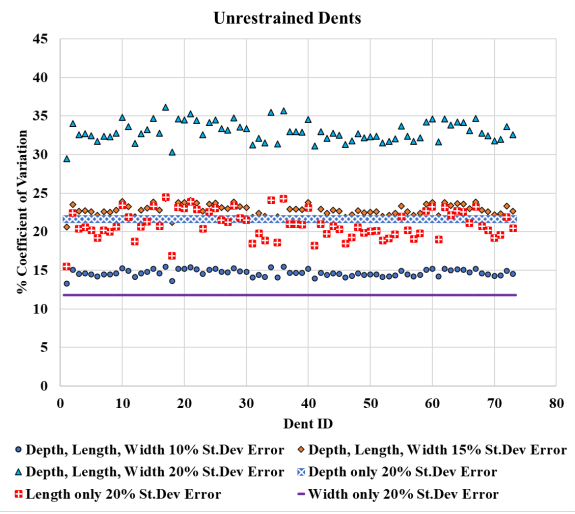

(c) Set 3 – Unrestrained

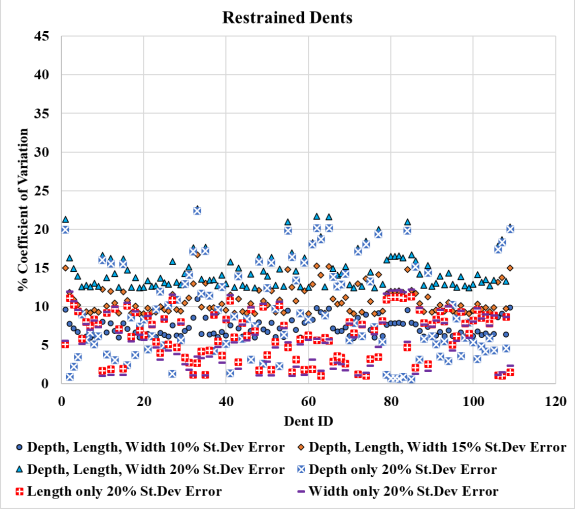

(d) Set 3 – Restrained

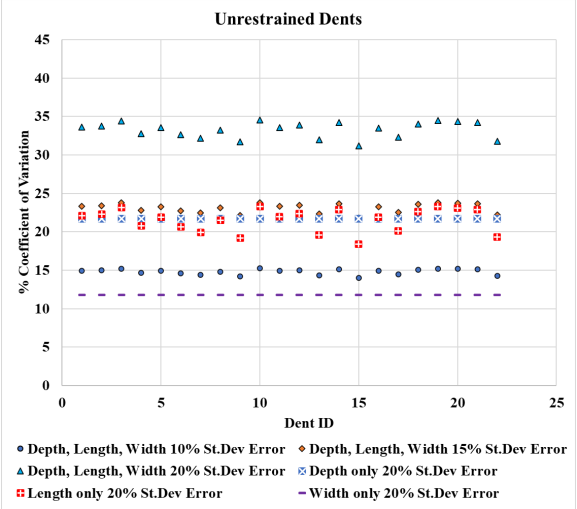

(e) Set 7 - Unrestrained

Figure 29- Coefficient of Variation of the Dent Fatigue Life Distributions

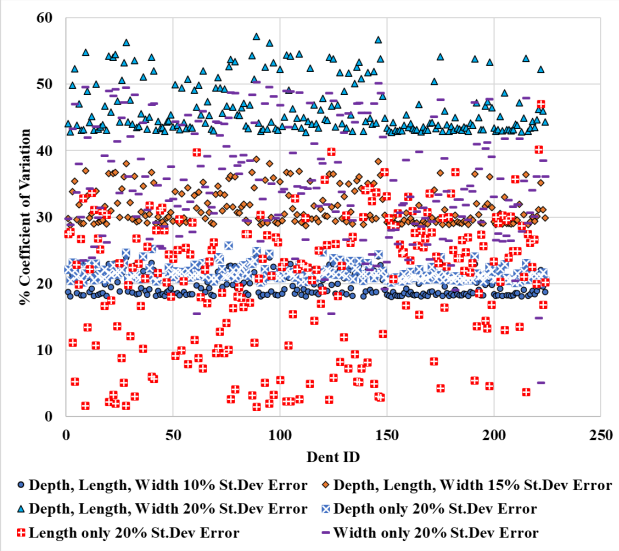

(a) Set 1 – All dents

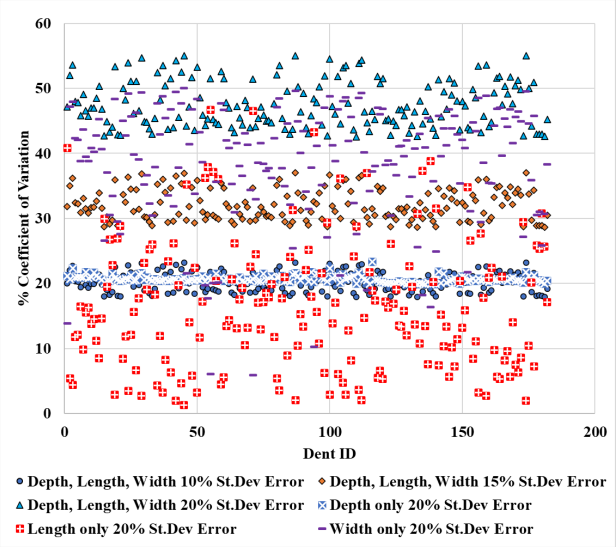

(b) Set 3 – All dents

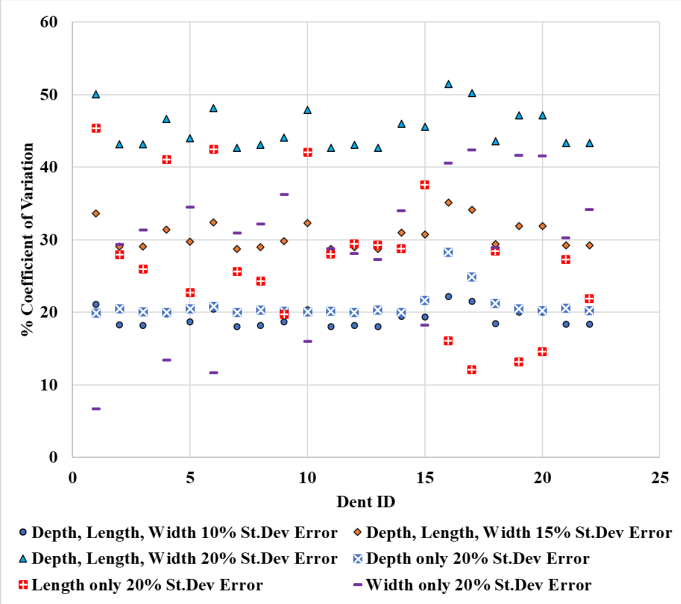

(c) Set 7 – All dents

Figure 30- Coefficient of Variation of the ASME Effective Strain Distributions

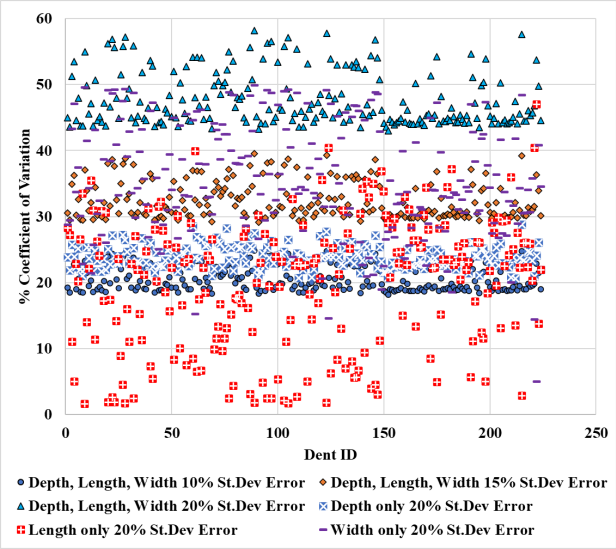

(a) Set 1 – All dents

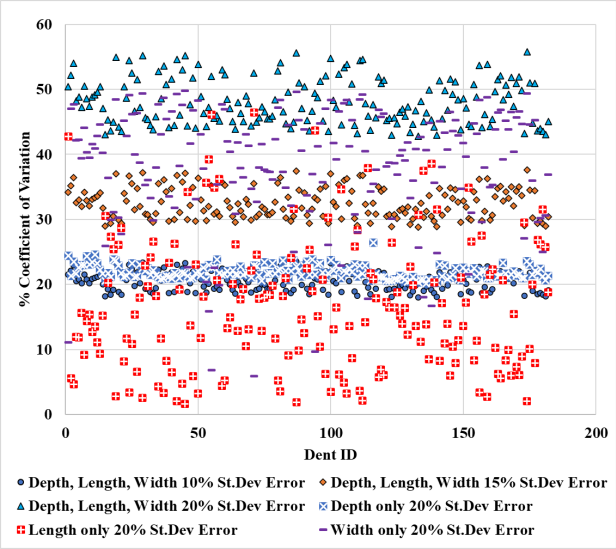

(b) Set 3 – All dents

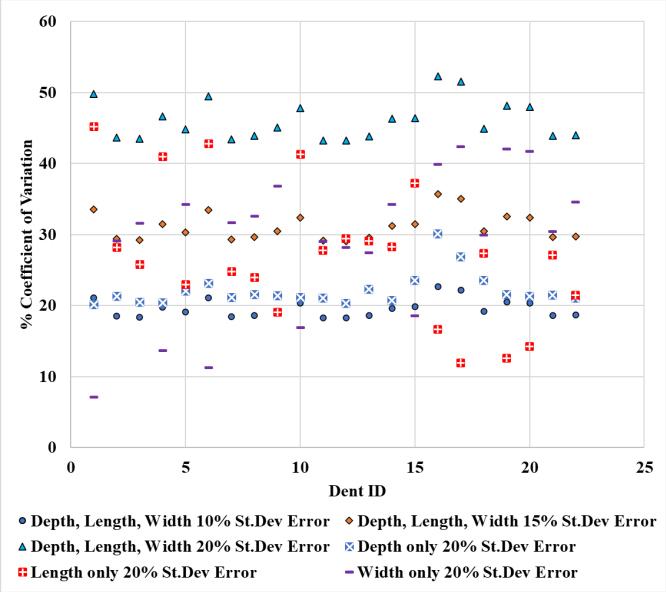

(c) Set 7 – All dents

Figure 31- Coefficient of Variation of the Modified ASME Effective Strain Distributions

5.2 Comparison of Fatigue Life and Strain Estimates Evaluated using Laser Scan and ILI Dent Geometry

As mentioned earlier, in addition to the Monte Carlo simulations performed to investigate the effects of shape variation on the fatigue life and strain estimates, ILI pull trial data from multiple ILI Service Providers and laser scan dent data were also used to understand the impact of dent shape measurement variations. As part of the PRCI MD NDE-4-18 PHMSA contract 693JK31910014 project, a series of dents had been measured by multiple ILI Service Providers. Under the ILI trial program, each ILI vendor had to perform multiple passes of the pipe strings at different speeds. As a result, multiple measurements of the same dents by each vendor were available. The dents had also been laser scanned. Data from 53 single peak dents were employed for this analysis and each dent had up to 50 ILI and one laser scan measurements, providing a sizable family of variations for each dent. As in the cases in Section 5.1, the dent reference data (laser scan data) and ILI data were used to evaluate fatigue life and strain estimates. The resulting distribution of estimates were collated for the family of variations of each dent and the coefficient of variation of these distributions were evaluated. These coefficient of variation in fatigue life, ASME strain and modified ASME strain estimates, for each dent, is provided in Figure 32.

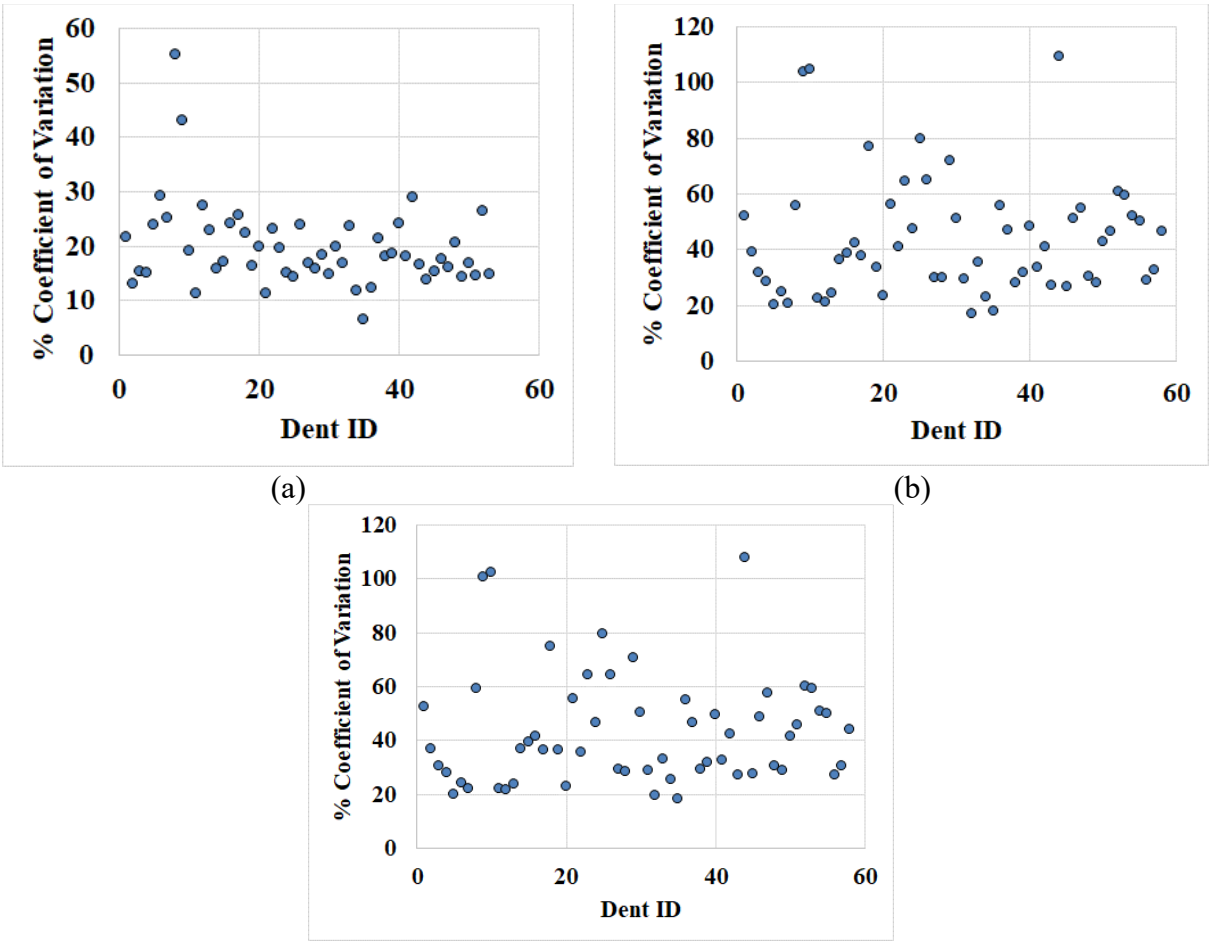

Figure 32- Coefficient of Variation

Of (a) Fatigue Life (b) ASME Effective Strain (c) Modified ASME Effective Strain Estimates

The unity plots comparing the estimates evaluated from laser scan and ILI data are presented below in Figure 33. Approximately 66% and 91% of the errors in fatigue life estimates are within 20% and 40% error bands, respectively. About 41% and 81% of the errors in ASME strain estimates are within 30% and 60% error bands, respectively, and about 41% and 85% of the errors in modified ASME strain estimates are within 30% and 60% error bands, respectively. This is also evident in Figure 32, as almost all data points are below 40% coefficient of variation for fatigue life estimates, and the majority below 60% for the strain estimates. These values are also comparable to the Monte Carlo simulation results (Figure 29 - Figure 31). It can be observed that the upper bounds of the percentage coefficient of variation for the fatigue life and strain estimates are about 40% and 60%, respectively. In Figure 32, for the few dents having errors outside these bounds, it was found that a few of their ILI profiles were highly distorted leading to high overall error, but these are rare cases and do not represent the majority of the profiles.

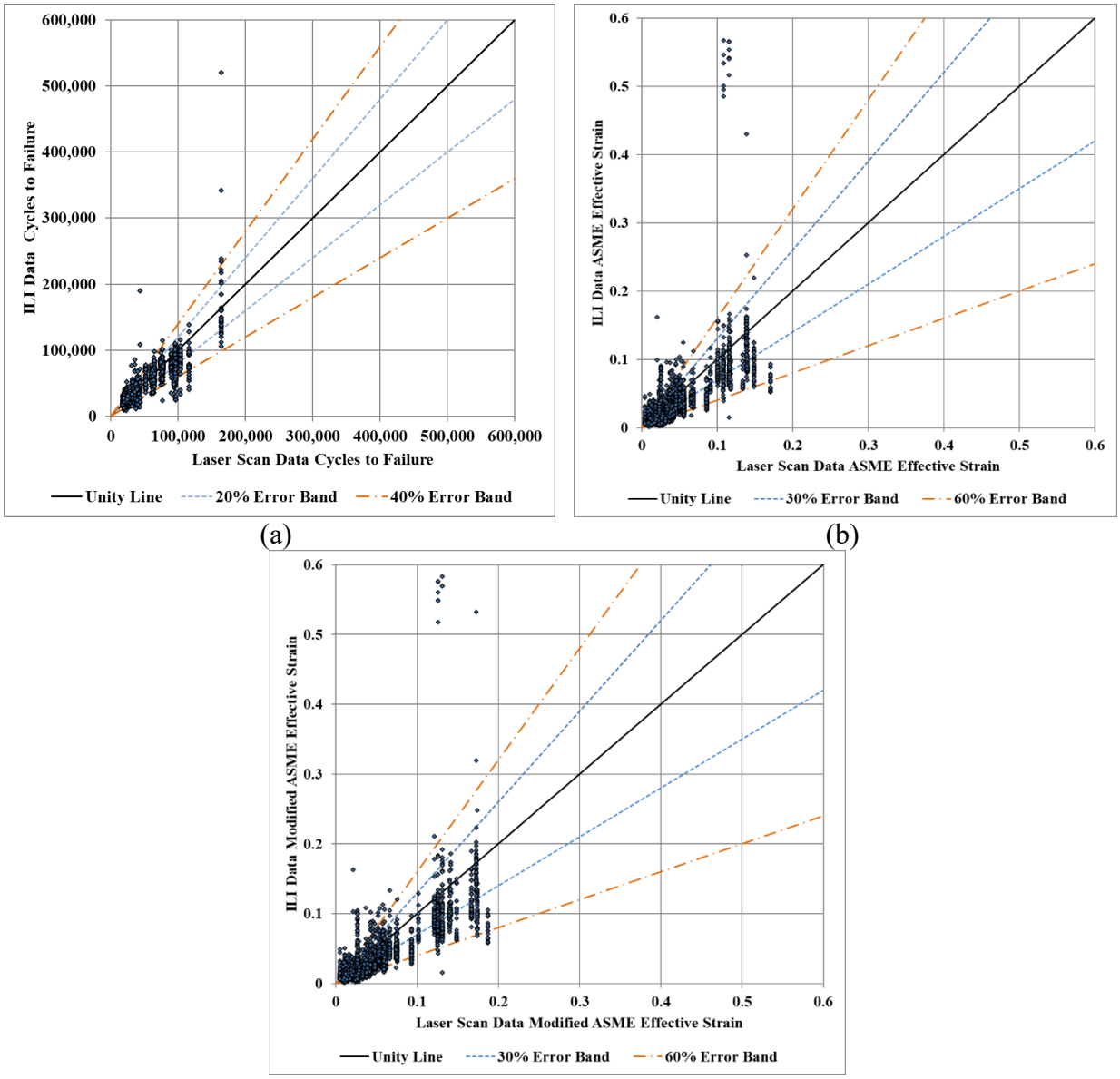

Figure 33- Unity Plots of ILI vs Laser Scan Data Estimates

Of (a) fatigue life (b) ASME effective strain (c) modified ASME effective strain

6 Dent Fatigue Life Assessment Safety Quantification

The objective of this task was to ascertain safety factors that are inherent in the dent fatigue life estimation of plain dents and dents interacting with coincident features. This was accomplished by defining scale factors (s) that can be applied to the calculated fatigue lives to return life estimates that have minimum factors of safety (R) with a specified certainty (α). These scale factors were evaluated by comparing experimental full-scale dent fatigue life data with the estimates from the fatigue life assessment methodologies developed under PRCI- and CEPA-sponsored research and incorporated in API RP 1183 [1] [12]. Histograms of the ratio of experimental to predicted fatigue

lives (safety factor) were developed and continuous probability distribution functions were fitted onto these. These functions provided estimates of the probability of the safety factor being above certain values. These fitted probability density functions were scaled so that a minimum factor of safety, with a specified certainty, could be achieved and the factor by which these functions were scaled are denoted as scaling factors. The evaluated scaling factors can be used to scale the estimated fatigue life to ensure that a minimum amount of factor of safety can be ensured with a specified amount of certainty, for a particular fatigue life assessment methodology.

6.1 Comparison of Experimental Dent Fatigue Lives with Estimated Values

As mentioned earlier, the first step in developing the scale factors was to compare experimental fatigue lives with estimates from various fatigue life assessment methodologies. For this purpose, data from 127 full-scale dent fatigue life tests were used. Out of the 127 dents, there were 61 plain dents, 29 dents interacting with metal loss and 37 dents interacting with welds (girth welds and long seam welds). Twenty-four (24) dents out of the total of 127 dents were field dents removed from in-service pipelines and the rest were created in the lab. These tests were performed on pipes of different geometries (OD/t = 10.75/0.219, 18/0.312, 20/0.281, 24/0.25, 24/0.311, 24/0.35, 24/0.375, 36/0.312, 40/0.312, 40/0.344 inches). The lab fabricated dents were created using different sized indenters (2, 4, 8, 12, 24, 48-inch diameter elliptical, 10-inch and 20-inch long bars applied along the pipe axis, and a 20-inch long bar applied transverse to the pipe axis) and cycled at different pressure ranges (P = 5% to 55%, 10% to 60%, 10% to 70%, 10% to 80% SMYS). The dent and pipe geometry data from these dents formed in the full-scale trials were used along with the associated pressure range data to predict the number of cycles to failure (N_{pred}) using the dent fatigue life models. Additionally, for the dents interacting with welds, a life reduction factor of 10 was applied to the predicted cycles as recommended in API RP 1183. Similarly, a life reduction factors were employed for interaction with metal loss, based on surface finish and wall thickness reduction as recommended in API RP 1183 [1]. The predicted fatigue lives were compared with the experimental number of cycles to failure (N_{exp}). The life predictions were made using three different dent fatigue life prediction models described in API RP 1183:

- Level 0 (API 1183 Dent Spectrum Severity Indicator Fatigue Life) [API RP 1183 Section 7.4.2],
- Level 0.5 (API 1183 Dent Operational Pressure Spectrum Fatigue Life) [API RP 1183 Section 7.4.3], and
- Level 2 Shape Parameter Life Assessment [API RP 1183 Section 8.3.4].

The ratio of experimental to predicted number of cycles to failure (r) was calculated for each prediction model (Appendix C). This ratio is the multiple by which the experimental lives are greater than the predicted lives i.e., modeling bias. In this report the modeling bias has been referred to as the factor of safety. Histograms of r were generated and lognormal statistical distributions were fitted onto the nine sets of r data. The three fatigue life assessment methodologies applied to plain dents, dents interacting with metal loss and dents interacting with welds. These sets were calculated using BS 7608 Class D Mean and BS 7608 Class D Mean – 1sd S-N curves. Using these lognormal distributions, the probability of occurrence of experimental to calculated life ratios less than 1 (i.e., unconservative predictions) and greater than 1 (i.e., conservative predictions) may be evaluated. The lognormal distributions were modified by applying scale factors (s) such that

the resulting distribution of effective ratios of experimental to predicted fatigue life (r') may be used to define Target Safety Factors (R) for defined confidence levels (α).

$$r = \frac{N_{exp}}{N_{pred}} \tag{6.1}$$

$$r' = \frac{N_{exp}}{N_{pred}'} = \frac{N_{exp}}{N_{pred}/s} = \frac{N_{exp}}{N_{pred}} * s = r * s \tag{6.2}$$

Where, r is the ratio of experimental to predicted number of cycles to failure, N_{exp} is the experimental number of cycles to failure, N_{pred} is the predicted number of cycles to failure, N_{pred}' is the effective predicted number of cycles to failure, r' is the effective ratio of experimental to predicted number of cycles to failure and s is the scale factor which when applied to N_{pred} can result in r' greater than a specified target safety factor (R). The level of confidence that $r' > R$ is given by α, which is the probability of exceedance of R in the r' probability distribution (scaled lognormal distribution).

The procedure described above on the method to ensure a specific factor of safety on a fatigue life estimation with a specified certainty, is illustrated in Figure 34. A sample *r* ratio and its scaled (*r'*) probability distributions is displayed in the figure. Based on the original *r* distribution, the probability that the actual fatigue life of a dent is at least double the predicted fatigue life is 0.62. If it is required that at least a safety factor of 2 is to be ensured with a probability of 0.9, then the original *r* distribution has to be scaled so that 90% of the area under the distribution is above a value of *r* = 2. This can be achieved by scaling the *r* distribution by 1.528. Therefore, applying this factor to the fatigue life estimate, it can be expected with 90% certainty that the effective fatigue life estimate has at least a safety factor of 2 (Equation (6.3)).

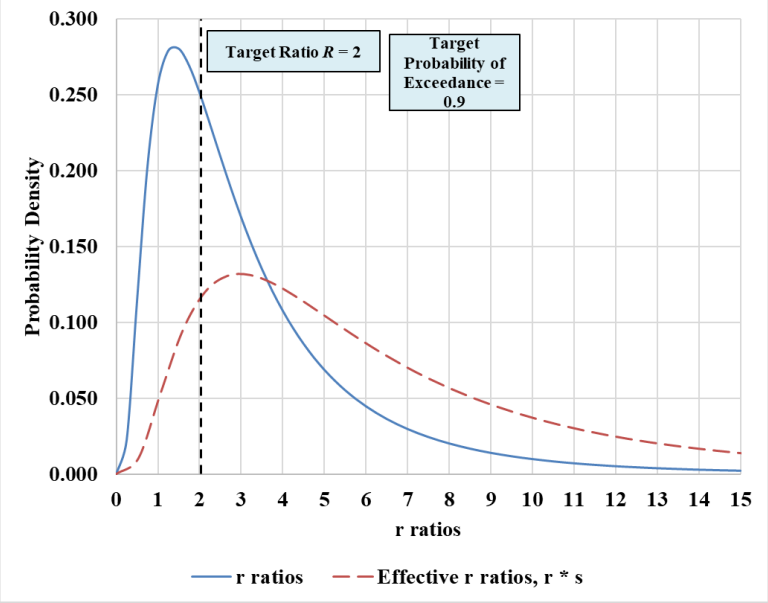

Figure 34- Sample Probability Distribution Function and Scaled Distribution Function of *r* Ratios

$$N_{pred}{}'(for\ r > R, with\ certainity\ \alpha) = \frac{N_{pred}}{s} \tag{6.3}$$

6.1.1 Scaling Factors for Fatigue Life Assessment Models Applied to Plain Dents

As discussed earlier, the first step in developing the scaling factors to ensure a target safety factor with a specified certainty, was to evaluate and fit the experimental to predicted fatigue lives ratio distribution for all the listed fatigue life estimation methodologies. These predicted fatigue lives were evaluated using BS 7608 mean and mean -1sd S-N curves. The resulting *r* ratio distributions for plain dents are presented in Figure 35. The scaling factors for various target safety factors have been listed for the three fatigue life assessments of plain dents in Table 12. It can be observed from the results that Level 0 fatigue life estimates, with both mean and mean -1sd, curves are very conservative and can ensure high safety factors with high levels of certainty. Level 0.5 estimates are less conservative and require scaling for target safety factors greater than 1 at higher levels of certainty. Level 0.5 can ensure a minimum factor of safety of one with certainty as high as 0.9. As expected, the mean -1sd curve provides greater conservatism. Level 2 is the least conservative assessment model and cannot provide minimum factor of safety of 1 with high certainty when using mean curve and up to 0.8 with mean -1sd curve. For target minimum safety factors greater than 1, scaling factors are required across most certainty levels.

Table 12- Scaling Factors Associated with Level 0, 0.5 and 2 Dent Fatigue Life Assessment, for Plain Dents

Level 0, Mean						
Scaling Factor Matrix		Probability of Exceedance of Target Ratio α				
		0.9	0.8	0.7	0.6	0.5
Safety Factor (Target Ratio R)	1	1	1	1	1	1
	2	1	1	1	1	1
	3	1	1	1	1	1
	4	1	1	1	1	1
	5	1	1	1	1	1
	10	1.04	1	1	1	1

Level 0, Mean -1sd						
Scaling Factor Matrix		Probability of Exceedance of Target Ratio α				
		0.9	0.8	0.7	0.6	0.5
Safety Factor (Target Ratio R)	1	1	1	1	1	1
	2	1	1	1	1	1
	3	1	1	1	1	1
	4	1	1	1	1	1
	5	1	1	1	1	1
	19	1.02	1	1	1	1

Level 0.5, Mean						
Scaling Factor Matrix		Probability of Exceedance of Target Ratio α				
		0.9	0.8	0.7	0.6	0.5
Safety Factor (Target Ratio R)	1	1	1	1	1	1
	2	1.68	1.25	1.01	1	1
	3	2.52	1.88	1.52	1.27	1.07
	4	3.36	2.51	2.03	1.69	1.43
	5	4.2	3.13	2.54	2.12	1.79
	6	5.04	3.76	3.04	2.54	2.15

Level 0.5, Mean -1sd						
Scaling Factor Matrix		Probability of Exceedance of Target Ratio α				
		0.9	0.8	0.7	0.6	0.5
Safety Factor (Target Ratio R)	1	1	1	1	1	1
	2	1.04	1	1	1	1
	3	1.56	1.16	1	1	1
	4	2.07	1.55	1.25	1.04	1
	5	2.59	1.93	1.56	1.31	1.1
	6	3.11	2.32	1.87	1.57	1.33

Level 2, Mean						
Scaling Factor Matrix		Probability of Exceedance of Target Ratio α				
		0.9	0.8	0.7	0.6	0.5
Safety Factor (Target Ratio R)	1	N/A	N/A	1	1	1
	2	3.03	2.21	1.75	1.44	1.2
	3	4.55	3.31	2.63	2.16	1.8
	4	6.07	4.42	3.51	2.88	2.4
	5	7.58	5.52	4.38	3.61	3
	6	9.11	6.62	5.26	4.33	3.6

Level 2, Mean -1sd						
Scaling Factor Matrix		Probability of Exceedance of Target Ratio α				
		0.9	0.8	0.7	0.6	0.5
Safety Factor (Target Ratio R)	1	N/A	1	1	1	1
	2	1.87	1.36	1.08	1	1
	3	2.81	2.04	1.62	1.33	1.11
	4	3.75	2.73	2.17	1.78	1.48
	5	4.68	3.41	2.71	2.23	1.85
	6	5.62	4.08	3.25	2.67	2.22

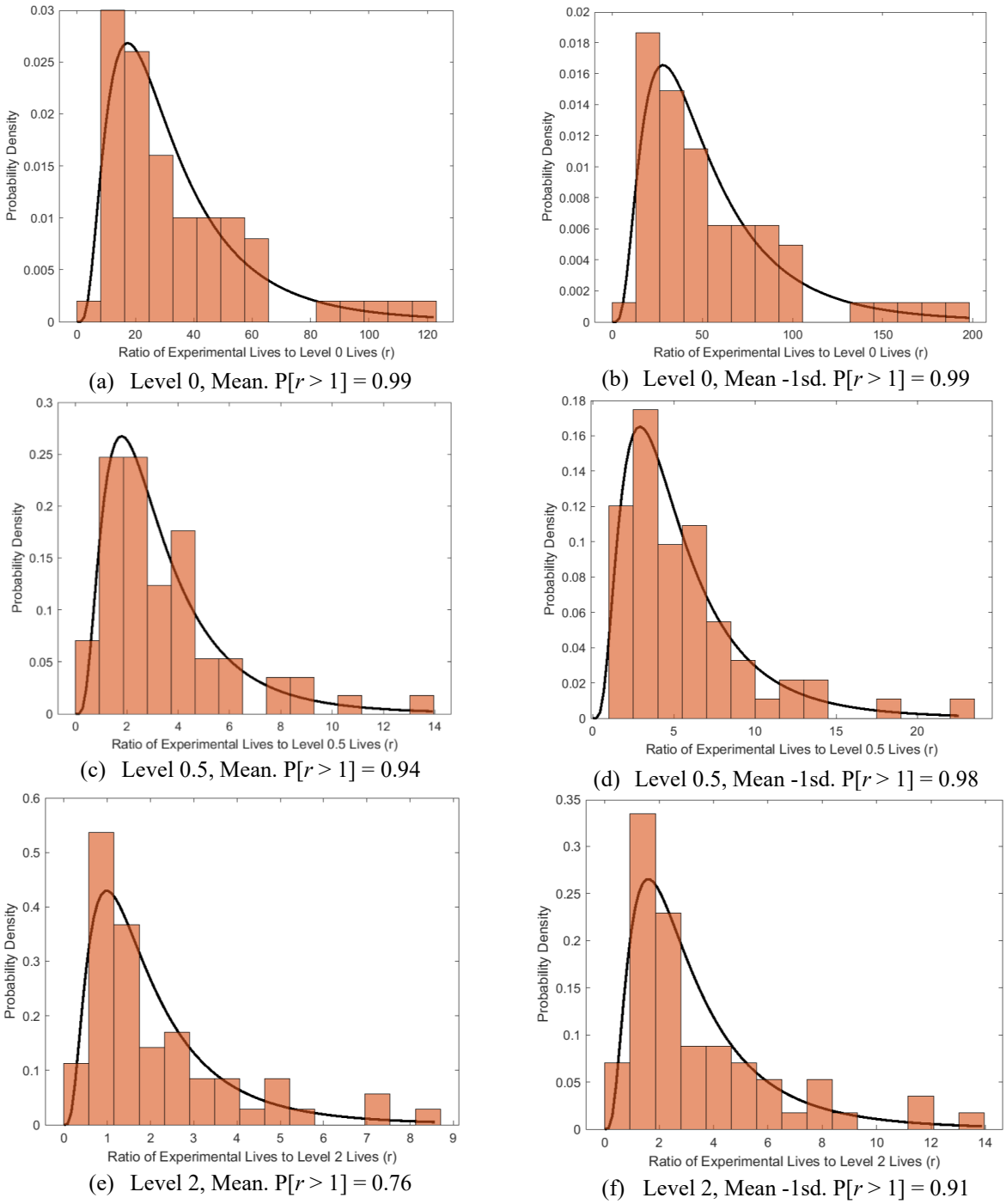

(a) Level 0, Mean. P[$r > 1$] = 0.99

(b) Level 0, Mean -1sd. P[$r > 1$] = 0.99

(c) Level 0.5, Mean. P[$r > 1$] = 0.94

(d) Level 0.5, Mean -1sd. P[$r > 1$] = 0.98

(e) Level 2, Mean. P[$r > 1$] = 0.76

(f) Level 2, Mean -1sd. P[$r > 1$] = 0.91

Figure 35- *r* Ratio Distributions of Various Fatigue Life Estimation Criteria, for Plain Dents

6.1.2 Scaling Factors for Fatigue Life Assessment Models Applied to Dents Interacting with Metal Loss

The same process was followed as in the case of plain dents to evaluate the *r* ratio distributions and the scaling factors to obtain minimum target factors of safety for dents interacting with metal loss. For dents interacting with metal loss, fatigue life reduction factors are required to be applied to the plain dent fatigue life estimates. These reductions factors are based on the maximum depth

of the metal loss and surface finish (API RP 1183) [1]. Besides the application of reduction factors, the remaining steps are the same as in plain dents. The *r* ratio distribution plots are presented in Figure 36, and the scaling factor values have been listed in Table 13. As in the case of plain dents, Level 0 is very conservative with Level 2 being the least, and greater conservatism using mean -1sd S-N curve is also apparent. It can also be observed that the application of the reduction factor makes the estimates more conservative as fewer scaling factors are required to ensure minimum target factors of safety, when compared to plain dents.

Table 13- Scaling Factors Associated with Level 0, 0.5 and 2 Dent Fatigue Life Assessment For Dents Interacting with Metal Loss

Level 0, Mean						
Scaling Factor Matrix		Probability of Exceedance of Target Ratio α				
		0.9	0.8	0.7	0.6	0.5
Safety Factor (Target Ratio R)	1	1	1	1	1	1
	2	1	1	1	1	1
	3	1	1	1	1	1
	4	1	1	1	1	1
	5	1	1	1	1	1
	15	1.03	1	1	1	1

Level 0, Mean -1sd						
Scaling Factor Matrix		Probability of Exceedance of Target Ratio α				
		0.9	0.8	0.7	0.6	0.5
Safety Factor (Target Ratio R)	1	1	1	1	1	1
	2	1	1	1	1	1
	3	1	1	1	1	1
	4	1	1	1	1	1
	5	1	1	1	1	1
	24	1.02	1	1	1	1

Level 0.5, Mean						
Scaling Factor Matrix		Probability of Exceedance of Target Ratio α				
		0.9	0.8	0.7	0.6	0.5
Safety Factor (Target Ratio R)	1	1	1	1	1	1
	2	1	1	1	1	1
	3	1.38	1.04	1	1	1
	4	1.84	1.39	1.14	1	1
	5	2.3	1.74	1.42	1.19	1.01
	6	2.76	2.08	1.71	1.44	1.22

Level 0.5, Mean -1sd						
Scaling Factor Matrix		Probability of Exceedance of Target Ratio α				
		0.9	0.8	0.7	0.6	0.5
Safety Factor (Target Ratio R)	1	1	1	1	1	1
	2	1	1	1	1	1
	3	1	1	1	1	1
	4	1.14	1	1	1	1
	5	1.42	1.07	1	1	1
	6	1.7	1.29	1.05	1	1

Level 2, Mean						
Scaling Factor Matrix		Probability of Exceedance of Target Ratio α				
		0.9	0.8	0.7	0.6	0.5
Safety Factor (Target Ratio R)	1	N/A	1	1	1	1
	2	2.2	1.66	1.35	1.14	1
	3	3.3	2.49	2.03	1.71	1.45
	4	4.39	3.32	2.71	2.28	1.93
	5	5.49	4.14	3.38	2.84	2.42
	6	6.59	4.97	4.06	3.41	2.9

Level 2, Mean -1sd						
Scaling Factor Matrix		Probability of Exceedance of Target Ratio α				
		0.9	0.8	0.7	0.6	0.5
Safety Factor (Target Ratio R)	1	1	1	1	1	1
	2	1.36	1.02	1	1	1
	3	2.03	1.53	1.25	1.05	1
	4	2.71	2.05	1.67	1.4	1.19
	5	3.39	2.56	2.09	1.76	1.49
	6	4.07	3.07	2.51	2.11	1.79

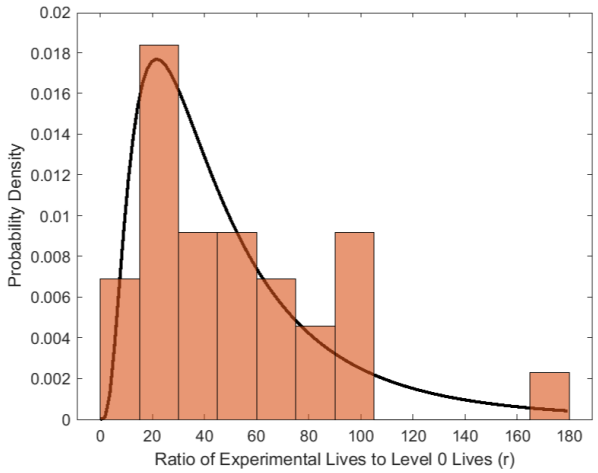

(a) Level 0, Mean. P[r > 1] = 0.99

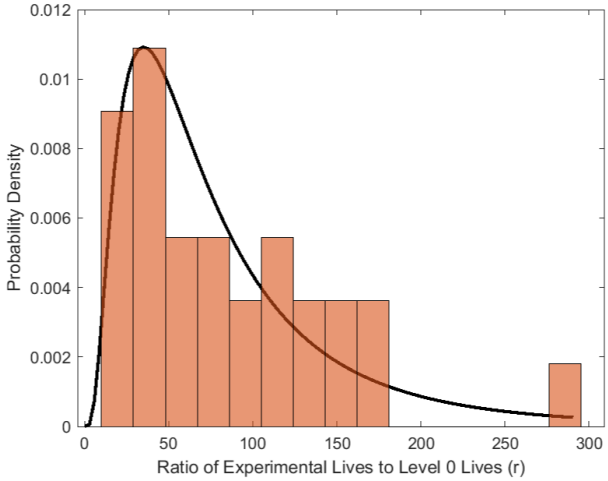

(b) Level 0, Mean -1sd. P[r > 1] = 0.99

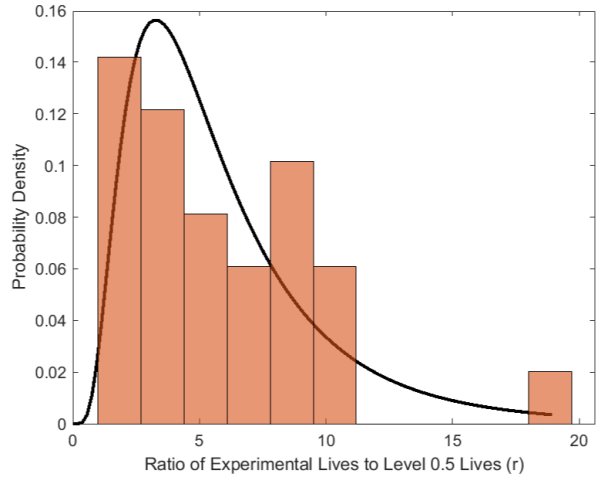

(c) Level 0.5, Mean. P[$r > 1$] = 0.99

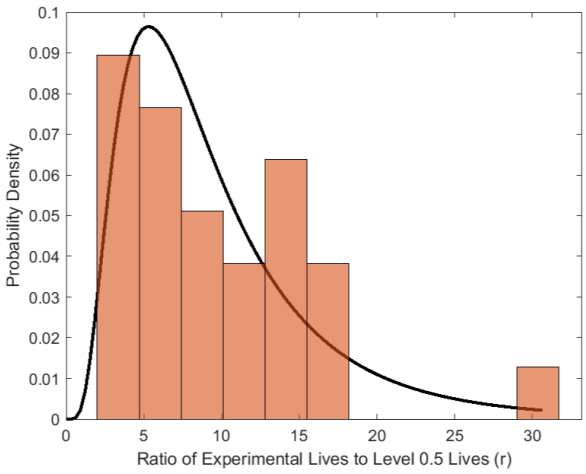

(d) Level 0.5, Mean -1sd. P[$r > 1$] = 0.99

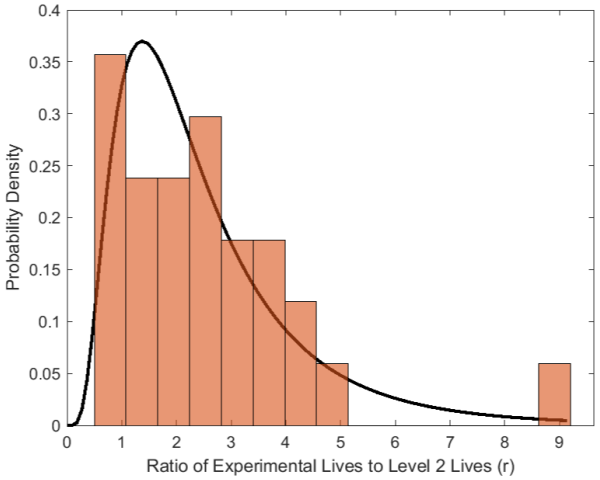

(e) Level 2, Mean. P[$r > 1$] = 0.87

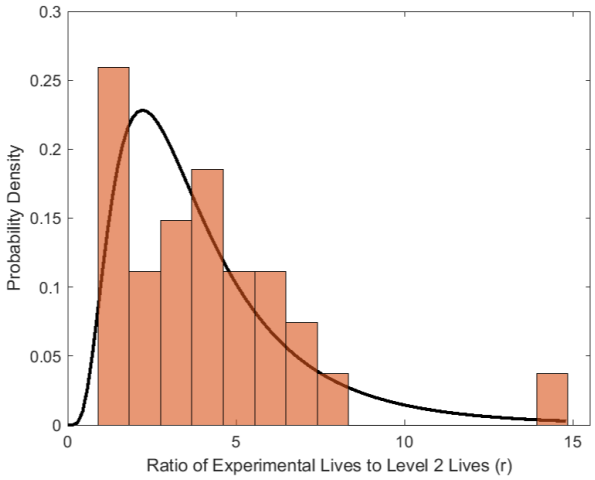

(f) Level 2, Mean -1sd. P[$r > 1$] = 0.97

Figure 36- *r* Ratio Distributions of Various Fatigue Life Estimation Criteria, for Dents Interacting with Metal Loss

6.1.3 Scaling Factors for Fatigue Life Assessment Models Applied to Dents Interacting with Welds

The same process was followed as in the case of plain dents to evaluate the *r* ratio distributions and the scaling factors to obtain minimum target factors of safety. For dents interacting with welds, a fatigue life reduction factor of 10 is applied to the plain dent fatigue life estimates as per API RP 1183 [1]. Besides the application of the fatigue life reduction factor, the remaining steps are same as in plain dents. The *r* ratio distribution plots are presented in Figure 37, and the scaling factor values have been listed in Table 14. Compared to the other cases, the reduction factor of 10 renders the fatigue life estimates very conservative as is evident from the results, where only a few cases require the application of scaling factors to ensure a minimum target factor of safety. Scaling factors were also evaluated by considering a reduction factor of 5 instead of 10. The results are tabulated in Table 15 and appear to be less conservative than for the reduction factor of 10, but the values are still more conservative than for plain dents and metal loss cases. It is to be noted that the maximum reduction in fatigue life due to dent girth weld interaction and dent long seam weld interaction was 6.5X and 1.8X respectively [8].

Table 14- Scaling Factors Associated with Level 0, 0.5 and 2 Dent Fatigue Life Assessment For Dents Interacting with Welds, with a Fatigue Life Reduction Factor of 10 Applied

Level 0, Mean							Level 0, Mean -1sd						
Scaling Factor Matrix		Probability of Exceedance of Target Ratio α					Scaling Factor Matrix		Probability of Exceedance of Target Ratio α				
		0.9	0.8	0.7	0.6	0.5			0.9	0.8	0.7	0.6	0.5
Safety Factor (Target Ratio R)	1	1	1	1	1	1	Safety Factor (Target Ratio R)	1	1	1	1	1	1
	2	1	1	1	1	1		2	1	1	1	1	1
	3	1	1	1	1	1		3	1	1	1	1	1
	4	1	1	1	1	1		4	1	1	1	1	1
	5	1	1	1	1	1		5	1	1	1	1	1
	25	1	1	1	1	1		25	1	1	1	1	1
Level 0.5, Mean							**Level 0.5, Mean -1sd**						
Scaling Factor Matrix		Probability of Exceedance of Target Ratio α					Scaling Factor Matrix		Probability of Exceedance of Target Ratio α				
		0.9	0.8	0.7	0.6	0.5			0.9	0.8	0.7	0.6	0.5
Safety Factor (Target Ratio R)	1	1	1	1	1	1	Safety Factor (Target Ratio R)	1	1	1	1	1	1
	2	1	1	1	1	1		2	1	1	1	1	1
	3	1	1	1	1	1		3	1	1	1	1	1
	4	1	1	1	1	1		4	1	1	1	1	1
	5	1	1	1	1	1		5	1	1	1	1	1
	9	1.07	1	1	1	1		14	1.03	1	1	1	1
Level 2, Mean							**Level 2, Mean -1sd**						
Scaling Factor Matrix		Probability of Exceedance of Target Ratio α					Scaling Factor Matrix		Probability of Exceedance of Target Ratio α				
		0.9	0.8	0.7	0.6	0.5			0.9	0.8	0.7	0.6	0.5
Safety Factor (Target Ratio R)	1	1	1	1	1	1	Safety Factor (Target Ratio R)	1	1	1	1	1	1
	2	1	1	1	1	1		2	1	1	1	1	1
	3	1	1	1	1	1		3	1	1	1	1	1
	4	1	1	1	1	1		4	1	1	1	1	1
	5	1.12	1	1	1	1		5	1	1	1	1	1
	6	1.34	1	1	1	1		8	1.1	1	1	1	1

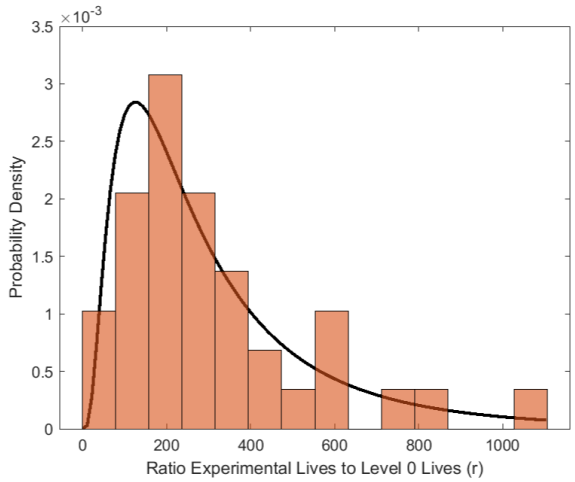

(a) Level 0, Mean. P[$r > 1$] = 0.99

(c)

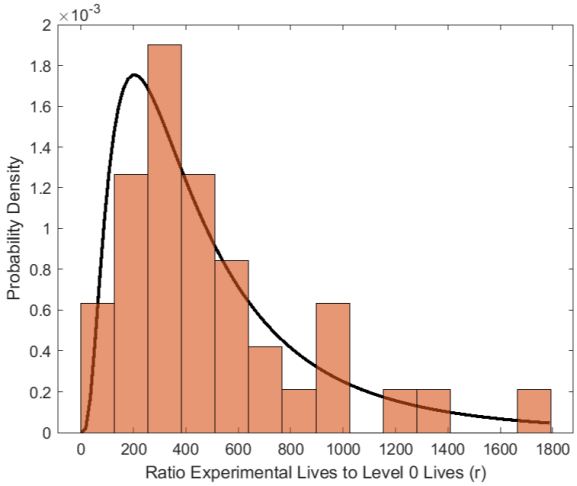

(b) Level 0, Mean -1sd. P[$r > 1$] = 0.99

(d)

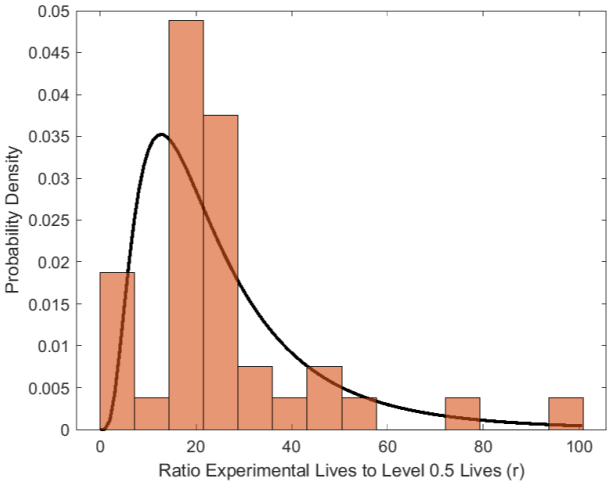

(e) Level 0.5, Mean. P[$r > 1$] = 0.99

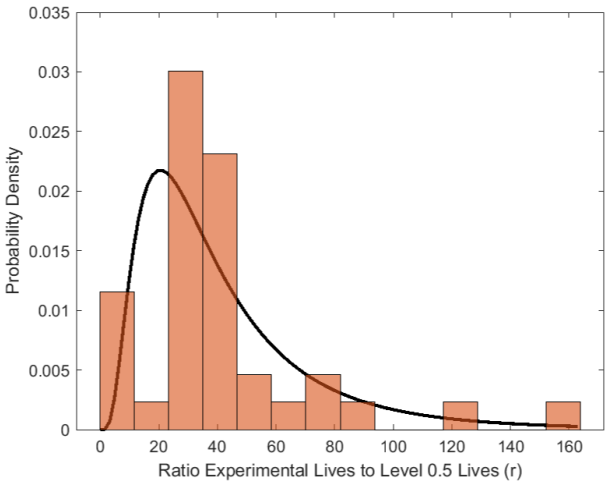

(f) Level 0.5, Mean -1sd. P[$r > 1$] = 0.99

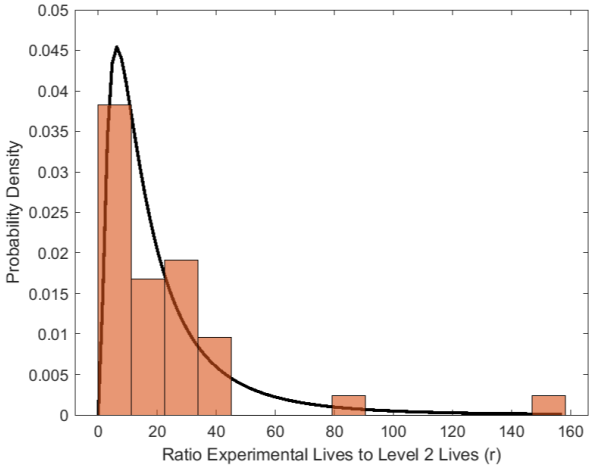

(g) Level 2, Mean. P[$r > 1$] = 0.99

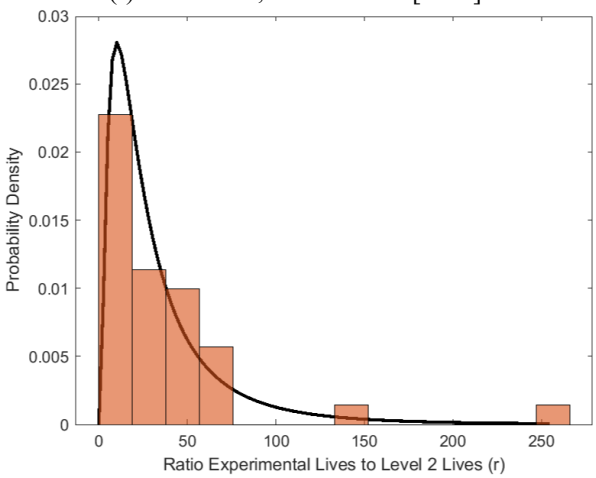

(h) Level 2, Mean -1sd. P[$r > 1$] = 0.99

Figure 37- r Ratio Distributions of Various Fatigue Life Estimation Criteria, for Dents Interacting with Welds

Table 15- Scaling Factors Associated with Level 0, 0.5 and 2 Dent Fatigue Life Assessment For Dents Interacting with Welds, with a Fatigue Life Reduction Factor of 5 Applied

Level 0, Mean						
Scaling Factor Matrix		Probability of Exceedance of Target Ratio α				
		0.9	0.8	0.7	0.6	0.5
Safety Factor (Target Ratio R)	1	1	1	1	1	1
	2	1	1	1	1	1
	3	1	1	1	1	1
	4	1	1	1	1	1
	5	1	1	1	1	1
	25	1	1	1	1	1

Level 0, Mean -1sd						
Scaling Factor Matrix		Probability of Exceedance of Target Ratio α				
		0.9	0.8	0.7	0.6	0.5
Safety Factor (Target Ratio R)	1	1	1	1	1	1
	2	1	1	1	1	1
	3	1	1	1	1	1
	4	1	1	1	1	1
	5	1	1	1	1	1
	25	1	1	1	1	1

Level 0.5, Mean						
Scaling Factor Matrix		Probability of Exceedance of Target Ratio α				
		0.9	0.8	0.7	0.6	0.5
Safety Factor (Target Ratio R)	1	1	1	1	1	1
	2	1	1	1	1	1
	3	1	1	1	1	1
	4	1	1	1	1	1

Level 0.5, Mean -1sd						
Scaling Factor Matrix		Probability of Exceedance of Target Ratio α				
		0.9	0.8	0.7	0.6	0.5
Safety Factor (Target	1	1	1	1	1	1
	2	1	1	1	1	1
	3	1	1	1	1	1
	4	1	1	1	1	1

	5	1.19	1	1	1	1		**Ratio R)**	**5**	1	1	1	1	1
	6	1.42	1.05	1	1	1			**7**	1.03	1	1	1	1
Level 2, Mean								**Level 2, Mean -1sd**						
Scaling Factor Matrix		**Probability of Exceedance of Target Ratio α**						**Scaling Factor Matrix**		**Probability of Exceedance of Target Ratio α**				
		0.9	**0.8**	**0.7**	**0.6**	**0.5**				**0.9**	**0.8**	**0.7**	**0.6**	**0.5**
Safety Factor (Target Ratio R)	**1**	1	1	1	1	1		**Safety Factor (Target Ratio R)**	**1**	1	1	1	1	1
	2	1	1	1	1	1			**2**	1	1	1	1	1
	3	1.34	1	1	1	1			**3**	1	1	1	1	1
	4	1.79	1.19	1	1	1			**4**	1.1	1	1	1	1
	5	2.23	1.49	1.11	1	1			**5**	1.38	1	1	1	1
	6	2.68	1.79	1.33	1.04	1			**6**	1.65	1.1	1	1	1

6.1.4 Additional Information Regarding Fatigue Life Estimates

The evaluation of Level 0 and 0.5 fatigue life estimates involves the prediction of stress magnification factors to predict the fatigue life estimates based on BS 7608 mean S-N as per API RP 1183 [1]. The Level 2 assessment model was formulated using the BS 7608 mean -1sd S-N curve and directly predicts the fatigue life estimate based on that S-N curve. In order to obtain a Level 2 fatigue life estimate based on the BS 7608 mean S-N curve, the original output must be multiplied by 1.62. The scaling factors and *r* ratio distribution for Level 2 with mean S-N curve were evaluated using this technique.

It is noted that the S-N curves employed in the development of the fatigue life modelling approaches are selected such that they mathematically are a lower bound to the full-scale test data, rather than suggesting that the BS 7608 structural class applies to the full-scale test data.

7 Sample Estimation of Fatigue Life and Effective Strain

Sample calculations of various fatigue life estimation methodologies and effective strain assessments were carried out as part of this project. The detailed sample calculations of Level 0 and Level 0.5 dent fatigue life screening approach, Level 2 dent fatigue life assessment, ASME B31.8 Appendix R Strain, "Blade Energy Partners Simplified Model" Strain and BMT Modified ASME Strain have been presented in Appendix A. For the sample application of dent fatigue life screening and assessment, geometry information of a dent has been provided and along with the characteristic length and areas evaluated as per API RP 1183. Sample pressure loading has also been provided where applicable. For the strain evaluations, the axial and transverse profile of a dent have been provided and this information is applied in the calculation of the three strain formulations. The process involves curve fitting of the dent peak region, evaluation of slopes, curvatures and arc lengths of the dent peak region and application of the evaluated values into the strain formulations to calculate the effective strains.

8 Concluding Remarks

The present study builds on mechanical damage (MD) assessment and management tools, developed over several years and incorporated in API RP 1183 [1]. The current project enhances previously developed tools being adopted in an industry recommended practice (API RP 1183) for pipeline MD integrity assessment and management. Three main tasks of the project were to assess and

improve the indentation strain prediction models, to assess the effect of ILI data variability on fatigue life and strain estimations and to develop safety factors regarding fatigue life estimation.

Indentation Strain

- Comparisons between FE dent indentation strains and strain estimates using predictive models (ASME B31.8 Appendix R and Blade Energy Partners Simplified Model) were carried out. The comparisons were performed using a large data set of dents comprising of field dents, in-service field dents and hypothetical dents.
- The prediction results for ASME strains were found to agree well with the FE strains for restrained dents except in cases of deep (>6%OD) dents with radius of curvature less than 200 mm. The deficiency in the ASME strain model was concluded to be due to the absence of circumferential membrane strain and use of inappropriate constant used in the axial membrane strain formulation.
- The prediction results for Blade Energy Partners Simplified Model were found to agree well with the FE strains for restrained dents.
- ASME strain and Blade strain methodology does not work for unrestrained dents. This was owing to the change in shape experienced by the unrestrained dents due to dent re-rounding after indenter removal and under pressure.
- A modified ASME strain model was proposed consisting of modifications made to the original axial membrane strain formulation and a circumferential membrane strain formulation developed along similar lines to the axial membrane strain model. The BMT Modified ASME strain estimates were compared against the FE strains and were found to be in good agreement across all restrained dents.
- A prediction model was developed to predict indentation strains for unrestrained dents for ASME and BMT Modified ASME formulations.
- DFDI model was compared against full-scale test data. Based upon the least conservative (critical strain (ε_0) = 0.5, DFDI cracking limit = 1) and the most conservative options (critical strain (ε_0) = 0.3, DFDI cracking limit = 0.6) 0 out of 47 or 16 out of 47 tests were predicted to have cracks during indentation based on Blade formulation.
- Strain limit criterion of 6% in ASME B31.8 Appendix R is very conservative. Full scale indentation strain data was compared against ASME B31.8 Appendix R strain limit criterion and predicted 32 out of 47 tests exceeded the 6% strain limit.

Impact of Variation in Dent Shape on Fatigue Life and Strain Estimation

The following summarizes the results of generalized variation schemes in dent shapes implemented in the current project and is not associated with any tool specifications.

- Monte Carlo simulations where ILI dent shapes were randomized and estimates of fatigue life and strain were evaluated for the family of variations of each dent. Additionally, the fatigue life and strain estimates were evaluated using the reference data and ILI data from pull trials carried out by multiple vendors across the same set of dents. This allowed the comparison of estimates from the actual dent shape measurements against estimates made using sample measurements from multiple ILI Service Providers, made across multiple pulls.

- In Monte Carlo simulations for restrained dents the average coefficient of variation of fatigue life estimate ranged between 3% - 17%. The maximum variation in fatigue life was induced by depth, length and width variation scheme with standard deviation of 20% (average coefficient of variation 15% - 17%). Maximum variation in fatigue life was induced by depth variation scheme (average coefficient of variation 3% - 13%) when compared to variation schemes where the dimensions were varied individually, indicating the higher sensitivity to depth in fatigue life estimation of restrained dents.
- In Monte Carlo simulations for unrestrained dents the average coefficient of variation of fatigue life estimate ranged between 12% - 34%. The maximum variation in fatigue life was induced by combined depth, length and width variation scheme with standard deviation of 20% (average coefficient of variation 32% - 34%). Maximum variation in fatigue life was induced by depth variation scheme (average coefficient of variation 22% - 23%) when compared to variation schemes where the dimensions were varied individually, indicating the higher sensitivity to depth in fatigue life estimation of un-restrained dents.
- In Monte Carlo simulations for ASME strain estimates the average coefficient of variation ranged between 9% - 51%. The maximum variation in strain estimates was induced by depth, length and width variation scheme with standard deviation of 20% (average coefficient of variation 45% - 51%). Maximum variation in strain estimates was induced by width variation scheme (average coefficient of variation 29% - 44%) when compared to variation schemes where the dimensions were varied individually, indicating the higher sensitivity to width in strain estimation.
- In Monte Carlo simulations for modified ASME strain estimates the average coefficient of variation ranged between 9% - 52%. The maximum variation in strain estimates was induced by depth, length and width variation scheme with standard deviation of 20% (average coefficient of variation 46% - 52%). Maximum variation in strain estimates was induced by width variation scheme (average coefficient of variation 29% - 44%) when compared to variation schemes where the dimensions were varied individually, indicating the higher sensitivity to width in strain estimation.
- Strain estimates were more sensitive to dent shape variation as compared to fatigue life estimates.
- The statistical measure of variation for the fatigue life and strain estimates using dent data from pull trials agreed very well with the Monte Carlo simulations. The majority of dents had coefficient of variation within 40% and 60% for fatigue life estimates and strain estimates, respectively. This agreement validated the approach taken to simulate variability of fatigue life estimate and strain estimate due to variation of dent shapes.

Safety Factor Quantification

- Quantification of safety factors associated with fatigue life estimation was accomplished by compiling safety factor histograms using full-scale dent experimental and estimated fatigue life values. Lognormal probability distributions were fitted onto the safety factor histograms and these distributions were scaled to achieve the required safety factor at a specified probability of exceedance. The process was carried out for fatigue life estimation for plain dents, dents interacting with welds and dents interacting with corrosion.

- Safety factors and associated confidence levels were derived for fatigue life screening (Level 0 and Level 0.5) and Level 2 fatigue life estimation approaches for plain dents and dents interacting with weld and corrosion.
- Safety factors were also derived for Level 2 approach using mean BS7608 S-N curve instead of recommended BS7608 mean -1sd S-N curve. The users can then select the scale factors to scale predicted lives based on desired safety factors and confidence levels. This allows for consistency (using same S-N curve) in Level 0, Level 0.5 and Level 2 approaches.
- Safety factors for dents interacting with welds were reevaluated using fatigue life reduction factor of 5 instead of recommended fatigue life reduction factor of 10. Using a lower fatigue life reduction factor of 5 still allows for a safety factor of 5 at 80% confidence level. Having this option allows the users to select the scaling factors based on their desired safety factors and associated confidence level especially for the cases in long seam welds that are known to be free of defects.

9 Recommendations

- Further work is required to define the critical strain values for pipeline steels and address the conservatism in ASME B31.8 Appendix R 6% strain limit criteria.
- Fatigue life reduction factor of 10, as recommended in API RP 1183, in dent weld interaction leads to very conservative fatigue life estimates and further work is required to address the conservatism.
- Safety factor calculations in the current project were carried out for plain dents using combined experimental data for restrained dents and unrestrained dents. Further work is required to explore the differences between the two dent restraint conditions as experimental data suggests restrained dents have much longer fatigue lives as compared to unrestrained dents.

10 Acknowledgements

BMT would like to acknowledge the support provided for this project by US DOT and PRCI. Special thanks to PRCI MD SRP team for their support during this project.

11 Referenced Publications

[1] American Petroleum Institute, *API RP 1183, Assessment and Management of Dents in Pipelines,* API, 2020.

[2] American Society of Mechanical Engineers, *ASME B31.8-2018, Gas Transmission and Distribution Piping System,* ASME, 2018.

[3] R. W. Revie, Oil and Gas Pipelines: Integrity and Safety Handbook, John Wiley & Sons, 2015.

[4] M. Gao, R. Krishnamurthy, S. Tandon and U. Arumugum, "Critical Strain Based Ductile Damage Criterion and its Application to Mechanical Damage in Pipelines," *13th International Conference on Fracture,* 2013.

[5] M. Gao, R. McNealy, R. Krishnamurthy and I. Colquhoun, "Strain-Based Models for Dent Assessment – A Review," *ASME 7th International Pipeline Conference,* 2008.

[6] S. A. Lukasiewicz, J. A. Czyz, C. Sun and S. Adeeb, "Calculation of Strains in Dents Based on High Resolution In-Line Caliper Survey," *ASME 6th International Pipeline Conference,* 2006.

[7] M. J. Rosenfeld, P. C. Porter and J. A. Cox, "Strain Estimation Using Vecto Deformation Tool Data," *ASME 2nd International Pipeline Conference,* 1998.

[8] S. Tiku, V. Semiga, A. Dinovitzer and B. John, "Full Scale Fatigue Testing of Dents (Plain Dents and Dents Interacting with Welds and Metal Loss) MD4-2," PRCI Catalog No. PR-214-073510-R01, 2018.

[9] S. Tiku, A. Eshragi, B. John and A. Dinovitzer, "Full Scale Testing of Interactive Features for Improved Models," US DOT PHMSA DTPH56-14-H-00002, 2017.

[10] S. Tiku, A. Eshragi, B. John and A. Dinovitzer, "Full Scale Testing of Shallow Dents with and without Interacting Features MD4-14," PRCI Catalog No. PR-214-163714, 2019.

[11] MATLAB, "Solve Nonlinear Least-Squares (Nonlinear Data-Fitting) Problems," [Online]. Available: www.mathworks.com/help/optim/ug/lsqnonlin.html. [Accessed 7 September 2020].

[12] S. Tiku, A. Eshragi, A. Rana and A. Dinovitzer, "Fatigue Life Assessment of Dents with and without Interacting Features MD4-9," PRCI Catalog No. PR-214-114500-R01.

[13] E. A. de Souza Neto, D. Perić and D. R. J. Owen, Computational Methods for Plasticity: Theory and Applications, John Wiley & Sons, 2008.

[14] U. Arumugum, M. Gao and R. Krishnamurthy, "Study of a Plastic Strain Limit Damage Criterion for Pipeline Mechanical Damage Using FEA and Full-Scale Denting Tests," *International Pipeline Conference,* 2016.

[15] MATLAB, "Normal random numbers," [Online]. Available: https://www.mathworks.com/help/stats/normrnd.html. [Accessed 2 1 2022].

[16] A. Rana, S. Tiku and V. Semiga, "Management of Dents," CEPA, 2021.

[17] I. D. Faux and M. J. Pratt, Computational Geometry for Design and Manufacture, Horwood, 1987.

Appendix A - Sample Calculations

This section includes sample calculations for restraint parameter, Levels 0, 0.5, 1 and 2 for dent fatigue life assessment as incorporated in API RP 1183 document and dent strain assessment based on ASME B31.8 effective strain, "Blade Energy Partners Simplified Model" effective strain and modified ASME effective strain.

A1. Restraint Parameter Calculation, Level 0 and Level 0.5 Dent Screening and Level 2 Dent Fatigue Life Estimation Examples

The following provides details of the sample calculations for restraint parameter evaluations and Level 0 and Level 0.5 dent fatigue life assessment developed in CEPA sponsored project and adopted in API RP 1183 recommended practice document.

The procedures detailed below are applicable to plain unrestrained, shallow restrained and deep restrained dents, with use of the appropriate equations. In addition, restrained parameter calculation to assess restraint condition of the dent is also included. Dent restraint condition needs to be determined prior to performing any of the CEPA/PRCI fatigue life assessment as incorporated in API RP 1183.

A1.1 Example 1: Restraint Parameter Calculation

The BMT Restraint Parameter (RP) is a metric that can be used to estimate the restraint condition of a dent feature based on the characteristic lengths and areas obtainable from the ILI data. The restraint parameter equation is given by,

$$RP = max\left\{\frac{18 * \left|A_{15\%}^{AX} - A_{15\%}^{TR}\right|^{1/2}}{L_{70\%}^{TR}}, 8 * \left(\frac{L_{15\%}^{AX}}{L_{30\%}^{AX}}\right)^{1/4} * \left(\frac{L_{30\%}^{AX} - L_{50\%}^{AX}}{L_{80\%}^{TR}}\right)^{1/2}\right\} \qquad \text{(A.1)}$$

The restraint parameter defined above is a dimensionless parameter. A dent with RP value greater than 20 is a restrained dent and a dent with RP value below 20 is an unrestrained dent. The RP should be evaluated for all four combinations of the upstream (US)/downstream (DS) axial profiles with the clockwise (CW)/counterclockwise (CCW) transverse profiles (i.e., combinations of the US/CW, US/CCW, DS/CW, and DS/CCW profiles). The maximum RP from the four combinations should be adopted as the restraint parameter value. The other option is to estimate fatigue lives based on both the restrained and un-restrained equations if the restraint parameter is between 15-25 and determine minimum fatigue life.

Figure A.1 and Figure A.2 show dent axial and transverse profiles extracted from ILI data. The dent characteristic lengths and areas are listed in Table A.1. To evaluate whether the given dent is a restrained or unrestrained dent, Equation 11.1 needs to be evaluated for all four combinations of DS/US/CW/CCW as follows.

Table A.1 - Characteristic Length and Area of the Example Dent

	OD (inch)	WT (inch)	Depth (mm)	Depth (%OD)				
	32	0.281	28.5	3.51%				
Axial	5%	10%	15%	30%	50%	75%	85%	90%
DS Length (mm)	1262	1000	860	540	315	160	115	100
US Length (mm)	1290	990	840	520	260	125	80	55
DS Area (mm²)	23322	16771	12890	5875	2077	431	175	
US Area (mm²)	24304	17009	13463	6341	1921	412	160	
Transverse	15%	30%	50%	70%	75%	80%	85%	90%
CW Length (mm)	150	130	86	52	47	41	33	25
CWW Length (mm)	221	178	138	104	95	85	74	63
CW Area (mm²)	1735	1303	578		136		63	
CCW Area (mm²)	2291	1339	657		201		85	

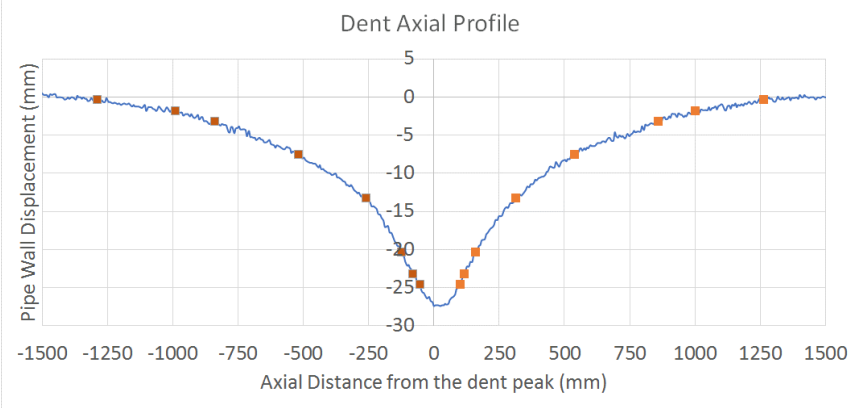

Figure A.1 - Hypothetical Dent Axial Profile

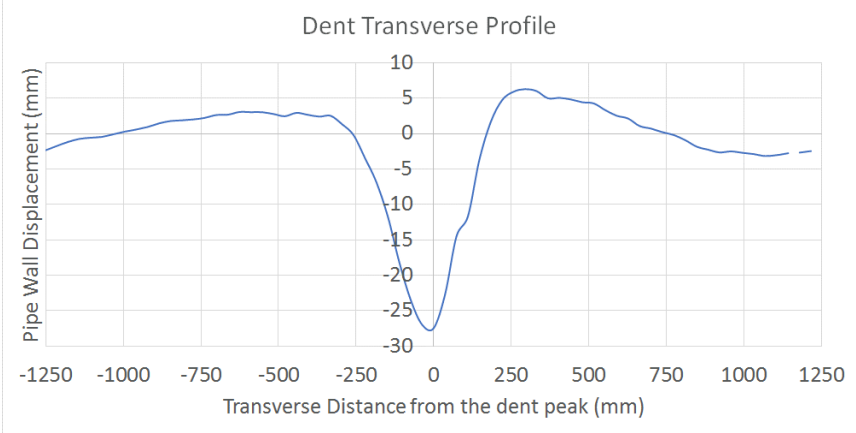

Figure A.2 - Hypothetical Dent Transverse Profile

$$RP^{US/CW} = max\left\{\frac{18 * |13463 - 1735|^{1/2}}{52}, 8 * \left(\frac{840}{520}\right)^{1/4} * \left(\frac{520 - 260}{41}\right)^{1/2}\right\} = max(37.49, 22.71) = 37.49$$

$$RP^{US/CCW} = max\left\{\frac{18 * |13463 - 2291|^{1/2}}{104}, 8 * \left(\frac{840}{520}\right)^{1/4} * \left(\frac{520 - 260}{85}\right)^{1/2}\right\} = max(18.29, 15.77) = 18.29$$

$$RP^{DS/CW} = max\left\{\frac{18 * |12890 - 1735|^{1/2}}{52}, 8 * \left(\frac{860}{540}\right)^{1/4} * \left(\frac{540 - 315}{41}\right)^{1/2}\right\} = max(36.56, 21.05) = 36.56$$

$$RP^{DS/CCW} = max\left\{\frac{18 * |12890 - 2291|^{1/2}}{104}, 8 * \left(\frac{860}{540}\right)^{1/4} * \left(\frac{540 - 315}{85}\right)^{1/2}\right\} = max(17.82, 14.62) = 17.82$$

The maximum value of the RP from all the 4 combinations is 37.49 which is greater than 20. Therefore, the dent under consideration is a restrained dent. As discussed earlier, the other option is to estimate fatigue lives based on both the restrained and un-restrained equations, if the restraint parameter is between 15-25 and determine minimum fatigue life.

To evaluate whether the dent is shallow restrained or deep restrained dent, the criterion presented in PRCI MD 4-9 project and API 1183 can be applied as follows.

The shallow restrained dent criterion states that: for pipe ODs less than 12.75" the dent is a shallow restrained dent if its depth is less than 4% OD. For pipe ODs above 13 inches the dent is a shallow restrained dent if its depth is less than 2.5% OD. For the dent in this example the pipe OD is greater than 13" and the dent depth is 3.51% OD. Therefore, the dent in this example is a **deep restrained** dent.

A1.1.1 Example 2: Level 0 Dent Screening

BMT has developed conservative approaches for screening dents as fail/pass. A "pass" indicates dent meets the integrity requirement whereas a "fail" means next level integrity assessment needs to be performed. It should be mentioned that a Level 0 "fail" flag does not mean that the dent possesses an integrity issue, but it requires further investigation based on the next level integrity assessment.

For deep restrained dents, the maximum stress magnification factor K_M^{Max}, can be related to the pipe geometry, OD/t, [16]

$$K_M^{Max} = 0.1071 * \left(\frac{OD}{t}\right) + 0.1332 \quad \text{(A.2)}$$

Consider the deep restrained dent with the pipe geometry listed in Table A.1. Assume that the dent has seen one cycle of hydrotest pressure (90% P_{SMYS}) since it was formed. The pressure severity spectrum indicator (SSI) for this line is 100 cycles. The maximum K_M^{Max} that can exist in this line for deep restrained dents is given by Equation (A.2).

$$K_M^{Max} = 0.1071 * \left(\frac{32}{0.281}\right) + 0.1332 = 12.4$$

For class D mean curve $\log_{10} C = 12.6007$ and $m = 3$. For a target life of $Y = 150$ years and the line operational pressure $SSI = 100$, the $K_M^{Allowable}$ is calculated as follows using Equation *(A.3)*,

$$K_M^{Allowable} = 10^{[(log_{10} C - log_{10}(SSI*Y)]/m}/90 \quad (A.3)$$

$$K_M^{Allowable} = 10^{[(12.6007 - log_{10}(100*150)]/3}/90 = 7.14$$

The dent $K_M^{Max} > K_M^{Allowable}$; therefore, it fails the Level 0 integrity assessment for the given operational pressure $SSI = 100$ and the target life of $Y = 150$ based on the BS7608 Class D mean curve. This warrants further investigation based on higher levels of integrity assessments.

A1.1.2 Example 3: A.3 Level 0.5 Dent Assessment

The Level 0.5 assessment is similar to the Level 0 assessment, but with a lower level of conservatism. It includes the effect of pressure range in evaluating the maximum stress magnification factor.

Consider again the deep restrained dent from the previous examples (Table A.1). Let us assume that the dent is on a X52 grade pipe ($\sigma_{SMYS} = 358$ MPa). The detailed pressure data for this line is listed in Table A.2 It is assumed that there are only 3 pressure ranges in the loading spectrum. Using the BS7608 Class D mean S-N curve, it is desired to evaluate if the dent meets a target life of $Y_{targ} = 150$ years. The SSI of the given pressure cycle is 100 cycles per year.

Table A.2 - Pressure Cycles for Level 0.5 Assessment

Cycle #	P_{min} (psi)	P_{max} (psi)	P_{min} (%P_{SMYS})	P_{max} (%P_{SMYS})	ΔP (%P_{SMYS})	P_{mean} (%P_{SMYS})	No of cycles per year (n)
1	90	180	10	20	10	15	90
2	180	365	20	40	20	30	40
3	270	550	30	60	30	45	40

It was observed in Example 2 in Section A1.1.1 that for a target life of 150 years, Level 0 assessment yielded $K_M^{Max} > K_M^{Allowable}$, hence, the dent failed Level 0 assessment. This necessitated the next level of integrity assessment.

To perform the Level 0.5 screening for this dent, Equation (A.4) shown below must be used for the calculation of the maximum K_M^{Max} for each pressure range [16].

$$K_M^{Max} = a_2 * \Delta P^2 + a_1 * \Delta P + a_0 \quad (A.4)$$

For OD/t = 32/0.281 = 114, the coefficients are reproduced below in Table A.3. The specific row from which the coefficients have been extracted, has been highlighted in Table A.3.

Table A.3 - Quadratic Function Constants for Equation (A.4) for Various the Pipe Geometries

OD (in)	WT (in)	OD/t	a2	a1	a0
4.5	0.188	24	-2.4E-05	-0.00196	2.577475
6.625	0.188	35	-0.00034	0.008566	3.409317
8.625	0.218	40	-4.6E-05	-0.02301	4.610979
10.75	0.188	57	0.000447	-0.10299	7.817281
12.75	0.312	41	-0.00011	-0.01147	4.285955
16	0.218	73	0.000582	-0.13666	9.686782
18	0.312	58	0.000164	-0.06131	6.527629
20	0.281	71	0.000559	-0.10867	7.901048
24	0.25	96	0.002017	-0.2779	12.79732
24	0.281	85	0.001622	-0.2372	11.81594
30	0.25	120	0.003232	-0.41884	16.74678
32	0.281	114	0.003184	-0.41642	16.77947
36	0.281	128	0.002118	-0.29807	13.62747
42	0.42	100	0.003223	-0.42328	17.11699

For $\Delta P = 10\%\ P_{SMYS}$:

$$K_M^{Max} = 0.003184 * (10)^2 - 0.41642 * (10) + 16.77947 = 12.9$$

Similarly, for $\Delta P = 20\%\ P_{SMYS}$:

$$K_M^{Max} = 0.003184 * (20)^2 - 0.41642 * (20) + 16.77947 = 9.7$$

And for $\Delta P = 30\%\ P_{SMYS}$:

$$K_M^{Max} = 0.003184 * (30)^2 - 0.41642 * (30) + 16.77947 = 7.1$$

The corresponding maximum stress range for each pressure cycle can be obtained using the following equation:

$$\Delta S^{Max} = K_M^{Max} * (\Delta P/100) * \sigma_{SMYS}$$

Knowing that for grade X52 line $\sigma_{SMYS} = 358$ MPa.

$$\Delta P = 10\%\ P_{SMYS} \rightarrow \Delta S^{Max} = 12.9 * (0.1) * 358 = 462\ MPa$$
$$\Delta P = 20\%\ P_{SMYS} \rightarrow \Delta S^{Max} = 9.7 * (0.2) * 358 = 695\ MPa$$
$$\Delta P = 30\%\ P_{SMYS} \rightarrow \Delta S^{Max} = 7.1 * (0.3) * 358 = 763\ MPa$$

Once the maximum stress range for each pressure cycle is calculated the accumulated damage associated to each pressure cycle bin can be calculated as follows:

$$D_i = n_i/N_i$$

where $N_i = 10^{(\log_{10} C - m*\log_{10} \Delta S_i^{Max})}$. For the BS7608 Class D mean S-N curve, $\log_{10}$ C=12.6007 and m=3. Therefore, the 1-year cumulative damage for the given pressure spectrum is given by,

$$D_{total} = D_1 + D_2 + D_3 = \frac{90}{10^{(12.6007-3\,log_{10}\,462)}} + \frac{40}{10^{(12.6007-3\,log_{10}\,695)}} + \frac{40}{10^{(12.6007-3\,log_{10}\,763)}}$$

$$D_{total} = 0.01003$$

Therefore, the total fatigue life of this dent is given by $Y_{total} = 1/D_{total} = 100$ years. Because Y_{total} is less than the target life of $Y_{targ} = 150$ years, the dent fails the Level 0.5 screening assessment. Table A.4 summarizes the above calculations in a tabulated format. Therefore, the next integrity assessment level needs to be considered.

Table A.4 - Calculated Level 0.5 Maximum Stress Magnification Factor for Example 3

Sl. no	ΔP (%P_{SMYS})	No of cycles per year (n)	ΔS_{nom} (Mpa)	K_M^{Max}	ΔS_i (Mpa)	N_i	D_i
1	10	90	35.3	12.9	462	40484	0.00222
2	20	40	72.6	9.7	695	11903	0.00336
3	30	40	109.9	7.1	763	8993	0.00445
						D_{total}	0.01003
						$Y_{total} = \frac{1}{D_{total}}$ (years)	**100**

A1.1.3 Example 4: Level 2 Dent Assessment

The Level 2 assessment [12] is the least conservative fatigue life assessment method, which utilizes the dent geometric information in form of the characteristic lengths and areas of axial and transverse profiles and pressure loading history to predict the dent fatigue life.

The same dent used in Example 3 is employed here (OD 32 in, t 0.312 in, Grade X52). The characteristic lengths and areas are listed in Table A.1. The dent is subjected to pressure loading listed in Table A.2 . Level 2 fatigue life prediction Equation (A.5) consists of a dimensionless parameter called shape parameter (*SP*), which is calculated using the dent geometry, pipe material grade and pressure loading information, along with coefficients (*A* and *B*) which depend on the cyclic pressure loading. The output of Equation (A.5) is the number of cycles to failure. The equation has been developed using the BS7608 Class D mean -1SD S-N curve,

$$N = A\,(SP)^B \qquad \text{(A.5)}$$

The formulation of *SP* depends on the restraint condition of the dent and dent depth (for restrained dent). For deep restrained dents the formulation of *SP* is as given below,

$$PF = (Pmean * \Delta P/P_{SMYS}^2)^{1/3} \qquad \text{(A.6)}$$

$$R = -2.3053 * PF + 1.5685 \quad \text{(A.7)}$$

$$G_{SF} = \left[\frac{\sigma_{SMYS}\ (MPa)}{358}\right]^{M} \quad \text{(A.8)}$$

$$x_L = \left[\frac{\sqrt{A^{AX}_{30\%} * A^{AX}_{75\%}}}{t * L^{AX}_{75\%}}\right]^{3/2} * \left(\frac{L^{AX}_{75\%}}{L^{TR}_{75\%}}\right)^{1/2}$$
$$x_H = \left[\frac{A^{AX}_{10\%}}{L^{AX}_{10\%} * L^{AX}_{75\%}}\right]^{3/4} * \left(\frac{L^{TR}_{75\%}}{L^{AX}_{75\%}}\right) \quad \text{(A.9)}$$

$$SP = [R * x_L + +(1 - R) * x_H] * G_{SF} * (OD/t)^{0.25} \quad \text{(A.10)}$$

For the deep restrained dent under consideration (Table A.1) and pressure cycle 1 from Table A.2 , the sample calculation of Equations (A.5) to (A.10) is given below. Since the dent under consideration is an asymmetric dent, 4 combinations of x_L and x_H parameters can be evaluated and 4 values of number of cycles to failure can be obtained from Equation (A.5). The smallest value of N is then adopted as the most conservative option. Here, the calculations for US-CW combination from Table A.1 has been demonstrated.

For pressure cycle 1,

Pmax = 20% P_{SMYS}, Pmin = 10% $P_{SMYS,}$ Pmean = 15% P_{SMYS}, Prange = 10% P_{SMYS}

$$PF = (15 * 10/100^2)^{1/3} = 0.2466$$

$$R = -2.3053 * 0.2466 + 1.5685 \approx 1$$

For restrained dents M = 4,

$$G_{SF} = \left[\frac{358}{358}\right]^4 = 1$$

Taking the characteristic length and area values for US and CW from Table A.1,

$$x_L = \left[\frac{\sqrt{6341 * 412}}{7.9248 * 125}\right]^{3/2} * \left(\frac{125}{47}\right)^{\frac{1}{2}} = 3.399$$

$$x_H = \left[\frac{17009}{990 * 125}\right]^{3/4} * \left(\frac{47}{125}\right) = 0.0848$$

$$SP = [1 * 3.399 + +0 * 0.0848] * 1 * \left(\frac{812.8}{7.9248}\right)^{0.25} = 10.81$$

For deep restrained dents under cyclic pressure loading of Pmax = 20% P_{SMYS}, Pmin = 10% $P_{SMYS,}$ the coefficients of Equation (A.5) are,

$$A = 10^{6.0873}$$

$$B = -0.773$$

$$N = 10^{6.0873} * (10.81)^{-0.773} = 194085$$

$$N^{US\ CW} = 10^{6.0873} * (10.81)^{-0.773} = 194085$$

Similarly, the number of cycles to failure for the other combinations are as follows,

$$N^{US\ CCW} = 254746$$

$$N^{DS\ CW} = 239181$$

$$N^{DS\ CCW} = 313937$$

Since the value of US-CW combination is the lowest, it is taken as the value of N. Since the number of cycles per year of pressure cycle 1 is 90, the damage incurred due to this pressure loading throughout the year is,

$$D_1 = \frac{n_1}{N_1} = \frac{90}{194085} = 0.000464$$

The damage incurred under pressure cycles 2 and 3 can be evaluated, following the procedure described above. The damage values are as given below,

$$D_2 = 0.000643$$

$$D_3 = 0.0013$$

Therefore, the total damage is D_{total} = 0.000464 + 0.000643 + 0.0013 = 0.002407 and the total fatigue life of the dent is,

$$Y_{total} = \frac{1}{D_{total}} = \frac{1}{0.002407} = 415\ years$$

A1.1.4 Effect of Pipe Grade on Fatigue Life Screening and Estimation

Pipe grade information in form of SMYS is required for the screening and fatigue life estimation methods presented earlier. Level 0 screening analysis does not require pipe grade information. For Level 0.5, the cyclic pressure range is required to be input in form of percentage of PSMYS (pressure that would induce nominal hoop stress equal to SMYS. For Level 2, the coefficients in the Equation A.5 are chosen based on cyclic minimum and maximum pressure in form of percentage of PSMYS (rounded to multiples of 10). Additionally, the effect of material grade is also introduced into the SP formulation in form of the Grade Scale Factor (G_{SF}), Equation A.8. The regression models, where applicable, were created using nominal pressure inputs in form of percentage of PSMYS and the SMYS information is required to translate the pressure information back into absolute values.

A1.2 Sample Effective Strain Calculations

The effective strain measure provided in ASME B31.8, can be used as a measure of ductile damage incurred in a dent. The measure requires the input of dent axial and transverse profile curvatures, dent length and depth, to calculate a scalar strain measure similar to the accumulated plastic strain formulation. The process of evaluating these quantities from dent ILI Caliper data is given in the following paragraphs.

For the initial step, the geometry data of the axial and circumferential profile through the dent apex should be extracted (Figure A.3 and Figure A.4). The circumferential profile has to be mapped onto the polar coordinate system to simplify the curve fitting process (Figure A.4 (b)). The axial (z) and angular (θ) should be offset so that the dent peaks are at zero for both axial and transverse profiles. Then a span of points about the dent apex has to be extracted for curve fitting, from the axial profile. The span was centered on the dent apex and extended up to the upstream and downstream points corresponding to 85% dent depth, as per the dent depth points used to extract characteristic lengths and areas for fatigue life estimation. Similar process should be repeated for the circumferential profile in the polar coordinate system. The ends of the span corresponded to the 85% dent depth clockwise and counterclockwise points, and the span was centered at the dent peak. The 85% dent depth points were used because these points are close to the peak and the resulting spans capture the shape of the peak region well. Fourth order polynomials (Equations (A.11) and (A.12)) were fitted to the axial and circumferential spans. The degree of polynomials depends on the goodness of fit. A good fit was achieved using 4th order polynomials in this example (Figure A.5 and Figure A.6). The polynomials used for axial and circumferential profiles are as follows,

$$y = b_0 + b_1 z + b_2 z^2 + b_3 z^3 + b_4 z^4 \quad \text{(A.11)}$$

$$r = c_0 + c_1 \theta + c_2 \theta^2 + c_3 \theta^3 + c_4 \theta^4 \quad \text{(A.12)}$$

The Trendline function in Excel graphing tool can be used to evaluate the fitting coefficients (b_i and c_i). The evaluated coefficients are given below,

b0	b1	b2	b3	b4
-1.4799E-06	2.5765E-05	6.2951E-03	-5.6343E-04	-2.0947E+01

c0	c1	c2	c3	c4
-2.8663E+03	-2.6831E+02	2.8932E+02	6.7827E+00	2.3305E+02

After the coefficients have been extracted the derivative and second derivative of the above equations should be evaluated (Equations (A.13) and (A.14)).

$$y' = b_1 + 2\,b_2\,z + 3b_3z^2 + 4b_4z^3, \quad y'' = 2\,b_2 + 6b_3z + 12b_4z^2 \tag{A.13}$$

$$r' = c_1 + 2c_2\theta + 3c_3\theta^2 + 4c_4\theta^3, \quad r'' = 2c_2 + 6c_3\theta + 12c_4\theta^2 \tag{A.14}$$

Plugging in the coefficient values and the axial and angular coordinates of the dent peak (z = 0 mm and θ = 0 rad) (Figure A.5 and Figure A.6), in the above equations gives,

y' = -5.6343E-04, y" = 1.2590E-02

r = 233.05, r' = 6.7827, r" = 578.64

The derivative and second derivative values computed so far must be applied to the following equations to evaluate the curvature and radius of curvature values at the dent peak,

$$\kappa_1 = \frac{r^2 + 2r'^2 - rr''}{(r^2 + r'^2)^{1.5}} \tag{A.15}$$

$$\kappa_2 = \frac{y''}{(1 + y'^2)^{1.5}} \tag{A.16}$$

$$R = \frac{1}{\kappa} \tag{A.17}$$

Where, κ_1 and κ_2 are the curvatures of circumferential and axial profiles at the dent peak. R is the respective radius of curvature. Applying the values evaluated so far to the above equations gives,

κ_1 = -6.3477E-03, κ_2 = 1.2590E-02, R_1 = -157.53, R_2 = 79.43

In addition to the curvature values which define the bending strains, axial dent depth and length values need to be evaluated to calculate the axial membrane strain. Specific guidelines on evaluating the axial dent depth and length have not been provided in ASME B31.8. In this example the length is defined as the sum of US and DS $L_{85\%}^{AX}$ defined as per API 1183 and depth is defined as (100-85)% of dent depth (API 1183). This procedure was adopted because the 85% depth station is close to the dent peak and will provide a better approximation of the membrane strain near the peak (Figure A.7).

d =3.151, L = 47.958

Now all of the inputs for the strain evaluation have been collected and plugging in the necessary values into Equations (4.1) to (4.4) yields,

$\varepsilon_1 = 0.0367$, $\varepsilon_2 = 0.0449$, $\varepsilon_3 = 0.0022$, ε_{eff} OD = 0.079, ε_{eff} ID = 0.084

There are alternate measures of effective strain besides the ASME B31.8 strain. "Blade Energy Partners Simplified Model" is an alternative which takes into account the contribution of axial and circumferential membrane strain more rigorously. Both strains are evaluated based on the change in arc length of the profile when compared to the undeformed configuration. A deformed and the corresponding undeformed span about the dent peak have to be extracted and the lengths of these spans have to be calculated (Figure A.8 and Figure A.9). As mentioned earlier, the dent peak spans have been extracted with reference to the 85% dent depth points (or points close to them) and curves have been fitted onto them. These polynomials and their derivatives can be used to calculate the deformed arc lengths (L_S) for the axial and circumferential dent peak spans. For axial membrane strain evaluation, L_S is given by the following equation,

$$L_S = \int \sqrt{\left(1 + \frac{du}{dz}\right)^2 + \left(\frac{dv}{dz}\right)^2}\, dz \tag{A.18}$$

Where, dv/dz is the derivative of Equation (A.11) and du/dz is given by the following equation,

$$\frac{du}{dz} = \frac{\left(\frac{d^2v}{dz^2}\right)\left(\frac{dv}{dz}\right)}{2.6} \tag{A.19}$$

This equation can be evaluated using the derivatives of Equation (A.11). Equation (A.19) is integrated across the span of points taken for axial curve fitting, z_1 = -24 mm to z_2 = 24 mm in this case. This yields the following values,

L_S = 48.527 mm, L_0 = 48 mm.

Plugging these values into Equation (4.5) yields the following,

Blade axial membrane strain, $\varepsilon_3 = 0.011$

For the circumferential membrane strain L_S is given by the following equation,

$$L_S = \int \sqrt{\left(\frac{dr}{d\theta}\cos\theta - r\sin\theta\right)^2 + \left(\frac{dr}{d\theta}\sin\theta + r\cos\theta\right)^2}\, d\theta \tag{A.20}$$

Where, r and θ are as defined in Equation (A.12). The above equation is integrated from the angular coordinate of the counterclockwise to clockwise 85% dent depth points, θ_1 = -0.1193 to θ_2 = 0.1052 radians, respectively, in this case. L_0 can be approximated using the following equation,

$$L_0 = \left(\sin^{-1}\left(\frac{r}{R}\sin\theta\right)|_{\theta=\theta_2} - \sin^{-1}\left(\frac{r}{R}\sin\theta\right)|_{\theta=\theta_1}\right)R \tag{A.21}$$

Where, r is evaluated at θ_1 and θ_2 as listed above and R is the nominal pipe radius. After performing the necessary evaluations, the calculated values are as listed below,

L_S = 53.097, L_0 = 53.048

Circumferential membrane strain, ε_4 = 0.0009.

The strain values evaluated above are plugged into the Blade effective strain equation (Equation (4.6)),

ε_{eff} OD = 0.069, ε_{eff} ID = 0.094

An improved modified ASME strain model has been presented in this document and evaluations based on it are presented here. Since the bending strains have already been evaluated, the membrane strains based on the modifications proposed have to be evaluated. The axial membrane strain formulation is functionally same as that for ASME strain and can be evaluated using Equation (4.9). The same d and L values evaluated earlier are plugged into the equation.

d =3.151, L = 47.958, ε_3 = 0.0086

The same framework used so far is used for evaluating the circumferential membrane strain. The same transverse dent peak span, referenced to the 85% dent depth points, is employed. As mentioned in Section 4.4.2, the angular coordinates of the start and end of the span based on 85% dent depth points can be given as $\theta = L_{85}^{TR}/R$. The counterclockwise length angular coordinate can be given as $\theta_1 = -L_{85}^{TR}\ ccw/R$ and the clockwise as $\theta_2 = L_{85}^{TR}\ cw/R$, where L_{85}^{TR} ccw = -30.313 and L_{85}^{TR} cw = 26.733. Plugging in those values gives, θ_1 = -0.1193 to θ_2 = 0.1052 radians, same values used for Blade strain. In addition to these values the radial coordinates of the ends and dent peak are required and these can be evaluated by plugging in the angular coordinates of the ends and the peak ($\theta = 0$) into Equation (A.12).

r_1 = 236.235, r_2 = 236.304, r_p = 233.05

These values can be plugged into Equation (4.10) to obtain the counterclockwise and clockwise deformed and undeformed lengths,

$L_S\ ccw = \sqrt{{r_1}^2 + {r_p}^2 - 2\ r_1\ r_p\ \cos\theta_1}$ = 28.166,

$L_S\ cw = \sqrt{{r_2}^2 + {r_p}^2 - 2\ r_2\ r_p\ \cos\theta_2}$ = 24.901

$L_0 ccw = r_1\sqrt{2(1 - \cos\theta_1)}$ = 28.176,

$L_0 cw = r_2\sqrt{2(1 - \cos\theta_2)}$ = 24.859

Circumferential membrane strain, ε_4 = 0.0006.

The strain values evaluated above are plugged into the modified ASME effective strain equation (Equation (4.6)),

ε_{eff} OD = 0.072, ε_{eff} ID = 0.091

A comparison table listing the results for all three models has been given below,

Table A.5 - Consolidated Results For All Models Evaluated

Model	Circ. Bending Strain, $\boldsymbol{\varepsilon_1}$	Axial Bending Strain, $\boldsymbol{\varepsilon_2}$	Axial Membrane Strain, $\boldsymbol{\varepsilon_3}$	Circ. Membrane Strain, $\boldsymbol{\varepsilon_4}$	Max Effective Strain
ASME	0.0367	0.0449	0.0022	N/A	0.084
Blade	0.0367	0.0449	0.011	0.0009	0.094
Modified ASME	0.0367	0.0449	0.0086	0.0006	0.091

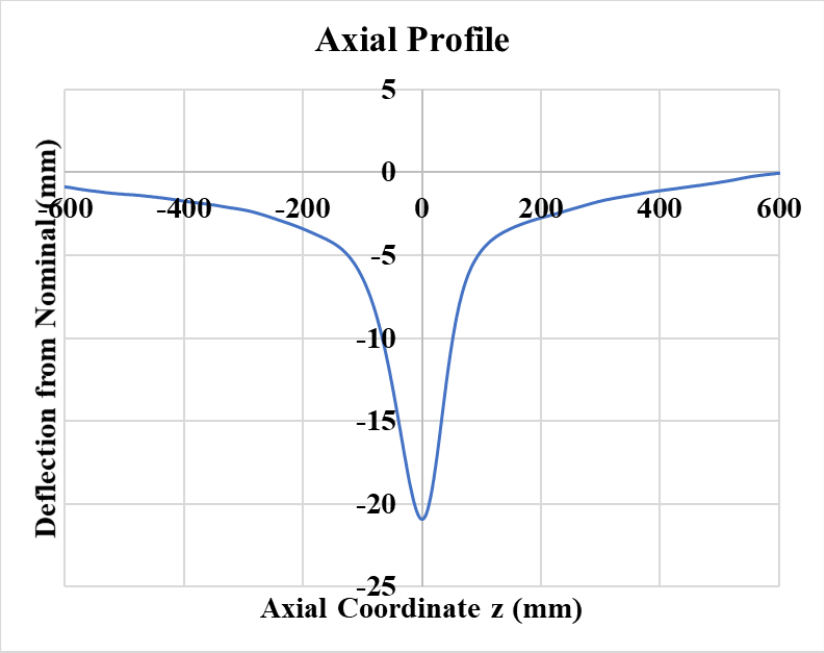

Figure A.3 - Dent Axial Profile

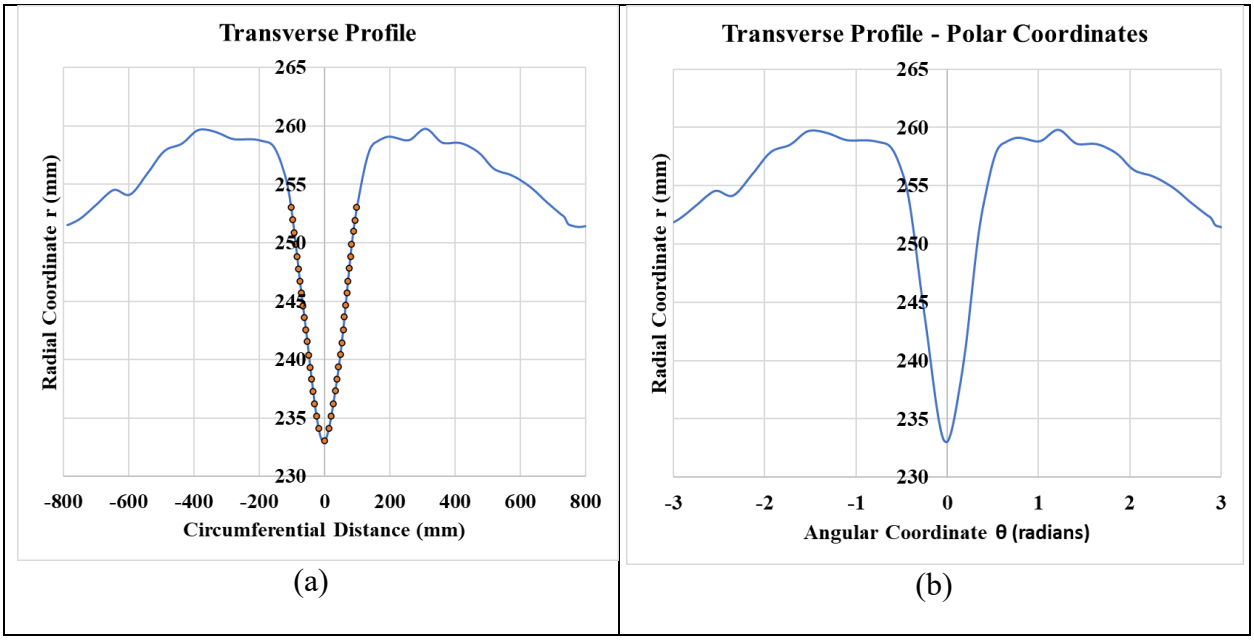

Figure A.4 - Dent Circumferential Profile in (a) Radial vs Circumferential Distance (b) Polar Coordinates

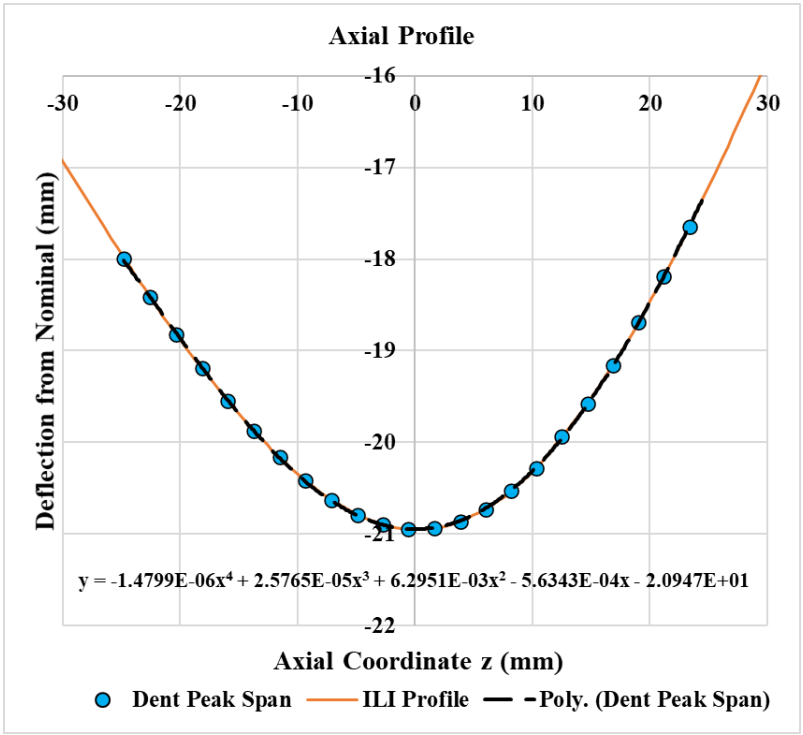

Figure A.5 - Axial Span of Points About the Dent Peak and a Quadratic Curve Fitting on the Span

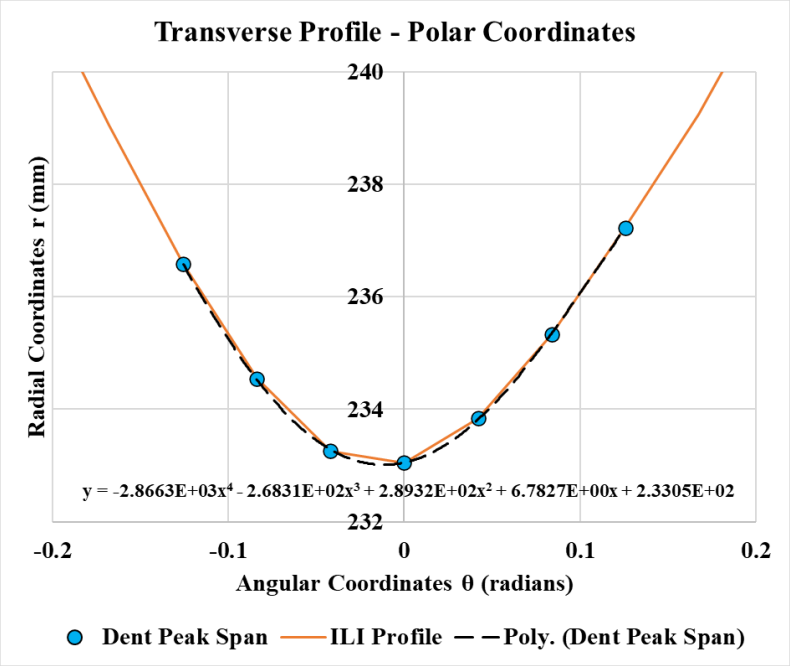

Figure A.6 - Circumferential Span of Points About the Dent Peak and a Quadratic Curve Fitting on the Span

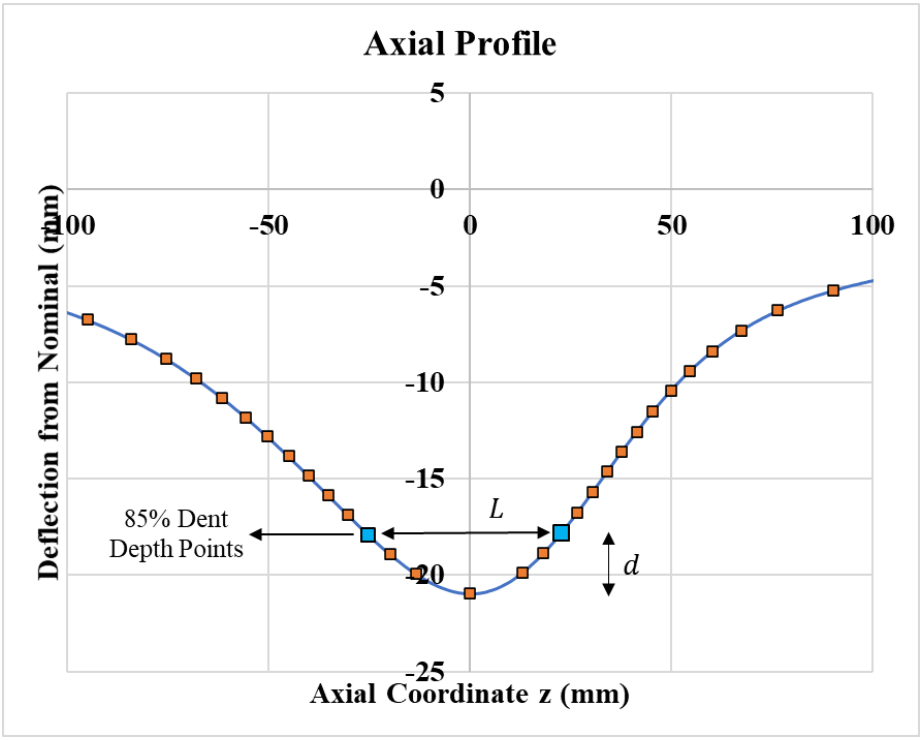

Figure A.7 - Evaluation of Depth and Length Parameters for Axial Membrane Strain using API RP 1183 Geometry Parameters

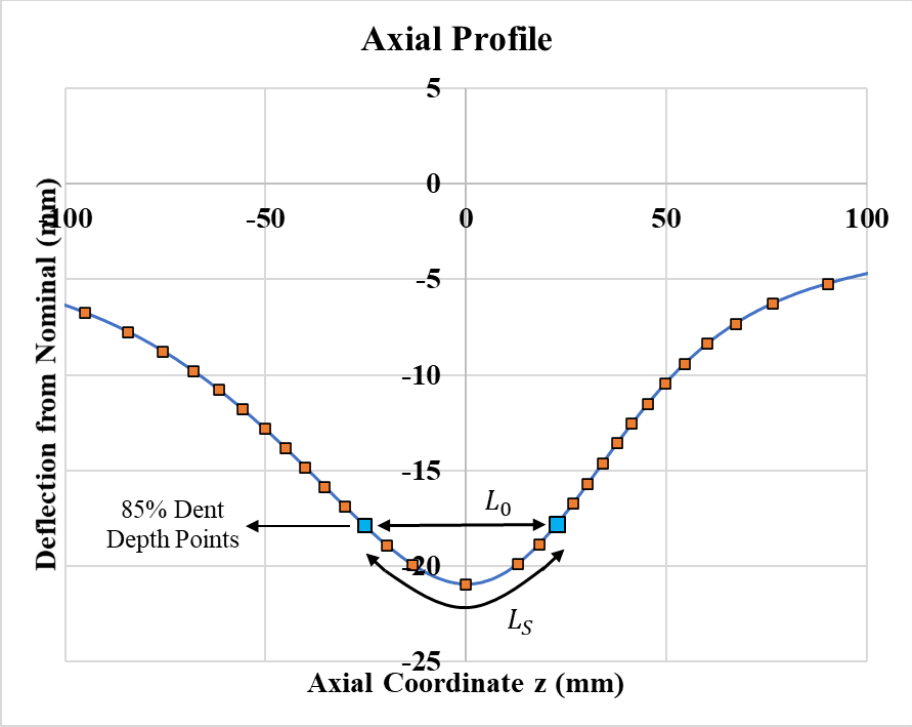

Figure A.8 – Evaluation of the Arc Length of the Deformed and Undeformed Axial Dent Peak Span

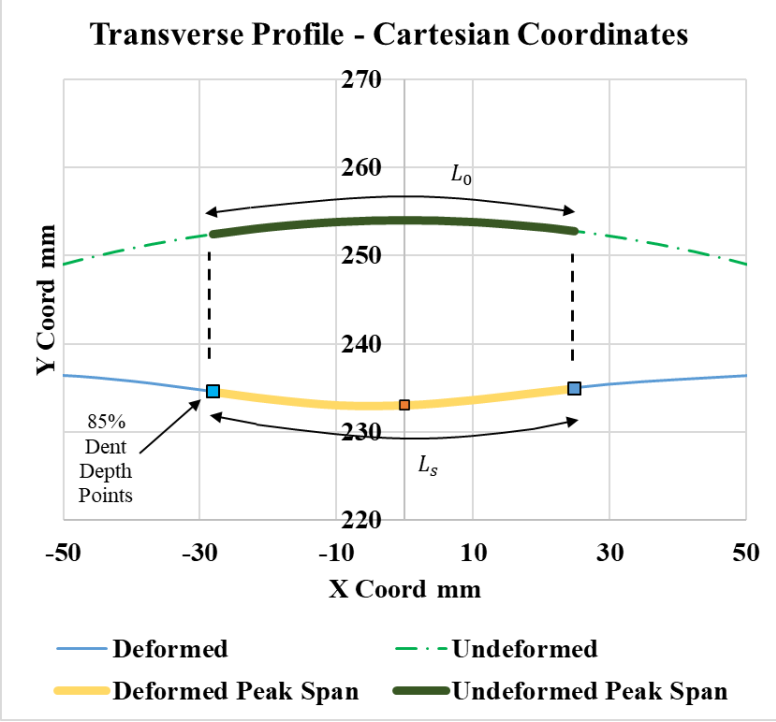

Figure A.9 - Evaluation of the Arc Length of the Deformed and Undeformed Circumferential Dent Peak Span

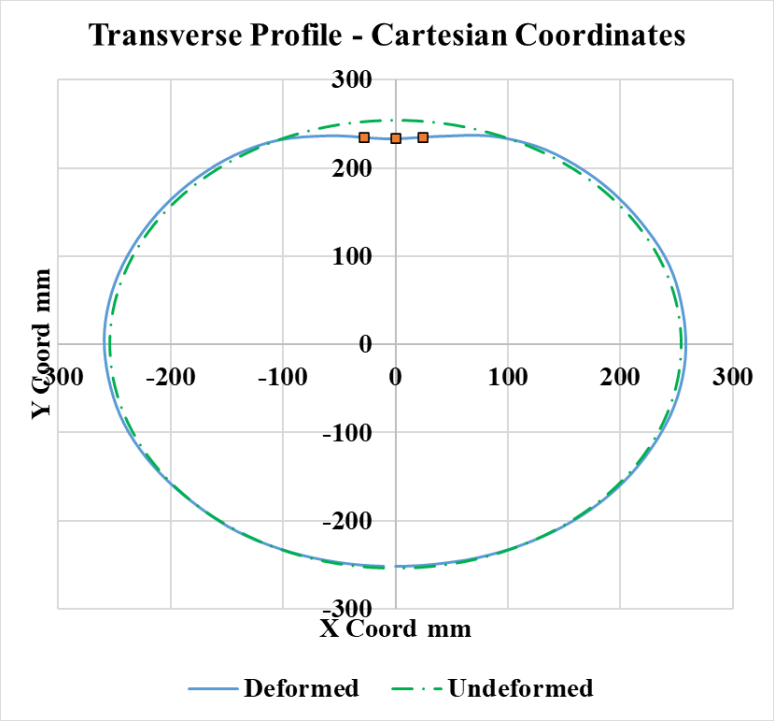

Figure A.10 – Deformed and Undeformed Circumferential Pipe Profile in Cartesian Coordinates

Appendix B - Additional Strain Estimate Unity Plots

This section shows some additional unity plots comparing strain estimates against FE strain results.

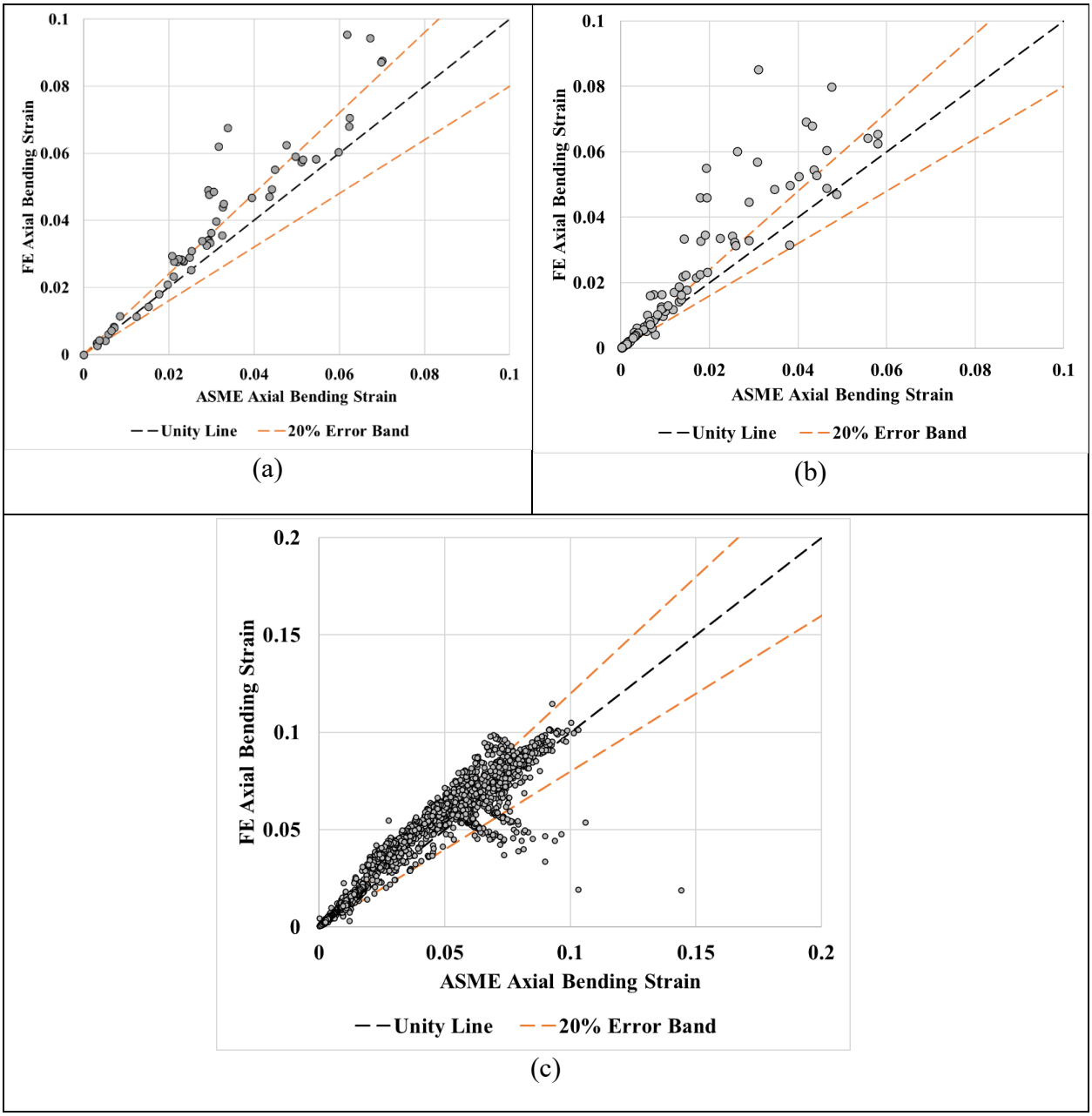

Figure B.1 - Unity Plots of ASME Axial Bending Strain vs FE Axial Bending Strain, Calculated using FE Models from (a) Full-Scale (b) Field Dents (c) Hypothetical Dents

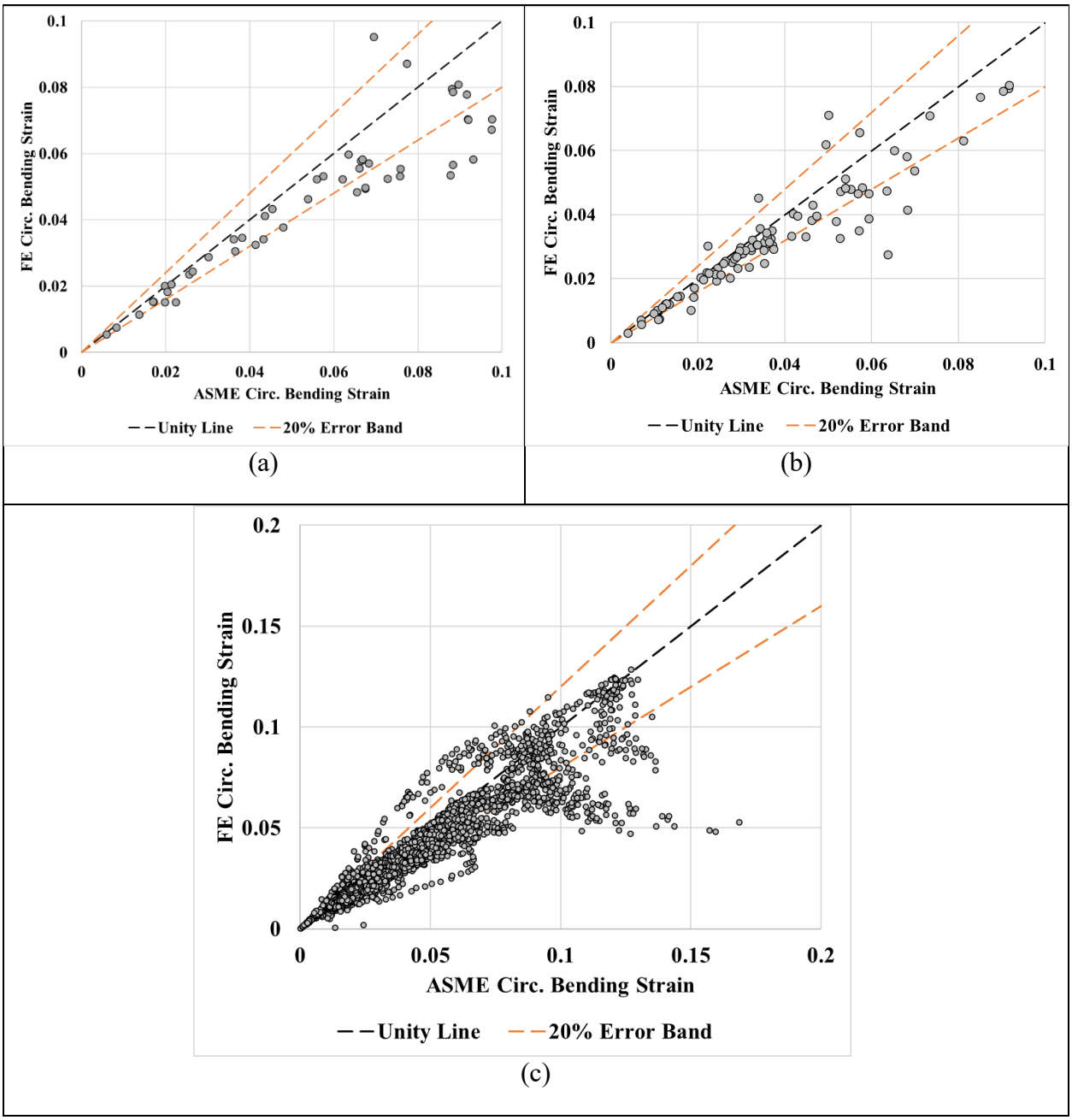

Figure B.2 - Unity Plots of ASME Circumferential Bending Strain vs FE Circumferential Bending Strain, Calculated using FE Models from (a) Full-Scale (b) Field Dents (c) Hypothetical Dents

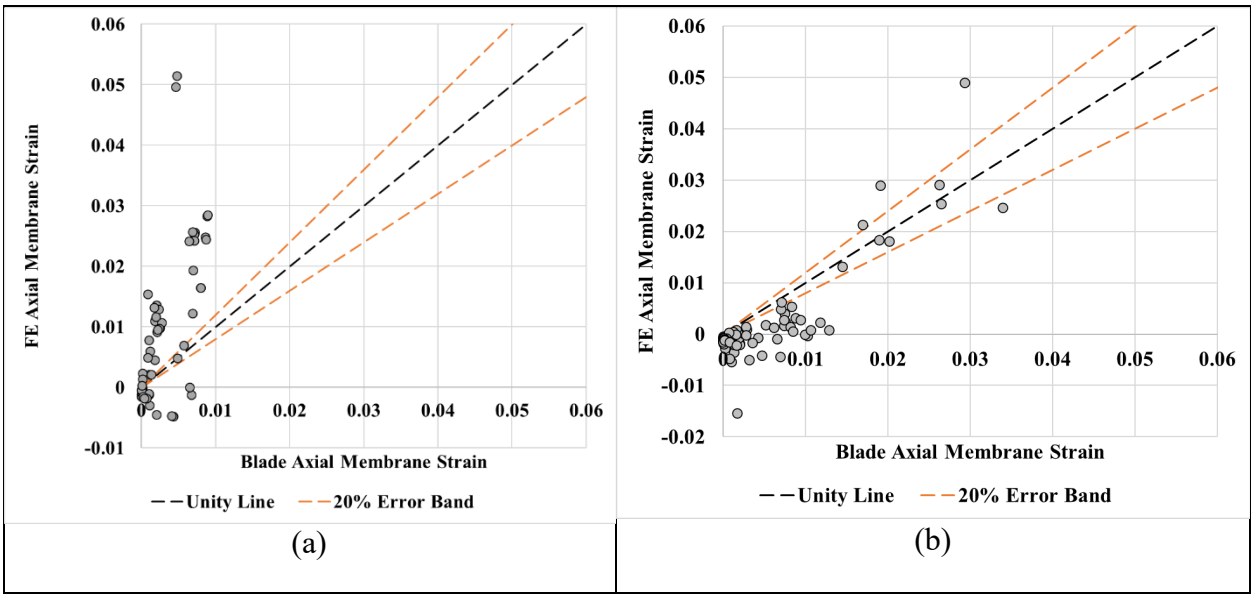

Figure B.3 - Unity Plots of Blade Axial Membrane Strain vs FE Axial Membrane Strain, Calculated using FE Models from (a) Full-Scale (b) Field Dents

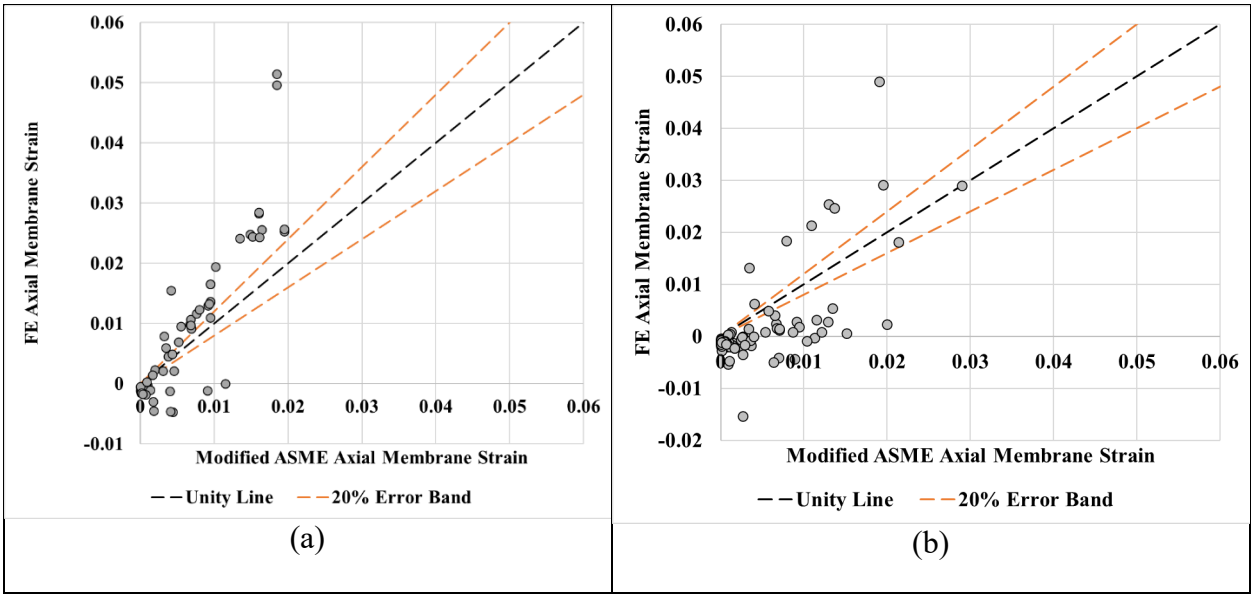

Figure B.4 - Unity Plots of Modified ASME Axial Membrane Strain vs FE Axial Membrane Strain, Calculated using FE Models from (a) Full-Scale (b) Field Dents

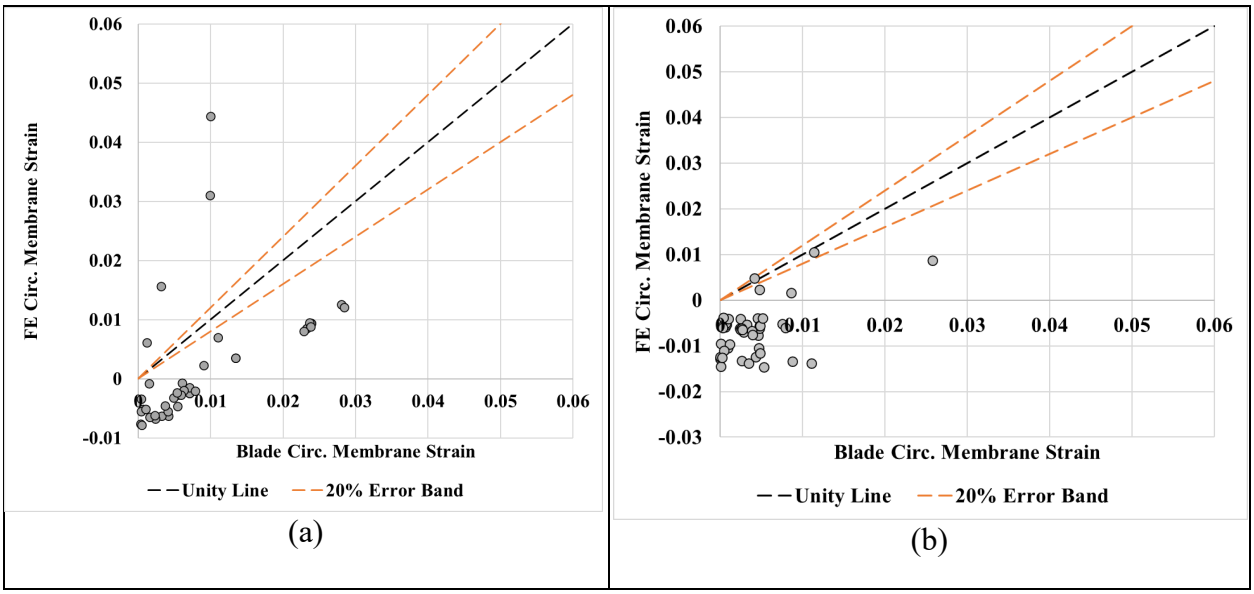

Figure B.5 - Unity Plots of Blade Circumferential Membrane Strain vs FE Circumferential Membrane Strain, Calculated using FE models from (a) Full-Scale (b) Field Dents

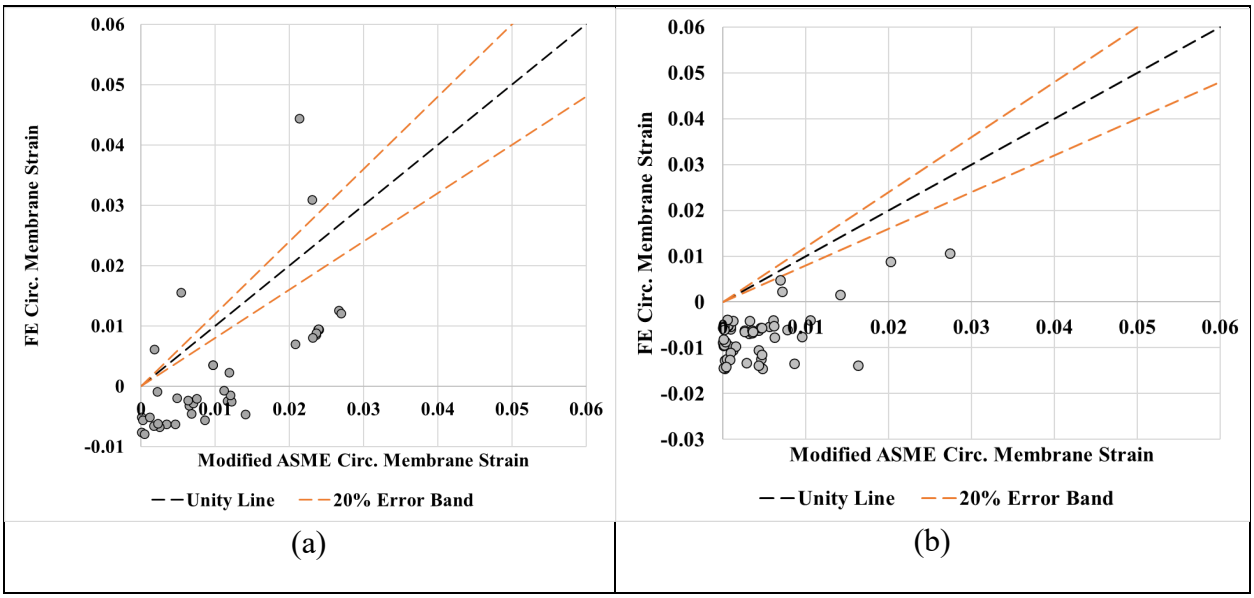

Figure B.6 - Unity Plots of Modified ASME Circumferential Membrane Strain vs FE Circumferential Membrane Strain, Calculated using FE models from (a) Full-Scale (b) Field Dents

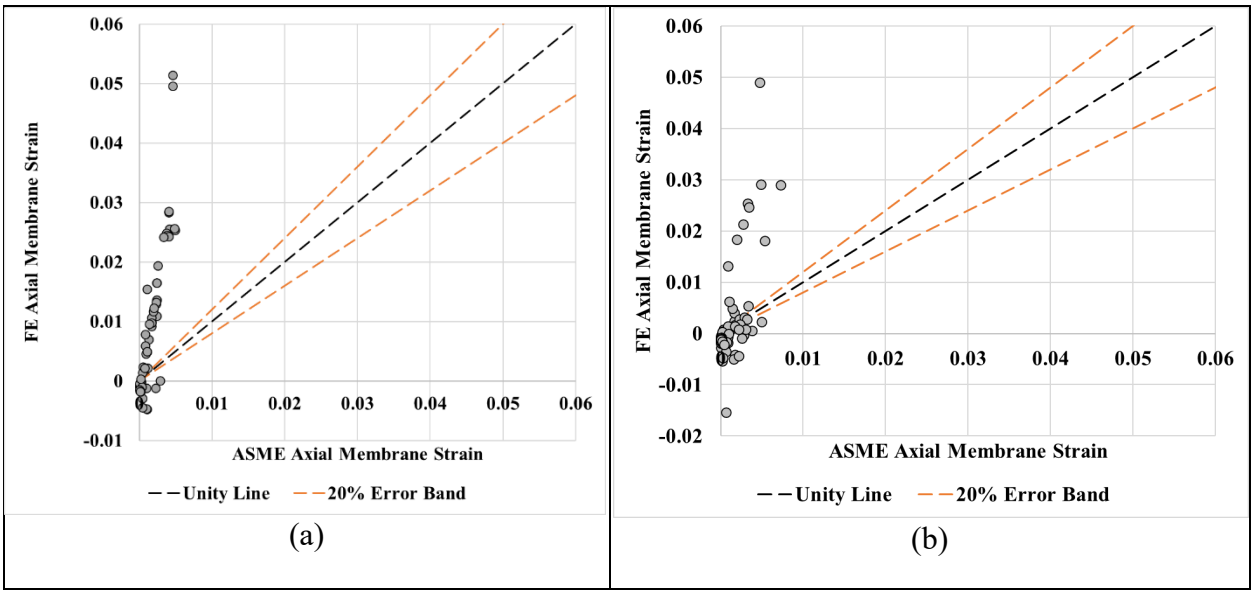

Figure B.7 - Unity Plots of ASME Axial Membrane Strain vs FE Axial Membrane Strain, Calculated using FE Models from (a) Full-Scale (b) Field Dents

Appendix C - Ratio of Experimental to Predicted Cycles to Failure

Table C.1 - Ratio of Experimental to Predicted Cycles to Failure for Plain Dents

	Nexp/Npred (BS 7608 Class D Mean -1sd SN Curve)				Nexp/Npred (BS 7608 Class D Mean SN Curve)			
Dent #	Level 0	Level 0.5	Level 0.5+	Level 2	Level 0	Level 0.5	Level 0.5+	Level 2
1	23.89	1.40	1.38	1.62	14.75	0.86	0.85	1.00
2	133.00	7.80	7.66	9.02	82.10	4.82	4.73	5.57
3	40.29	3.00	2.75	2.74	24.87	1.85	1.70	1.69
4	14.81	1.10	1.01	1.00	9.14	0.68	0.62	0.62
5	55.80	3.86	3.47	4.88	34.44	2.38	2.14	3.01
6	18.05	1.25	1.12	2.06	11.14	0.77	0.69	1.27
7	24.10	1.67	1.50	2.70	14.88	1.03	0.93	1.67
8	39.83	2.76	2.48	2.54	24.59	1.70	1.53	1.57
9	72.91	5.05	4.54	4.68	45.01	3.12	2.80	2.89
10	84.31	6.17	5.02	5.88	52.04	3.81	3.10	3.63
11	95.76	7.01	5.70	6.95	59.11	4.33	3.52	4.29
12	25.65	1.88	1.53	2.47	15.83	1.16	0.94	1.52
13	29.77	2.18	1.77	2.87	18.38	1.35	1.09	1.77
14	72.56	5.31	4.32	3.53	44.79	3.28	2.67	2.18
15	101.38	7.42	6.03	5.67	62.58	4.58	3.72	3.50
16	97.62	12.41	10.80	11.33	60.26	7.66	6.67	6.99
17	98.04	12.46	10.85	11.30	60.52	7.69	6.70	6.98
18	76.34	9.70	8.45	7.71	47.13	5.99	5.21	4.76
19	177.34	22.54	19.62	13.89	109.47	13.91	12.11	8.57
20	30.47	1.95	1.92	2.40	18.81	1.20	1.19	1.48
21	23.17	1.48	1.46	1.70	14.30	0.91	0.90	1.05
22	52.79	3.37	3.33	5.79	32.58	2.08	2.05	3.58
23	38.86	2.48	2.45	2.28	23.99	1.53	1.51	1.41

	Nexp/Npred (BS 7608 Class D Mean -1sd SN Curve)				Nexp/Npred (BS 7608 Class D Mean SN Curve)			
Dent #	Level 0	Level 0.5	Level 0.5+	Level 2	Level 0	Level 0.5	Level 0.5+	Level 2
24	35.39	2.26	2.23	2.65	21.85	1.40	1.38	1.64
25	50.28	4.62	4.97	1.36	31.04	2.85	3.07	0.84
26	38.96	3.58	3.85	1.16	24.05	2.21	2.38	0.72
27	32.66	4.20	4.48	1.47	20.16	2.59	2.76	0.91
28	22.98	2.96	3.15	0.55	14.18	1.82	1.95	0.34
29	149.38	13.74	14.77	3.06	92.21	8.48	9.12	1.89
30	91.42	8.41	9.04	1.79	56.44	5.19	5.58	1.10
31	17.51	2.84	3.00	0.85	10.81	1.76	1.85	0.52
32	20.82	3.38	3.57	1.73	12.85	2.09	2.20	1.07
33	29.59	3.24	2.95	1.80	18.27	2.00	1.82	1.11
34	58.02	6.35	5.77	2.69	35.82	3.92	3.56	1.66
35	43.91	4.63	3.90	1.15	27.11	2.86	2.41	0.71
36	54.72	5.77	4.85	2.41	33.78	3.56	3.00	1.49
37	52.56	5.55	4.66	1.34	32.44	3.42	2.88	0.83
38	56.09	5.92	4.98	1.53	34.63	3.65	3.07	0.94
39	82.91	8.75	7.36	3.49	51.18	5.40	4.54	2.16
40	89.18	9.76	8.88	4.42	55.05	6.02	5.48	2.73
41	63.63	6.71	5.65	1.61	39.28	4.14	3.48	0.99
42	24.38	2.57	2.16	1.28	15.05	1.59	1.34	0.79
43	24.12	2.64	2.40	1.38	14.89	1.63	1.48	0.85
44	32.21	3.40	2.86	0.87	19.88	2.10	1.76	0.54
45	39.46	6.41	6.76	2.70	24.36	3.96	4.17	1.67
46	26.58	2.80	2.36	0.76	16.41	1.73	1.46	0.47
47	41.51	4.38	3.68	1.14	25.62	2.70	2.27	0.70
48	29.02	7.08	7.49	3.98	17.91	4.37	4.63	2.46

	Nexp/Npred (BS 7608 Class D Mean -1sd SN Curve)				Nexp/Npred (BS 7608 Class D Mean SN Curve)			
Dent #	Level 0	Level 0.5	Level 0.5+	Level 2	Level 0	Level 0.5	Level 0.5+	Level 2
49	164.35	14.29	15.36	4.53	101.45	8.82	9.48	2.80
50	44.81	3.90	4.19	3.25	27.66	2.41	2.58	2.00
51	50.00	4.44	4.98	5.08	30.86	2.74	3.08	3.14
52	27.43	4.14	4.57	1.82	16.93	2.56	2.82	1.13
53	21.42	3.23	3.57	4.08	13.22	2.00	2.20	2.52
54	197.81	10.32	10.21	7.89	122.11	6.37	6.30	4.87
55	9.63	4.27	4.53	1.83	5.94	2.63	2.80	1.13
56	24.77	6.36	6.82	2.29	15.29	3.93	4.21	1.41
57	69.78	6.20	6.95	2.46	43.07	3.83	4.29	1.52
58	16.32	2.35	2.54	1.82	10.08	1.45	1.57	1.12
59	81.27	6.88	6.95	4.03	50.17	4.25	4.29	2.49
60	72.38	18.02	24.08	8.15	44.68	11.12	14.86	5.03
61	15.27	3.80	5.08	4.99	9.43	2.35	3.14	3.08

Table C.2 - Ratio of Experimental to Predicted Cycles to Failure for Dents Interacting with Corrosion

	Nexp/Npred (BS 7608 Class D Mean -1sd SN Curve)				Nexp/Npred (BS 7608 Class D Mean SN Curve)			
Dent #	Level 0	Level 0.5	Level 0.5+	Level 2	Level 0	Level 0.5	Level 0.5+	Level 2
1	87.15	6.03	5.42	5.56	53.80	3.72	3.35	3.43
2	41.34	3.03	2.46	2.01	25.52	1.87	1.52	1.24
3	15.62	2.54	2.68	1.30	9.64	1.57	1.65	0.80
4	36.24	5.88	6.21	3.02	22.37	3.63	3.83	1.86
5	21.55	3.50	3.69	1.05	13.30	2.16	2.28	0.65
6	25.76	4.18	4.41	1.25	15.90	2.58	2.72	0.77
7	24.69	4.01	4.23	2.06	15.24	2.47	2.61	1.27

	Nexp/Npred (BS 7608 Class D Mean -1sd SN Curve)				Nexp/Npred (BS 7608 Class D Mean SN Curve)			
Dent #	Level 0	Level 0.5	Level 0.5+	Level 2	Level 0	Level 0.5	Level 0.5+	Level 2
8	21.19	3.44	3.63	1.77	13.08	2.12	2.24	1.09
9	29.34	4.76	5.03	1.42	18.11	2.94	3.10	0.88
10	34.76	5.64	5.96	1.69	21.46	3.48	3.68	1.04
11	111.57	12.21	11.10	5.18	68.87	7.54	6.85	3.20
12	124.37	13.61	12.38	5.77	76.77	8.40	7.64	3.56
13	106.97	11.71	10.65	6.50	66.03	7.23	6.57	4.01
14	84.42	9.24	8.40	5.13	52.12	5.70	5.19	3.17
15	115.86	12.22	10.28	3.05	71.52	7.55	6.35	1.88
16	161.39	17.03	14.32	7.11	99.63	10.51	8.84	4.39
17	290.51	30.65	25.77	7.43	179.34	18.92	15.91	4.59
18	165.67	17.48	14.70	4.50	102.27	10.79	9.07	2.78
19	132.99	14.03	11.80	3.36	82.10	8.66	7.28	2.08
20	54.99	5.80	4.88	1.57	33.95	3.58	3.01	0.97
21	70.79	7.47	6.28	3.73	43.70	4.61	3.88	2.30
22	157.78	16.65	14.00	4.25	97.40	10.28	8.64	2.62
23	34.26	5.56	5.87	2.35	21.15	3.43	3.62	1.45
24	81.27	13.20	13.92	5.57	50.17	8.15	8.60	3.44
25	49.49	8.04	8.48	3.39	30.55	4.96	5.23	2.09
26	89.76	13.55	14.94	4.55	55.41	8.36	9.22	2.81
27	168.62	8.56	9.28	4.68	104.09	5.28	5.73	2.89
28	29.57	4.25	4.59	3.97	18.25	2.63	2.84	2.45
29	60.44	15.04	20.10	14.80	37.31	9.29	12.41	9.14

Table C.3 - Ratio of Experimental to Predicted Cycles to Failure for Dents Interacting with Welds, Life Reduction Factor of 10

	Nexp/Npred (BS 7608 Class D Mean -1sd SN Curve)				Nexp/Npred (BS 7608 Class D Mean SN Curve)			
Dent #	Level 0	Level 0.5	Level 0.5+	Level 2	Level 0	Level 0.5	Level 0.5+	Level 2
1	1787.16	119.29	109.54	133.82	1103.22	73.64	67.62	82.61
2	744.29	55.39	50.85	50.53	459.45	34.19	31.39	31.20
3	952.33	70.87	65.06	64.66	587.88	43.75	40.16	39.92
4	504.02	34.89	31.35	44.06	311.14	21.54	19.36	27.20
5	492.65	34.10	30.65	43.07	304.12	21.05	18.92	26.59
6	425.87	29.48	26.49	37.23	262.89	18.20	16.35	22.98
7	380.73	26.36	23.68	24.28	235.03	16.27	14.62	14.99
8	628.67	46.04	37.42	43.87	388.08	28.42	23.10	27.08
9	604.26	44.25	35.96	42.17	373.01	27.32	22.20	26.03
10	596.63	43.69	35.51	29.05	368.30	26.97	21.92	17.93
11	627.46	45.95	37.35	30.55	387.33	28.36	23.05	18.86
12	1268.71	92.91	75.51	61.77	783.18	57.35	46.61	38.13
13	989.59	72.47	58.90	48.18	610.88	44.73	36.36	29.74
14	153.85	9.83	9.70	11.52	94.97	6.07	5.99	7.11
15	472.59	60.07	52.29	47.75	291.73	37.08	32.28	29.47
16	219.51	14.03	13.84	6.38	135.50	8.66	8.54	3.94
17	213.07	23.80	20.71	25.97	131.53	14.69	12.78	16.03
18	278.01	31.06	27.02	25.33	171.62	19.17	16.68	15.64
19	366.48	40.94	35.62	33.38	226.23	25.27	21.99	20.60
20	88.42	9.88	8.59	11.44	54.58	6.10	5.30	7.06
21	119.86	7.66	7.56	6.61	73.99	4.73	4.67	4.08
22	142.02	9.07	8.95	5.97	87.67	5.60	5.53	3.69
23	455.14	29.08	28.70	12.45	280.96	17.95	17.71	7.69

	Nexp/Npred (BS 7608 Class D Mean -1sd SN Curve)				Nexp/Npred (BS 7608 Class D Mean SN Curve)			
Dent #	Level 0	Level 0.5	Level 0.5+	Level 2	Level 0	Level 0.5	Level 0.5+	Level 2
24	328.22	30.18	32.46	8.89	202.61	18.63	20.04	5.49
25	259.73	23.88	25.69	7.76	160.33	14.74	15.86	4.79
26	327.09	42.08	44.86	14.69	201.91	25.98	27.69	9.07
27	302.24	38.88	41.45	7.29	186.57	24.00	25.59	4.50
28	501.78	46.14	49.63	13.60	309.75	28.48	30.64	8.39
29	299.31	27.52	29.60	8.94	184.77	16.99	18.27	5.52
30	191.40	24.62	26.25	8.59	118.15	15.20	16.21	5.30
31	270.15	29.56	26.89	16.42	166.77	18.25	16.60	10.14
32	34.51	8.86	9.50	6.76	21.30	5.47	5.87	4.17
33	937.95	47.60	51.61	32.78	579.00	29.39	31.86	20.24
34	219.35	31.65	34.24	15.87	135.40	19.54	21.14	9.80
35	1295.04	42.67	29.16	60.48	799.44	26.34	18.00	37.34
36	802.20	42.84	37.88	58.41	495.20	26.45	23.38	36.05
37	714.07	162.89	168.77	254.72	440.80	100.55	104.19	157.24

Table C.4 - Ratio of Experimental to Predicted Cycles to Failure for Dents Interacting with Welds, Life Reduction Factor of 5

	Nexp/Npred (BS 7608 Class D Mean -1sd SN Curve)				Nexp/Npred (BS 7608 Class D Mean SN Curve)			
Dent #	Level 0	Level 0.5	Level 0.5+	Level 2	Level 0	Level 0.5	Level 0.5+	Level 2
1	893.58	59.64	54.77	66.91	551.61	36.82	33.81	41.30
2	372.14	27.69	25.42	25.27	229.73	17.09	15.69	15.60
3	476.16	35.43	32.53	32.33	293.94	21.87	20.08	19.96
4	252.01	17.45	15.68	22.03	155.57	10.77	9.68	13.60
5	246.33	17.05	15.32	21.54	152.06	10.53	9.46	13.29

	Nexp/Npred (BS 7608 Class D Mean -1sd SN Curve)				Nexp/Npred (BS 7608 Class D Mean SN Curve)			
Dent #	Level 0	Level 0.5	Level 0.5+	Level 2	Level 0	Level 0.5	Level 0.5+	Level 2
6	212.93	14.74	13.25	18.62	131.45	9.10	8.18	11.49
7	190.37	13.18	11.84	12.14	117.51	8.13	7.31	7.49
8	314.33	23.02	18.71	21.93	194.04	14.21	11.55	13.54
9	302.13	22.12	17.98	21.08	186.51	13.66	11.10	13.01
10	298.31	21.85	17.76	14.52	184.15	13.49	10.96	8.97
11	313.73	22.97	18.67	15.27	193.67	14.18	11.53	9.43
12	634.35	46.45	37.76	30.88	391.59	28.68	23.31	19.06
13	494.80	36.23	29.45	24.09	305.44	22.37	18.18	14.87
14	76.92	4.91	4.85	5.76	47.49	3.03	2.99	3.56
15	236.29	30.04	26.14	23.87	145.86	18.54	16.14	14.74
16	109.75	7.01	6.92	3.19	67.75	4.33	4.27	1.97
17	106.54	11.90	10.35	12.99	65.77	7.35	6.39	8.02
18	139.01	15.53	13.51	12.67	85.81	9.59	8.34	7.82
19	183.24	20.47	17.81	16.69	113.11	12.64	10.99	10.30
20	44.21	4.94	4.30	5.72	27.29	3.05	2.65	3.53
21	59.93	3.83	3.78	3.31	37.00	2.36	2.33	2.04
22	71.01	4.54	4.48	2.99	43.83	2.80	2.76	1.84
23	227.57	14.54	14.35	6.23	140.48	8.98	8.86	3.84
24	164.11	15.09	16.23	4.45	101.31	9.32	10.02	2.75
25	129.86	11.94	12.84	3.88	80.17	7.37	7.93	2.39
26	163.54	21.04	22.43	7.34	100.96	12.99	13.85	4.53
27	151.12	19.44	20.73	3.65	93.29	12.00	12.79	2.25
28	250.89	23.07	24.81	6.80	154.87	14.24	15.32	4.20
29	149.66	13.76	14.80	4.47	92.38	8.50	9.14	2.76
30	95.70	12.31	13.13	4.30	59.07	7.60	8.10	2.65

	Nexp/Npred (BS 7608 Class D Mean -1sd SN Curve)				Nexp/Npred (BS 7608 Class D Mean SN Curve)			
Dent #	Level 0	Level 0.5	Level 0.5+	Level 2	Level 0	Level 0.5	Level 0.5+	Level 2
31	135.08	14.78	13.44	8.21	83.38	9.12	8.30	5.07
32	17.25	4.43	4.75	3.38	10.65	2.73	2.93	2.09
33	468.97	23.80	25.80	16.39	289.50	14.69	15.93	10.12
34	109.67	15.83	17.12	7.94	67.70	9.77	10.57	4.90
35	647.52	21.34	14.58	30.24	399.72	13.17	9.00	18.67
36	401.10	21.42	18.94	29.20	247.60	13.22	11.69	18.03
37	357.04	81.44	84.39	127.36	220.40	50.28	52.09	78.62

Appendix D - Final Financial Section

The cost of this fixed-price project was 80% funded by the Government, with the other 20% cost-shared by the Project Team as identified on Page iv. Project expenses and billings were in strict accordance with the terms and conditions of Agreement #693JK31910011 and modifications. The final invoice, representing 100% completion, will be submitted through the final quarter, March 31, 2022. Note that the second DOT Peer Reviewed in Item 26, Task 6 will not be needed and has been eliminated from the final technical and deliverable milestone schedule. The removal of this task changes the final contract amount to $443,399, of which $352,084 is the Federal share and $91,315 is the PRCI share, as highlighted in the following final technical and deliverable milestone schedule.

Item N	Task N (per proposal)	Activity/Deliverable ACTIVITY/DELIVERABLE	Expected Completion Date/Mos	Payable Milestone TITLE	Projected Federal Payment	Projected Partner Cost-Sharing	Total
1	1	Project Kick Off Meeting	1	Project Kick-Off Meeting held	$4,604	$1,151	$5,755
3	6	Project Management and Reporting	3	Quarterly Status Report submitted	$3,500	$700	$4,200
		First Payable Milestone	**Date**	**SUBTOTAL**	**$8,104**	**$1,851**	**$9,955**
5	6	Project Management and Reporting	6	Quarterly Status Report submitted	$3,500	$700	$4,200
		Second Payable Milestone	**Date**	**SUBTOTAL**	**$3,500**	**$700**	**$4,200**
7	6	Project Management and Reporting	9	Quarterly Status Report submitted	$3,500	$700	$4,200
		Third Payable Milestone	**Date**	**SUBTOTAL**	**$3,500**	**$700**	**$4,200**
10	6	Project Management and Reporting	12	Quarterly Status Report submitted	$3,500	$700	$4,200
		Fourth Payable Milestone	**Date**	**SUBTOTAL**	**$3,500**	**$700**	**$4,200**
2	2	Improvement of Indentation Crack formation Strain Estimates	15	Plan of the review of full scale and FE data	$32,140	$7,535	$39,675
4	2	Improvement of Indentation Crack formation Strain Estimates	15	Completion of first set of FS test data	$30,540	$7,535	$38,075
6	2	Improvement of Indentation Crack formation Strain Estimates	15	Completion of the analysis of FS test data and first set of the FE model data	$32,240	$7,235	$39,475
8	2	Improvement of Indentation Crack formation Strain Estimates	15	Completion of the second set of analysis of the FE model data	$9,640	$3,035	$12,675
14	6	Project Management and Reporting	15	Quarterly Status Report submitted	$3,500	$700	$4,200
		Fifth Payable Milestone	**Date**	**SUBTOTAL**	**$108,060**	**$26,040**	**$134,100**
9	3	Impact of ILI Dent and Interacting Feature Sizing variation	18	Complete first set of analysis on dent shape variation impact	$46,009	$11,402	$57,411
12	3	Impact of ILI Dent and Interacting Feature Sizing variation	18	Complete second set of analysis on dent shape variation impact	$25,010	$5,602	$30,612
17	6	Project Management and Reporting	18	Quarterly Status Report submitted	$3,500	$700	$4,200
		Sixth Payable Milestone	**Date**	**SUBTOTAL**	**$74,519**	**$17,704**	**$92,223**
13	4	Dent Fatigue Life Assessment Safety Quantification	21	Complete first set of dent safety factor quantification	$27,087	$7,022	$34,108
16	4	Dent Fatigue Life Assessment Safety Quantification	21	Complete second set of dent safety factor quantification	$35,487	$9,022	$44,508
20	6	Project Management and Reporting	21	Quarterly Status Report submitted	$3,500	$700	$4,200
		Seventh Payable Milestone	**Date**	**SUBTOTAL**	**$66,073**	**$16,743**	**$82,817**
11	2	Improvement of Indentation Crack formation Strain Estimates	24	Completion of indentation crack formation strain estimate	$6,140	$2,335	$8,475
18	4	Dent Fatigue Life Assessment Safety Quantification	24	Complete dent fatigue life assessment safety quantification	$9,687	$2,022	$11,708
19	5	Sample Application of Enhancements	24	Complete first set of sample applications	$33,130	$9,183	$42,313
22	6	Project Management and Reporting	24	Quarterly Status Report submitted	$0	$0	$0
		Eighth Payable Milestone	**Date**	**SUBTOTAL**	**$48,957**	**$13,539**	**$62,496**
15	3	Impact of ILI Dent and Interacting Feature Sizing variation	27	Complete dent shape and feature size variation impact analysis	$13,009	$4,002	$17,012
21	5	Sample Application of Enhancements	27	Complete sample application of enhancements	$11,530	$1,982	$13,512
30	6	Project Management and Reporting	27	Quarterly Status Report submitted	$0	$0	$0
		Ninth Payable Milestone	**Date**	**SUBTOTAL**	**$24,539**	**$5,984**	**$30,524**
23	6	Dissemination of Results	30	One day workshop with stakeholders (DOT or PRCI event)	$1,500	$1,500	$3,000
24	6	Final Technical Review Meeting	30	Present final project presentation	$500	$500	$1,000
25	6	DOT Peer Review	N/A	Participate in annual DOT Peer Review	$1,000	$0	$1,000
26	6	DOT Peer Review	N/A	Participate in annual DOT Peer Review	$0	$0	$0
27	6	Public Paper	48	Publish Paper and/or Presentation at Pipeline Related Conference	$0	$0	$0
28	6	Draft Final Report	30	Draft final report submitted	$6,832	$3,853	$10,685
29	6	Final Report	N/A	Final Report submitted	$1,500	$1,500	$3,000
		Other		**SUBTOTAL**	**$11,332**	**$7,353**	**$18,685**
				GRAND TOTALS	**$352,084**	**$91,315**	**$443,399**